Highly Efficient Light-Emitting Electrochemical Cells

Antonio Pertegás Ojeda

D. Hendrik Jan Bolink y **D. Enrique Ortí Guillén**, Investigador de la Fundación General de la Universidad de Valencia en el Instituto de Ciencia Molecular (ICMol) y Catedrático del Departamento de Química Física, respectivamente, certifican que la memoria presentada por el licenciado Antonio Pertegás Ojeda con el título "Highly Efficient Light-Emitting Electrochemical Cells" corresponde a su Tesis Doctoral y ha sido realizada bajo su dirección, autorizando mediante este escrito la presentación de la misma.

En Valencia, a 20 de Noviembre del 2015

Dr. Hendrik Jan Bolink Prof. Dr. Enrique Ortí Guillén

Contents

1. Introduction

1.1. Electrical lighting technologies

Since humanity discovered fire, 400000 years ago,[1] the creation of light has determined the humans´ evolution to the contemporary modern societies. Along this evolution, light systems have been adapted to the different sources of power. In the 19th century, electrical lighting started with the design of the incandescent bulb. The enormous impact of that technology increased the quality of our lives such that it is considered "common", accessible and cheap. Electrical light has evolved, by different designs, in order to be adapted to the new human needs (fluorescent sources, Xenon lamps and now Light Emitting Diodes (LEDs) as relevant examples).

Nowadays, the creation of electrical light and its application is commonly available in developed societies. However, there is need for more energy efficient lighting systems. Since the world global population will be increasing to 10 billion of people by 2050,[2] the energy consumption will increase considerably in the future (Figure 1). As lighting represents 20% of electrical consumption,[3] new efficient lighting technologies, accessible for all population at low cost are needed in order to achieve remarkable energy savings.

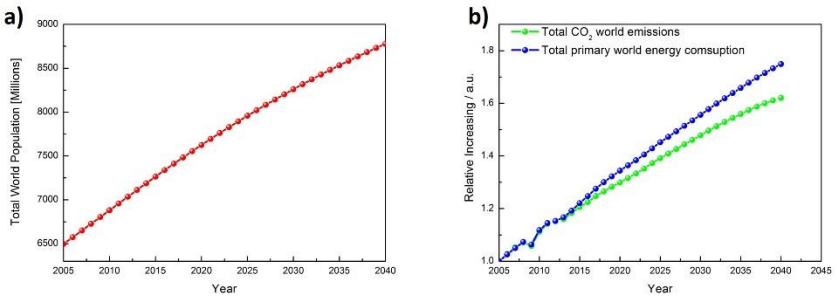

Figure 1. a) Total World Population prospections. b) Total world CO_2 emissions (green) and primary energy consumption (blue) prospections from 2005 (reference year). Source: Energy Information Administration (EIA).

Organic electronics offers high potential solutions in the field of lighting with promising achievements in a) design of new lighting prototypes, b) high lighting quality, c) easy and cheap manufacturing of materials and d) low electrical consumption.

1.2. Organic electronics for lighting applications

Electroluminescence (EL) from organic materials was first reported by A. Bernanose in 1953.[4-6] The process consisted in applying high voltage to organic fluorescent dyes. Afterwards, Helfrich and Pope[7,8] obtained EL in solid-state organic materials using anthracene and silver contact electrodes. Thick films of anthracence were used in these experiments and, as a result, the applied external voltages were very high (50-2000 V). The discovery of highly conductive organic materials by Heeger et al.[9] opened the way in the 1970s to the application of organic electronics in opto-electronic devices.

The continuous growth of the organic EL field led to the first Organic Light-Emitting Diode (OLED) in 1987.[10] This first OLED combined different hole- and electron-transport materials in a two-layer structure. The recombination occurred at the interface of the organic layers where electrons and holes meet forming excitons. In 1998, Baldo et al. incorporated in an OLED device a phosphorescent transition-metal complex (TMC) as the emitting active material[11], which strongly improved the efficiency of the device.

OLED technology has evolved reaching market-readiness in 2000. Currently, most mobile phones screens use OLED-based displays. The main strategy to reach this state has consisted in increasing the number of organic layers in the device, in order to separate the injection, transport and recombination processes (Figure 2). However, preparation of multilayer OLEDs requires thermal deposition techniques in high vacumm environment, which is undesirable for low cost manufacturing methods. Moreover, in order to get efficient electron injection, OLEDs require the use of low work function electrodes to generate an ohmic

contact. This feature increases the air sensitivity of OLEDs making rigorous encapsulation an absolute necessity. In this way, OLED technology leads to expensive prototypes for lighting applications at this moment and is not expected to have a high impact in energy saving.

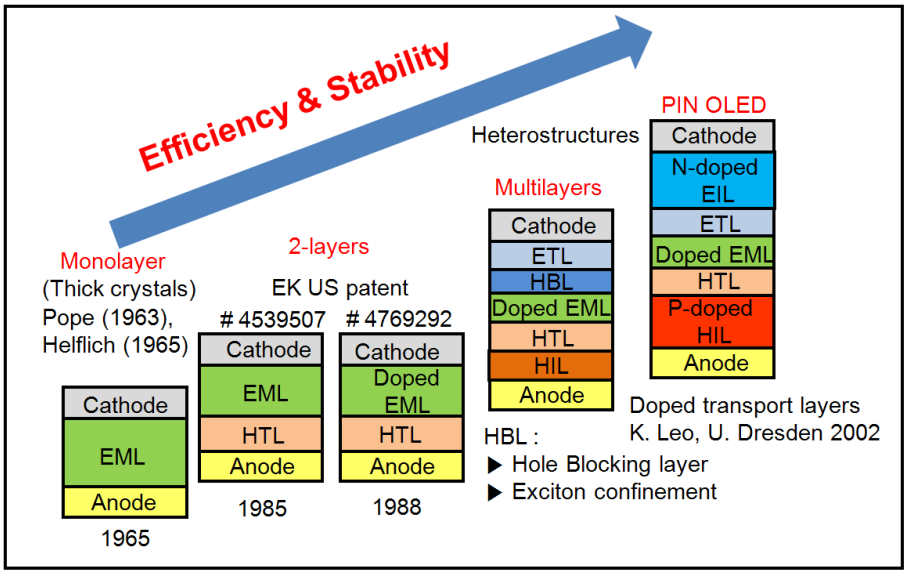

Figure 2. Evolution of OLED devices. From single layer to multilayer devices, performance increases with device complexity. (HIL: hole injection layer, HTL: hole transport layer, EML: emissive layer, HBL: hole blocking layer, ETL: electron transport layer). (Figure taken from ref. 12).

At this moment, there exists a simpler alternative for lighting applications: The light emitting devices called Light-Emitting Electrochemical Cells (LECs).

LECs have a much simpler architecture than OLEDs (Figure 3). They were first reported by Pei et al.[13] using as the electroluminescent material a fluorescent polymer mixed with an inorganic salt and an ionic conductive polymer, which were sandwiched between two electrodes in a single layer (p-LECs). Unlike OLEDs, LECs are: a) single-layer devices, b) compatible with air-stable electrodes like Au, Ag or Al and c) compatible with solution-processing techniques. The presence of ions in LECs plays a critical role in their operation mode. Under an applied bias,

the ions present in the active layer move toward the electrodes forming an ionic double-layer, which reduces the injection barrier for electrons and holes. This allows the use of a wide variety of electrodes, including air-stable electrodes.

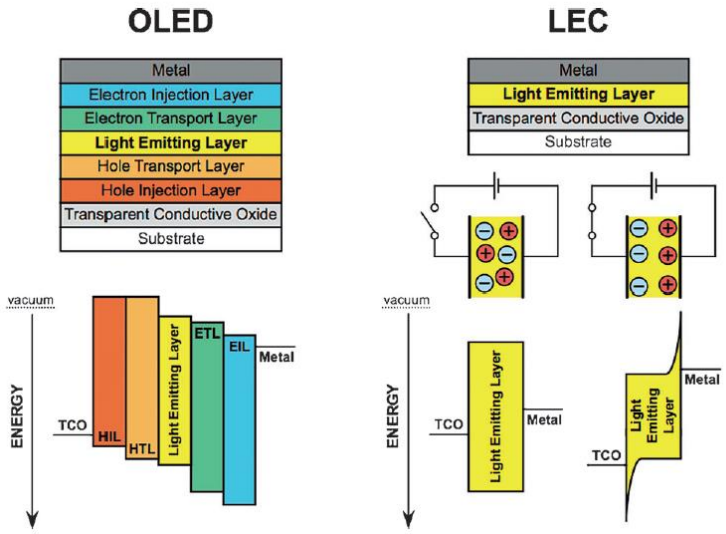

Figure 3. Schematic representation of a state-of-the-art OLED (left) and a state-of-the-art LEC (right). OLEDs require multiple layers, some of them processed by evaporation under high-vacuum conditions. Air-sensitive low work function metal or electron-injecting layers are needed for efficient charge carrier injection. LECs can be prepared from just a single active layer. The movement of the ions in the layer under an applied bias is the key to the LEC operation. [Figure taken from ref. 14].

The ionic nature of the active layer in LECs expanded the kind of organic materials with electronic properties suitable for the devices. Ionic Transition-Metal Complexes (iTMCs) are one type of intrinsic ionic materials with electron/hole transport properties, and luminescent properties. First examples of iTMC-LECs came soon after the emergence of p-LECs.[15-17] Both types of materials (polymers and iTMCs) lead to high performance devices.[14,18,19] However, iTMCs have a considerable advantage over polymers: iTMCs are phosphorescent emitters and,

therefore, can gather both singlet and triplets excitons for electroluminescence. In contrast, electroluminescence in p-LECs is restricted to singlet excitons, which leads to lower device efficiency.

1.3. Materials for Light-Emitting Electrochemical Cells

LECs are defined as light-emitting devices based on ionic materials. Hence, the presence of the adequate emitting material (neutral or ionic) and some ions (in case of neutral emitters) is required to prepare a LEC. Besides, the emitting layer should be able to: a) transport electrons and holes efficiently, and b) recombine electrons and holes forming excitons, which decay radiatively. On the one hand, transport of holes/electrons relies on the sequential oxidation/reduction of neighboring molecules. Therefore, the molecular redox states involved must be stable and reversible upon oxidation/reduction. On the other hand, the efficiency of the radiative process is mainly determined by the photoluminescent quantum yield (PLQY or ϕ_{PL}) of the material in a specific media, which is defined as the ratio of photons emitted by the number of absorbed photons in a photoluminescent process.

As we dicussed in seccion 1.2, p-LECs[20-28] and iTMC-LECs[29-37] have been widely studied. In this thesis, we only focus on iTMC-LECs, which from now will be simply referred to as LECs. The preparation of complexes derived from second- and third-row transition metal ions was found particularly attractive, because of their strong metal-ligand interaction and luminescent efficiencies.[38-41] The presence of heavy atoms in the complexes increases the spin-orbit coupling yielding an intersystem crossing from singlets to triplets. This results in a highly efficient phosphorescent emission, which makes them very interesting for electroluminescent applications.

There are examples of LECs based on Ru^{2+}, Os^{3+}, Ir^{3+} and Cu^{2+}.[42-45] However, only Ru- and Ir-iTMCs have been extensively explored, although the best performing LECs have been reached using iridium(III) complexes.[14,38] The effectiveness of the intersystem crossing increases

for iridium with respect to ruthenium because it is a heavier metal with a higher spin-orbit coupling.[46,47] In general, this fact leads to a better triplet harvesting of excitons and allows to achieve higher ϕ_{PL}.[46-48] Finally, iridium has the advantage of allowing the tunning of the color of emission by changing the ligands forming the iTMC.[14]

Ir-iTMCs consist of a combination of a neutral ligand (ancillary ligand), two negatively charged ligands (cyclometalating ligands) and the ion metal center. The total charge of the complex is +1. This positive charge is compensated by a counter-anion, which typically is PF_6 or BF_4. The role of the counter-anion is critical in the operation of the LEC,[39,49] as will be explained in section 1.4.

The ligands determine the luminescent properties of each complex. On the one hand, they determine the emission color of the complex, as the LUMO is often located on the ancillary ligand whereas the HOMO is normally located on the metal and the cyclometalating ligands (Figure 4). This particularity offers the possibility to tune the electroluminescence emission by modulating the energy of the HOMO-LUMO energy gap changing the chemical structure of the ligands. On the other hand, the presence of bulky substituent groups on the ligands increases the distance between neighboring molecules of the complex in the solid-state, and reduces the non-radiative pathways for the excitons. This leads to an increase of the ϕ_{PL} in the film, which if it is used in the appropriate way, contributes to increase the device efficiency.[50,51]

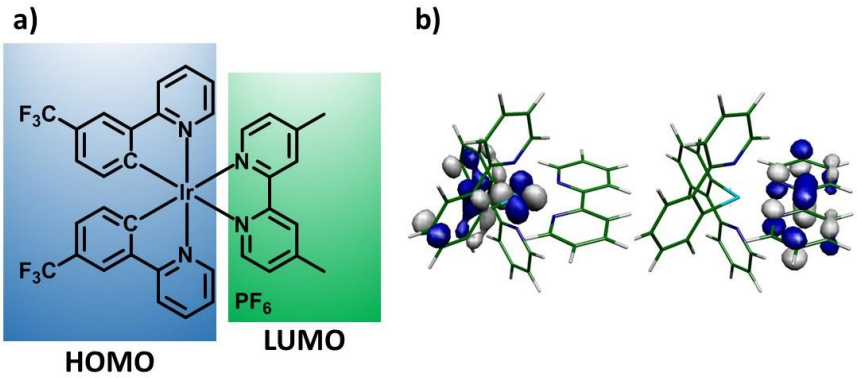

Figure 4. a) Schematic representation of the typical location of the Highest-Occupied Molecular Orbital (HOMO) and the lowest-unoccupied Molecular Orbital (LUMO) in a $[Ir(C\hat{}N)_2(N\hat{}N)]^+$ complex. b) Plot of the HOMO and LUMO obtained by theoretical calculations.

Recently, apart from iTMCs and polymers, small molecules (SMs) has emerged as a third group electroluminescent active materials in LECs.[52,53]

1.4. LECs operation mechanism

The performance of LECs is usually characterized by applying a constant voltage and monitoring the luminance and current density *versus* time (Figure 5).

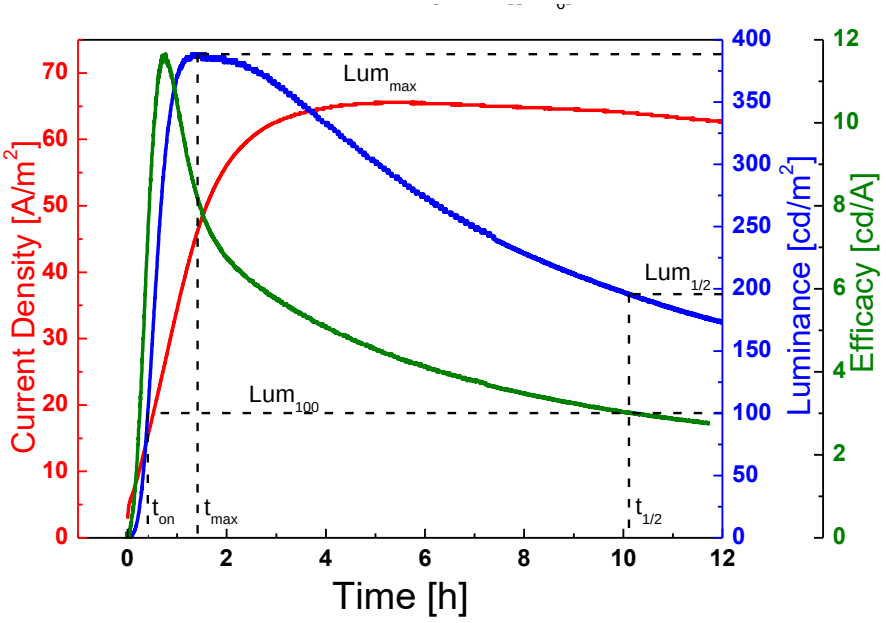

Figure 5. Time-dependent response of a LEC operated using constant voltage showing some of the most important figures of merit: luminance (blue), current density (red), efficacy (green), lifetime ($t_{1/2}$, 10.1 hours), turn-on time or time to reach a luminance of 100 cd/m^2 (t_{on}, 25 minutes) and time to reach the maximum luminance (t_{max}, 1.7 hours).

Under an applied voltage, at the initial state of the device, the system is not able to inject any electronic charge, because the injection happens from air-stable electrodes (high work function) to the LUMO or HOMO for electrons and holes, respectively. The difference between the energy of the frontier orbitals and the work function of the electrodes leads to a high-energy barrier to inject the charges. The situation changes *versus* time due to the movement of the ions present in the active layer, which migrate to the electrodes and facilitate the injection of both electronic charges in the material. Whereas electrons and holes are injected efficiently, the current going through the device slowly rises until a maximum is reached, and a quasi-simultaneously increase of the luminance is observed. The main characteristics for device evaluation will be further discussed in section 2.4.

The behavior described above about how LECs work is worldwide accepted. However, a controversial scientific debate regarding the detailed description of the operational mechanism has dominated the field for many years. In the late nineties, two models were proposed: a) the electrodynamical model[54-56] and b) the electrochemical model[13,57,58] (Figure 6).

The main difference between both models is that the electrodynamical model (ED) explains the charge injection by a decrease of the injection barrier due to the ion accumulation close to the electrode interface, which forms electric double-layers (EDLs). In contrast, the electrochemical model (ECD) describes the enhanced charge injection by the formation of doped regions (an oxidized or reduced molecule stabilized by an oppositely charged ion) adjacent to the electrodes after the EDLs formation. The propagation of the p- and n-doped regions reduces the intrinsic region in the center of the active layer where carriers recombine by exciton formation. As doping leads to an increase of conductivity, the voltage drops mostly over the non-doped intrinsic region. With operation time, the intrinsic region reduces leading to a larger voltage drop. Both models agree about ionic movement and their accumulation close to the electrodes thus generating EDLs, but they drastically differ in the profile of the potential across the active layer.

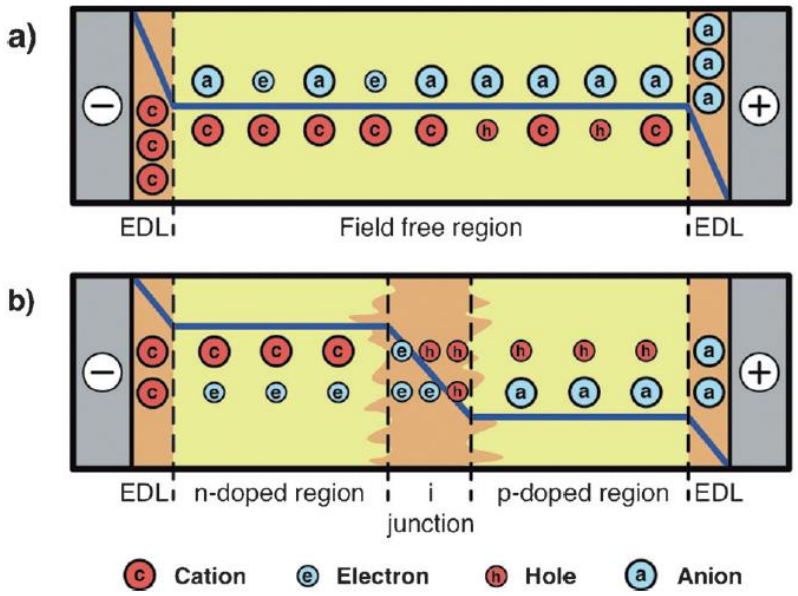

Figure 6. Schematic representation of (a) the electrodynamical model and (b) the electrochemical model during steady-state. The distribution of the electronic and ionic charges (see legend) as well as the potential profile (blue line) are represented. High- and low-field regions are highlighted in orange and light yellow color, respectively [Figure taken and adapted from ref. 14].

Experimental and theoretical works have alternatively supported the ED or the ECD mechanism.[59-64] van Reenen et al. and Lenes et al. found in 2010 [27,28,65] that depending on the electronic injection barrier either only the EDL is formed (supporting the ED model) or the electrochemical doping occurs (supporting the ECD model). These observations agreed with later proofs regarding the growing of the doped region carried out by Meier at al.[66,67] They showed that the ϕ_{PL} decreases reversibly *versus* time when the LEC is under operation. This implied that under normal operating conditions (at luminance levels of 10 cd·m^{-2}) the device operation is governed by the ECD model.

1.5. LECs: State of the art and limitations

For many years, LECs had significant limitations that prevented them to be considered for lighting systems. Three shortcomings were mainly considered: a) *turn-on* times above hours, b) low efficiencies and c) poor stabilities. Researchers from different groups have developed a wide range of strategies to solve these deficiencies. However, the combination of them is still not met.

Turn-on time and Lifetime: As the ionic movement is needed to allow the injection of electronic charges, the *turn-on time* is often large.[68,69] The turn-on time has been successfully reduced by: a) increasing the voltage applied to the LEC and b) adding ionic species with high mobility into the active layer in order to increase the ionic motion. However, both approaches lead to poor lifetimes due to a faster degradation and doping evolution of the active layer. In this way, a connection between the *turn-on time* and the device *lifetime* has been observed. Tordera et al. solved this undesired connection in 2012, by applying a pulsed current, which led to an instantaneous turn-on with a lifetime above 3000 hours.[70]

High Efficiencies and luminance levels: The device efficiency is mainly determinated by ϕ_{PL}, which depends both on the emitting iTMC and the composition of the active layer. The chemical design of iridium(III) complexes has allowed developing materials with ϕ_{PL} values above 70% using $[Ir(ppyF_2)_2(dtb\text{-}bpy)][PF_6]$ ($ppyF_2$ = (2-(2′,4′-difluorophenyl)pyridine and dtb-bpy = 4,4 ′- di-tert-butyl-2,2 ′-dipyridyl). Using this material an efficiency of 38 cd $A^{-1,}$ was achieved in a LEC.[71] This value was obtained by driving the LEC at a constant voltage of 3 V what results in a power efficiency of approximately 40 lm W^{-1}. This result is still far from the efficiencies reported for the current lighting technologies available (80-100 lm W^{-1} for LED lighting). In addition, the most efficient LECs have reached that value as a peak efficiency (Figure 5) and it is associated to luminance values that are too low for practical applications.[71-73] In this way, high efficiencies are usually linked to low luminances,[72-74] and are mostly reached at the initial stage of the LEC

operation when current density is still low and doping quenching is negligible.[31,66] For practical applications, high efficiency together with high luminance is desired during all the device operation. The best way to obtain this performance state has been reported for green LECs using pulsed current driving conditions, for which a maximum efficiency of 17.1 lm W^{-1} at luminances above 750 cd m^{-2} has been reached.[31]

In this way, pulsed current driving emerges as the best way to operate LECs in order to combine all the performance figures of merit in a unique device. However, in spite of all the achievements on this field during the last years, further research is still needed to introduce highly efficient LECs in lighting applications.

Color emission: Color emission mostly depends on the photophysical characteristics of the active material used to prepare the light-emitting device. LECs based on iridium complexes covering almost all the visible range have been created by combining the suitable ligands.[75] Nevertheless, only a few examples of blue emitting Ir-iTMCs have been successfully applied in LECs.[29,76-78] Other blue LECs employed conjugated polymers.[21,79] In both cases, the efficiencies and device lifetimes reached were insufficient for practical applications. Focussing on iridium complexes, the main difficulty lies in the red-shift usually observed in the EL spectrum compared to the PL spectrum.[77,80]

1.6. Aims

In this thesis we focused on the design and preparation of LEC devices in order to optimize their maximum efficiency by increasing the photoluminescence quantum yield. Three strategies were adopted to achieve this goal:

1) Chemical modification of the ancillary ligand.
2) The study of the effect of chloride impurities in LECs performance.
3) The use of host-guest systems.

2. Experimental & Methodology

2.1. Fabrication of LECs

Processing, preparation and subsequent characterization of the Light-Emitting Electrochemical Cells (LECs) devices were carried out in a class 10000 clean-room (Figure 7). The preparation of the devices consists of the following steps: a) cleaning of the substrates and coating of the layers, which were done inside the clean-room in atmospheric conditions, and b) evaporation of the cathode and characterization of the device, which were completed under inert conditions in a Braun glove box (< 0.1 ppm O_2 and H_2O).

Figure 7. MBraun glove box installed inside the clean-room at the Instituto de Ciencia Molecular (ICMol) of the Universidad de Valencia where all the devices were prepared and characterized.

The solvents were supplied by Aldrich (HPLC grade). 1-butyl-3-methyl imidazolium hexafluorophosphate [Bmim][PF_6] was obtained from Sigma-Aldrich (>98.5%). 2,7-Bis(diphenylphosphoryl)-9,9'-spirobifluorene (SPPO13) was purchased in Luminescent materials Corporation (Lumtec Corp. Taiwan). Cyanine dyes were supplied by Few Chemicals GmbH and poly(3,4-ethylenedioxythiophene) polystyrene sulfonate (PEDOT:PSS, CLEVIOS™ P VP AI 4083, aqueous dispersion, 1.3–1.7 %

solid content) was purchased from Heraeus. The rest of materials were synthetized in the group of Prof. Edwin C. Constable (University of Basel, Switzerland) or in the group of Prof. Mohammad K. Nazeeruddin (École Polytechnique Fédérale de Lausanne, Switzerland). Indium tin oxide ITO-coated glass plates (15 Ω $\square^{-1}$) were patterned by conventional photolithography (www.naranjosubstrates.com). The substrates were cleaned by 5-minute sonication steps in water-soap, water and 2-propanol baths, in that order. After drying, the substrates were placed in a UV-ozone cleaner (Jelight 42-220) for 20 minutes.

All the devices studied in this work have the stack architecture ITO/PEDOT:PSS/Active layer/Al shown in Figure 8. The composition of each active layer was varied depending on the purpose of the study.

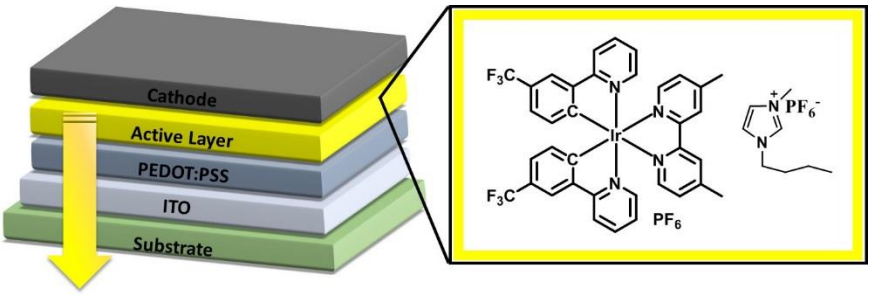

Figure 8. Left: device architecture of the LECs studied in this work. Right: chemical structure of one Ir-iTMC emitter and the ionic liquid [Bmim][PF_6] used in the active layer.

The devices were made as follows. First, a 80 nm layer of PEDOT:PSS was spin-coated on the ITO glass substrate. The purpose of this layer is to flatten the electrode, hence improving the reproducibility of the devices and preventing the formation of pinholes that can lead to shorts. Then, a transparent film composed of the active materials and the corresponding amount of [Bmim][PF_6] as ionic liquid (IL) were spin-coated from 20 to 30 mg mL^{-1} solutions. The IL was added to reduce the turn-on time and increases the performance of the devices. The devices were transferred to the inert atmosphere glove box. The LECs composed of iridium ionic transition-metal complexes (Ir-iTMCs)

were annealed at 100 ºC during a time of one hour. The aluminum electrode (70 nm) was thermally evaporated using a shadow mask under a vacuum ($<1 \times 10^{-6}$ mbar) with an Edwards Auto500 evaporator integrated in the glove box. The area of the cells was 6.5 mm^2. The devices were not encapsulated and were characterized inside the glove box at room temperature.

2.2. Thickness characterization of thin films.

In organic electronics, layer preparation from solution techniques forms amorphous thin films where accidental defects are usually present. The presence of defects as pin-holes creates ways where contact between the cathode and anode is easily reached. In consequence, the formation of short circuit or high leakage current could compromise the device effectiveness. By spin-coating, the layer quality is mainly governed by the solvent employed for the deposition, the concentration and solubility of the material. These parameters affect the morphology of the active layer as well as the thickness of the layer. For high soluble materials in common solvents, as Ir-iTMCs or ionic small molecules, the film formation leads to reproducible, good morphology and low defect concentration layers. In this case, the device preparation can be easily controlled by the thickness characterization. Prior to this thesis, it has been established that a minimum total stack of 150nm in needed to make reproducible devices, which concerns the PEDOT:PSS layer plus the active layer.

In this thesis, in order to guarantee the reproducibility of the study, the thickness of each deposited layer has been characterized by profilometer measurements (Ambios XP-1 profilometer) on control samples. These measurements allow us to optimize the spin-coating conditions (speed, solution concentration and solvent) in order to reach PEDOT:PSS layers with a controlled thickness of 80 nm and active layers with a thickness of 80− 150 nm. In this way, the two-layers stack reaches easily 200 nm, which is a sufficient thickness to make devices with low

leakage current and reasonable reproducibility. The thickness characterization of the deposited layers has been done complementarily by UV-Vis absorption using an Avantes Avaspec-2048 spectrometer as the absorption is proportional to the layer thickness.

2.3. Photoluminescence spectroscopy

In support of the electroluminescent properties of the materials in LECs, the photoluminescence (PL) properties of the complex used in the device and of the light-emitting layer containing the complex are crucial. Therefore, a photophysical study offers the possibility to evaluate the suitability of materials. This involves the determination of the PL spectrum and the PL quantum yield (ϕ_{PL}) in solution and in thin solid films. These characteristics are reflected in the electroluminescent properties of the device.

The PL spectrum gives the spectral region over which the complex emits when excited by light. The ϕ_{PL} is the relation between the emitted photons per photons absorbed by the emitter. It can be expressed in percentage or in a 0 to 1 scale, being 100% (or 1) a complete conversion of photons absorbed into photons emitted. For most iTMC emitters there is a direct relation between the ϕ_{PL} of the emitter and the electroluminescent efficiency in the device.[81] Particularly, since the emission of Ir-iTMCs arises from the triplet state and singlet excitons are efficiently converted into triplets, it has been shown that the external quantum efficiency (EQE) of a LEC device should be proportional to the solid-state ϕ_{PL} measured in thin films. Therefore, a preliminary photophysical characterization of the emitters in solid state allows to determine the maximum EQE that a LEC can achieve.

The PL spectrum and ϕ_{PL} were obtained by using a Hamamatsu C9920-02 Absolute PL Quantum Yield Measurement System. The system consists of an excitation light source (a xenon lamp linked to a monochromator), an integration sphere and a multi-channel spectrom-

eter. The PL in solution was measured on 10^{-5} M solutions of the emitter in solvents such as acetonitrile (CH_3CN) or dichloromethane (CH_2Cl_2). The solutions were previously degassed by bubbling argon for 10 minutes. The PL in thin film was measured in thin solid films using the device configuration, which consisted on a film of the complex mixed with the IL [Bmim][PF_6] in a 4 to 1 molar ratio. The films were spin-coated from solutions on quartz substrates.

2.4. Electroluminescent characterization of LECs

As we presented in chapter 1, LECs are usually operated by applying a constant voltage. Under these conditions, the behavior of LECs follows an increase of the current density and luminance vs time until a maximum value (Figure 5). The time scale observed such as the electroluminescent performance for each device differs depending on the ionic mobility, the active material, the electrodes used and the driving potential, among others. In order be able to make reliable comparisons between different devices, there are common parameters established as indicators of LECs behavior:

Electroluminescence Spectrum (EL spectrum): The EL spectrum gives information of the excited states of the active material involved in the emission and determines the color of the emitted light. The EL spectrum is a plot that results from measuring the intensity of radiation emitted by the device against the wavelength. The maximum emission peak of the EL spectrum is often reported and written as λ_{em}.

Luminance (Lum): The intensity of light measured per unit of surface (cd m^{-2}). It describes the quantity of light emitted by the device at a given moment.

Current Density: The intensity of current per unit of surface (A m^{-2}).

Voltage: The voltage applied to a device. For a pulsed driving scheme, the value is averaged over the on- and off-time of the pulse.

Lifetime ($t_{1/2}$): The time to reach half of the maximum luminance. It is the parameter most used to describe the stability of a LEC. Another parameter used to describe the stability that can be found in the literature is the total emitted energy (E_{tot}).[82]

Turn-on Time (t_{on}): The time needed to reach a determined value of luminance, usually 100 cd m^{-2} (Figure 5). Sometimes in the literature it is used as the time to reach maximum luminance, regardless of its value.

Current Efficiency: Often referred to as *Efficacy*, the flux in candelas per electrical ampere (cd A^{-1}). It is obtained by dividing the luminance by the current density.

Power Efficiency: The flux of light measured in lumens per electric watt (lm W^{-1}) measured by an integrated sphere or assuming lambertian emission by dividing the efficacy times π by the voltage. In case of pulsed-driven devices the duty cycle has to be taken into account as well.

External Quantum Efficiency (EQE): The ratio of photons emitted per injected electron in a given device. Theoretically it can be described by the following formula:

$$EQE = b\varphi/2n^2 \qquad (1)$$

where b is the recombination efficiency (equal to 1 for two ohmic contacts),[83] φ is the fraction of excitons that decay radiatively and n is the refractive index of the glass substrate which equals to 1.5. The factor $1/2n^2$ accounts for the coupling of light out of the device.

Commission Internationale de l'Eclairage coordinates (CIE coordinates): The maximum wavelength of the electroluminescent spectrum can only give a rough estimation of the true emission color, which depends on the specific bandwidth. To fully define a color, the sensitivity of the photoreceptors in the human eye has to be considered. For that, the CIE coordinates are used. The coordinates can be calculated from the electroluminescent spectrum and give an exact definition of the emission color according to universally accepted international

standards. The CIE coordinates are expressed (*x,y*) and are placed in a 2D plot (Figure 9) where the exact color point can be seen.

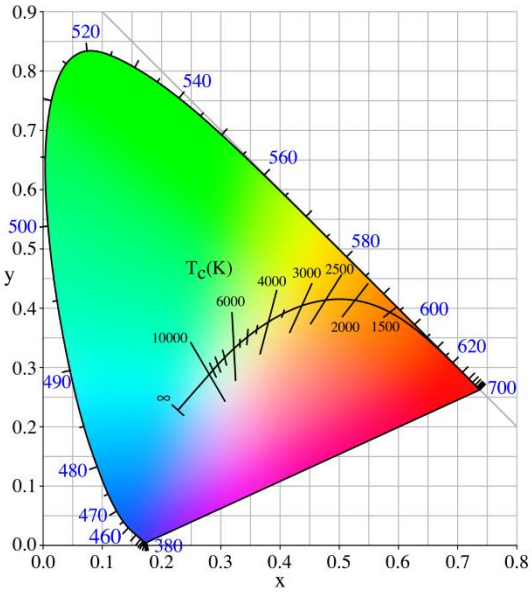

Figure 9. CIE coordinates plot. The color point of a given emitter is extracted from the electroluminescent spectrum and given as (*x,y*). The black curve shows the black body radiation.

The electrical and EL characterization of LECs was made as follows:

The electroluminescence spectra of the devices were measured by using an Avantes Avaspec-2048 luminance spectrometer.

The device lifetime was measured by applying a constant voltage or a pulsed current (block wave, 1000 Hz; duty cycle 50%) and monitoring the voltage, current and luminance by a True Colour Sensor MAZeT (MTCSiCT Sensor) with a Botest OLT OLED Lifetime-Test System. 3 V and 100 A m^{-2} were selected as standard driving conditions for constant voltage and pulsed current operation modes.

Radiance infrared measurements were obtained using an integrating sphere (UDT Instruments, model 2525LE) coupled to a Radiometric Sensor (UDT Instruments, model 247) and an optometer (UDT Instruments, model S370).

3. Improving LEC performance by chemical modification

3.1. Introduction

Recently, light-emitting electrochemical cells (LECs) with lifetimes exceeding 3000 hours have been demonstrated.[84] This breakthrough has been achieved by employing iridium ionic transition metal complexes (Ir-iTMCs) $[Ir(ppy)_2(pbpy)][PF_6]$ (ppy = phenylpyridine, pbpy = 6-phenyl-2,2′-bipyridine) that incorporates a phenyl pendant ring attached to the ancillary N^N ligand. The presence of this phenyl group induces the formation of a supramolecular-cage, due to π-π stacking interactions between the pendant phenyl ring and one coordinated phenylpyridine C^N ligand, that protects the complex from possible substitution with nucleophilic molecules.

Following the same strategy, several orange-emitting complexes have been developed.[51,84-87] However, besides the strong enhancement of the device lifetime, other device properties showed considerable limitations: i) the turn-on time (t_{on}) was, in general, long, ii) the maximum achievable luminance was rather low and iii) the corresponding efficiency was not constant over time. Specifically, the maximum efficiency using π-π stacking iTMCs was reported for the complex $[Ir(ppy)_2(C_{10}ppbpy)][PF_6]$ (C_{10}ppbypy = 4-(3,5-bis(decyloxy)phenyl)-6-phenyl-2,2′-bipyridine), which reached 15.3 lm W^{-1}, a maximum luminance of 284 cd m^{-2} and a lifetime ($t_{1/2}$) of 660 hours when operated at a constant voltage of 3 V.[51]

Another important breakthrough has been the introduction of pulsed current driving to operate a LEC which, when applied to devices using the above mentioned complex $[Ir(ppy)_2(C_{10}ppbpy)][PF_6]$, resulted in LECs with an instantaneous t_{on} and luminances above 600 cd m^{-2} during 550 hours.[70] The key aspect of this driving method is the stabilization of the doped zones, which form during device operation. However, with pulsed current driving, a much lower efficiency (1.8 lm W^{-1})[70] was achieved, when compared with the previous reported value (15.3 lm W^{-1}) using constant voltage driving.[51]

Due to the promising device performance of complexes using π-π stacking, research on these materials was continued with the aim of

increasing the efficiency of LECs, without sacrificing their lifetimes. In this perspective, the chemical modification of the ligand can again influence the device performance, mainly by varying the photoluminescence quantum efficiency (ϕ_{PL}) of the iTMC. One interesting approach consists in the use of bulky groups as spacers, which increase the distance between the emitters in the active layer reducing self-quenching processes.[51,88,89] This approach has been successfully used in Ir-iTMCs using remote functionalization, i.e. the insertion of groups at the periphery of the complex that do not strongly influence its electronic properties.

In this chapter, the evaluation in LECs of a series of iTMCs (Figure 10) with analogous chemical structures presenting intramolecular π-π stacking is discussed. The focus is on the enhancement of the ϕ_{PL} through two different strategies:

1) Remote functionalization of the ancillary ligand of the iTMC.
2) Substitution of the stacking group linked to the ancillary ligand of the iTMC.

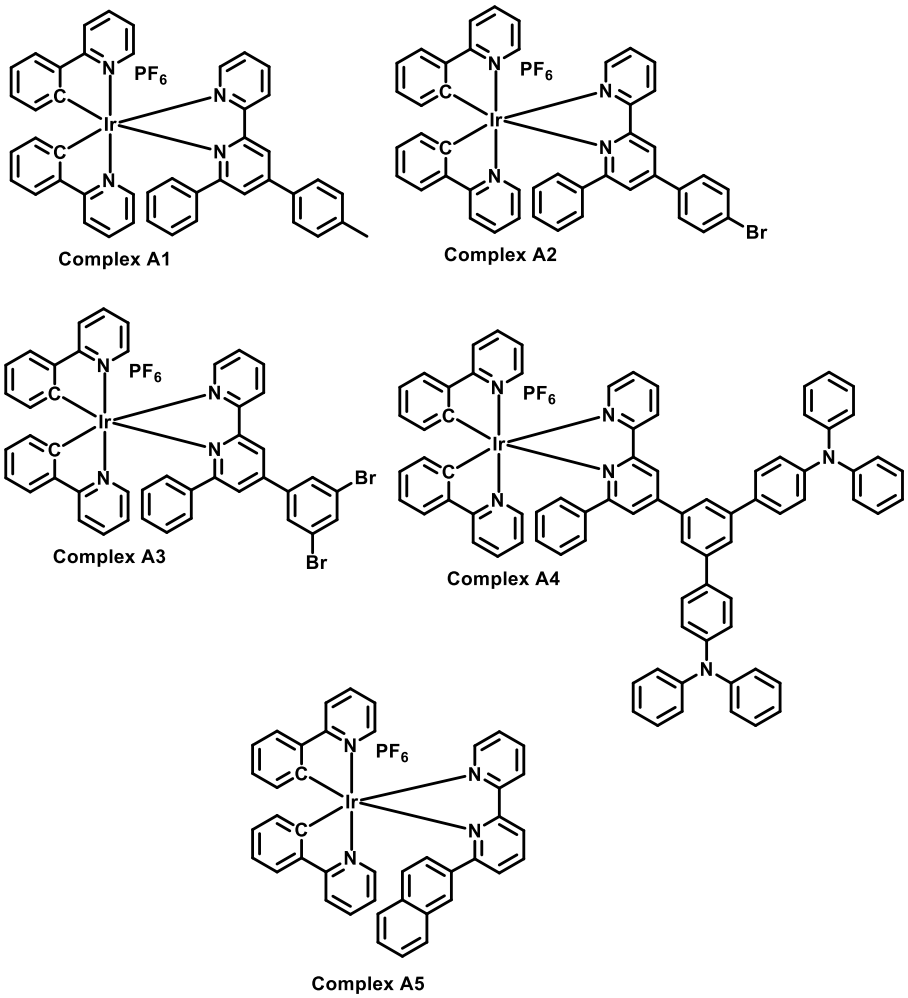

Figure 10. Chemical structure of the complexes evaluated in this chapter.

3.2. Results and discussion

The photophysical characterization of the iridium complexes **A1– A5** presented in Figure 10 consisted on the study of the photoluminescence (PL) spectrum and ϕ_{PL} both in solution and thin film (device configuration). PL data are summarized in Table 1.

Table 1. Photophysical properties of complexes **A1– A5**.

	Solution[a]		Thin film[b]	
Complex	λ_{max}^{PL} **[nm]**	ϕ_{PL} **[%]**	λ_{max}^{PL} **[nm]**	ϕ_{PL} **[%]**
A1	600	19.9	601	14.7
A2	608	14.0	608	11.4
A3	635	11.0	629	12.9
A4	604	5.2	604	7.8
A5	598	7.7	596	10.2

[a] Measured in deaered-dichloromethane 10^{-5}M solution using 320 nm as light source to excite the sample at room temperature. [b] Measured in a thin film composed with: iTMC:[Bmim][PF_6] 4:1 molar ratio using 320 nm as light source to excite the sample in atmosphere conditions.

All five complexes show similar orange-red emission spectrum in solution and thin film. The photophysical results obtained were rather surprising as they showed an unexpected trend in the ϕ_{PL}. By remote functionalization, the ϕ_{PL} in thin film was not severally affected, presenting values within 10.2% to 14.7%, except for complex **A4**, which showed a value of 7.8%. Hence, the presence of bulky substituents did not result in an improvement of the ϕ_{PL} compared to the archetype complex [Ir(ppy)$_2$(pbpy)][PF_6] (21.0%),[51] which bears a pendant phenyl group. In particular, complex **A4**, which is functionalized with the largest bulky substituent, showed the lowest ϕ_{PL}. Complex **A5**, which is modified by incorporating a naphthyl pendant as the stacking group, showed a ϕ_{PL} value (10.2%) that is only a half of that obtained for the [Ir(ppy)$_2$(pbpy)][PF_6] (21.0%).[51] An explanation for this unexpected result emerged from DFT calculations, which showed the existence of two low-lying triplet excited states close in energy but with different character (T_1 and T_2). T_1 has a mixed metal-to-ligand and ligand-to-ligand charge transfer (^{3}MLCT/^{3}LLCT) character, whereas T_2 involves electron excitations between molecular orbitals located on the pendant naphthyl group. It therefore has a ligand-centered (^{3}LC) character, which has no equivalent in analogous iTMCs lacking the naphthyl group.[68] The adiabatic energy difference between both triplet states was established to be 0.09 eV after full geometry relaxation, which is low enough to T_2

becomes competitive with the emissive triplet state T_1 during the population process and explains the relatively low ϕ_{PL} displayed by the complex.

All LECs prepared with iTMCs **A1– A5** were operated with a pulsed current driving regime using an average current density of 100 A m^{-2}. As previously mentioned, this driving method leads to faster t_{on} and better stabilities. Complex **A5** was further characterized through a range of different current densities (25 – 100 A m^{-2}). Additionally, LECs prepared using complex **A1** were driven using a constant voltage of 3 V, in order to evaluate how its performance is affected by the driving method. The performances of the LECs measured using a pulsed driving are summarized in Table 2. The device characteristics of complexes **A1** and **A5** are depicted, as representative examples, in Figure 11 and Figure 12, respectively.

Table 2. Performance of ITO/PEDOT:PSS/iTMC:[Bmim][PF_6] 4:1 molar ratio/Al LECs using a pulsed current driving of 100 A m^{-2} (1000 Hz, block wave and 50% duty cycle). [Bmim][PF_6] = 1-butyl-3-methylimidazolium hexafluorophosphate.

Complex	ϕ_{PL}[a] [%]	Lum_{max}[b] [cd m^{-2}]	PCE[c] [lm W^{-1}]	Efficacy[d] [cd A^{-1}]	$t_{1/2}$[e] [h]
A1	14.7	455	2.72	4.4	530
A2	11.4	115	0.33	1.1	8.3
A3	12.9	101	0.25	1.4	2.9
A4	7.8	83	0.25	0.8	250
A5	10.2	330	1.82	3.2	>3000

[a] Photoluminescent quantum yield in thin film using the device composition of the emissive layer. [b] Maximum luminance. [c] Maximum power conversion efficiency. [d] Maximum efficacy. [e] Lifetime evaluated as time to reach one-half of the maximum luminance.

All devices showed the typical LEC behavior for pulsed current driving: the luminance increases while voltage decreases *versus* time. Instead, when the LECs were operated using a constant voltage, both the luminance and current density increased with time due to the reduction of the injection barrier as consequence of the ionic movement. The LECs using **A5** will be discussed separately.

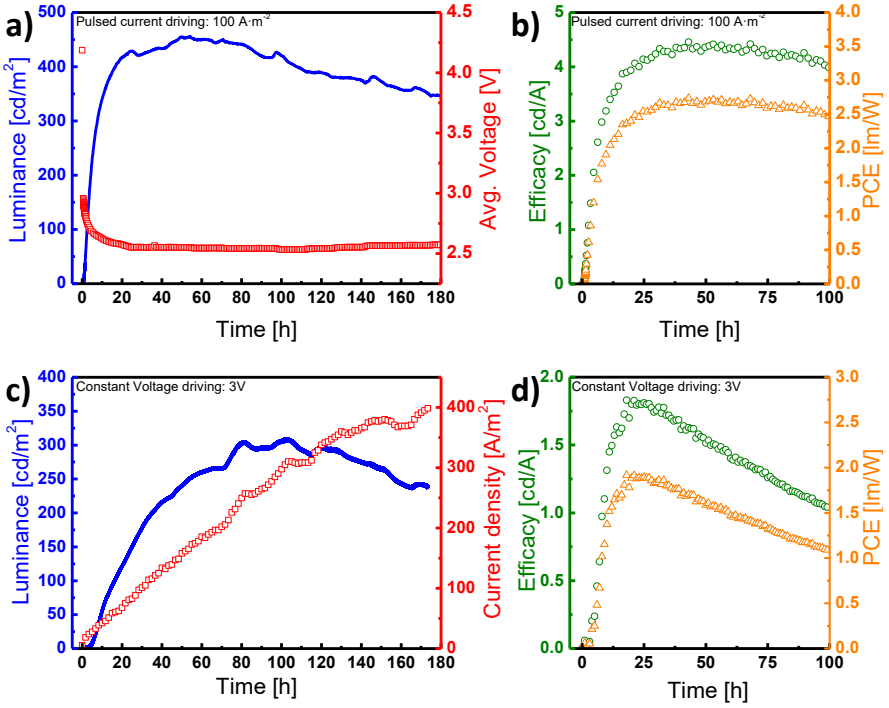

Figure 11. Performance for ITO/PEDOT:PSS/**A1**:[Bmim][PF_6] 4:1/Al LECs using either a pulsed current driving (a, b) of 100 A m^{-2} (1KHz, block wave and 50% duty cycle) or a constant voltage driving (c, d) of 3V. Luminance (solid line), average voltage or current density (open squares), efficacy (open circles) and power conversion efficiency (open triangles) are reported.

Remote functionalization has a large impact on the performance of LECs using iTMCs **A1** to **A4**. Devices using complexes **A2**, **A3** and **A4** showed low luminance (<100 cd m^{-2}) and efficiency (<1.2 cd A^{-1} or <1 lm W^{-1}), whereas LECs based on **A1** achieved luminance above 220 cd·m^{-2} ($Lum_{1/2}$) during 530 hours ($t_{1/2}$). The maximum efficacy achieved for all LECs is in agreement with the correspondent ϕ_{PL} trend, although a strong difference with respect to A1 was observed in spite of the small difference in the photophysical properties. This fact is rather surprising

since the complexes A1 and A2 differ only in the presence of the bromine atom (**A2**) instead of the methyl group (**A1**), suggesting that the lower performances should be related with the presence of the halogen, which is also true for complex **A3**. **A4** shows poor efficiencies in accordance with its rather low ϕ_{PL}. In agreement with ϕ_{PL} measurements, complex **A1** achieves the best efficiency (2.7 lm W^{-1}) using the pulsed current driving method. In contrast with what is usually observed for analogous π-π stacking complexes,[70] higher maximum efficiencies were obtained using a pulsed current driving mode than a constant voltage driving, what usually observed for analogous π-π stacking complexes.[70] Moreover, the presence of bromine in the ancillary ligand leads to unstable LECs, in spite of the presence of the π-π phenyl stacking group. Hence, complexes **A2** and **A3** showed a noticeable lifetime decay compared to analogous non-brominated complexes **A1** and **A4**.

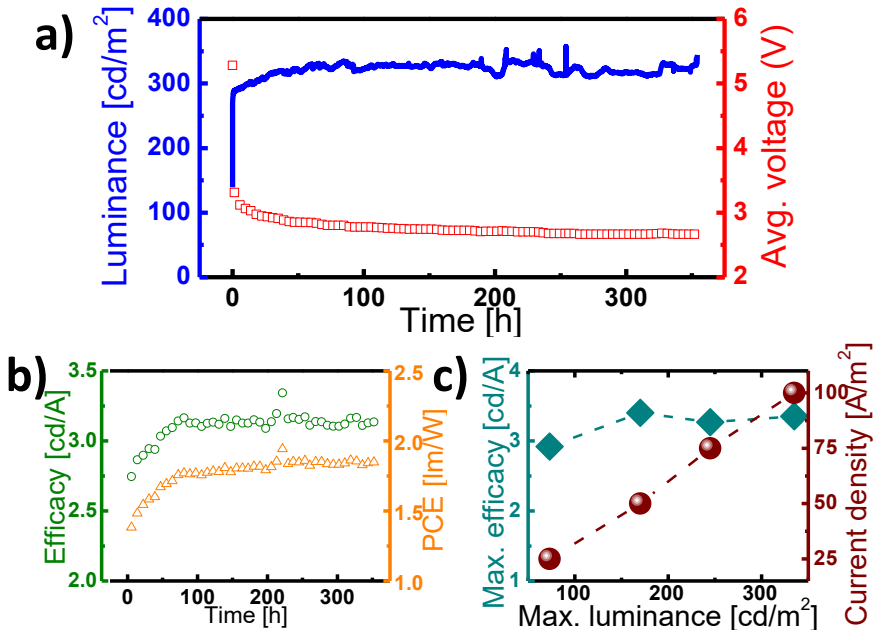

Figure 12. (a) Luminance (solid line) and average voltage (open squares) versus time for: ITO/PEDOT:PSS/**A5**:[Bmim][PF_6] 4:1/Al LECs using a pulsed current driving of 100 A m^{-2}. (b) Efficacy (open circles) and power conversion efficiency (open triangles) versus time for the same LEC. (c) Maximum efficacy (solid diamond) and current density needed (solid spheres) as function of the maximum luminance achieved.

Complex **A5** showed interesting features when incorporated in a LEC device. Using a pulsed current driving mode, LECs using **A5** showed: i) a fast t_{on} with an initial luminance above 100 cd m^{-2}, ii) a remarkable lifetime above 3000 hours, iii) high and stable efficiency compared to what obtained with similar complexes with higher ϕ_{PL}[51] and iv) a linear dependence of efficiency *versus* current density, which allows to tune the luminance of the LEC simply by changing the current density (Figure 12c).

3.3. Conclusions

Some conclusions can be drawn from the results reported in this chapter. First, the incorporation of bulky groups in the chemical structure of Ir-iTMCs show, in some cases, a detrimental effect on the ϕ_{PL} of Ir-iTMCs. As a matter of fact, the bulkiest complex (**A4**) showed unexpectedly low ϕ_{PL}. Furthermore, the ϕ_{PL} for the other four complexes was rather low. A thorough theoretical study has revealed the origin of the low ϕ_{PL} for complex **A5**, which is related with the presence of low-lying triplet states associated with the substituent. Moreover, the presence of bromine atoms was found to be detrimental for the device functioning, resulting in low device operation stability. In spite of the similar ϕ_{PL} measured for all the complexes, the performance of the LECs was found significantly different what demonstrated that the ϕ_{PL} is not the only parameter to take in account when designing iTMCs. Specifically, the LECs based on complexes **A4** and **A5** achieved interesting effiencies with respect to the reference $[Ir(ppy)_2(pbpy)][PF_6]$ under pulsed driving. Finally, LECs based on complex **A5** showed lifetimes above 3000 h, that are interesting for practical applications, and tunable luminance levels by changing the applied current, which can be an alternataive approach for more efficient systems.

3.4 – Contributions of the author

Article 1: ***Fine-tuning of photophysical and electronic properties of materials for photonic devices through remote functionalization.*** *European Journal of Inorganic Chemistry* **2012**, 3780-3788

Article 2: ***Bright and stable light-emitting electrochemical cells based on an intramolecularly .*** *Journal of Material Chemistry C* **2014**, *2*, 7047.

The following article has been deleted due to publisher copyright policy.

Bünzli, A. M., Bolink, H. J., Constable, E. C., Housecroft, C. E., Neuburger, M., Ortí, E., Pertegás, A. and Zampese, J. A. (2012), Fine-Tuning of Photophysical and Electronic Properties of Materials for Photonic Devices Through Remote Functionalization. Eur. J. Inorg. Chem., 2012: 3780–3788.

doi: 10.1002/ejic.201200394

The following article has been deleted due to publisher copyright policy.

Bünzli, A. M., Bolink, H. J., Constable, E. C., Housecroft, C. E., Neuburger, M., Ortí, E., Pertegás, A. and Zampese, J. A. (2012), Fine-Tuning of Photophysical and Electronic Properties of Materials for Photonic Devices Through Remote Functionalization. Eur. J. Inorg. Chem., 2012: 3780–3788.

doi: 10.1002/ejic.201200394

The following article has been deleted due to publisher copyright policy.

Bünzli, A. M., Bolink, H. J., Constable, E. C., Housecroft, C. E., Neuburger, M., Ortí, E., Pertegás, A. and Zampese, J. A. (2012), Fine-Tuning of Photophysical and Electronic Properties of Materials for Photonic Devices Through Remote Functionalization. Eur. J. Inorg. Chem., 2012: 3780–3788.

doi: 10.1002/ejic.201200394

The following article has been deleted due to publisher copyright policy.

Bünzli, A. M., Bolink, H. J., Constable, E. C., Housecroft, C. E., Neuburger, M., Ortí, E., Pertegás, A. and Zampese, J. A. (2012), Fine-Tuning of Photophysical and Electronic Properties of Materials for Photonic Devices Through Remote Functionalization. Eur. J. Inorg. Chem., 2012: 3780–3788.

doi: 10.1002/ejic.201200394

The following article has been deleted due to publisher copyright policy.

Bünzli, A. M., Bolink, H. J., Constable, E. C., Housecroft, C. E., Neuburger, M., Ortí, E., Pertegás, A. and Zampese, J. A. (2012), Fine-Tuning of Photophysical and Electronic Properties of Materials for Photonic Devices Through Remote Functionalization. Eur. J. Inorg. Chem., 2012: 3780–3788.

doi: 10.1002/ejic.201200394

The following article has been deleted due to publisher copyright policy.

Bünzli, A. M., Bolink, H. J., Constable, E. C., Housecroft, C. E., Neuburger, M., Ortí, E., Pertegás, A. and Zampese, J. A. (2012), Fine-Tuning of Photophysical and Electronic Properties of Materials for Photonic Devices Through Remote Functionalization. Eur. J. Inorg. Chem., 2012: 3780–3788.

doi: 10.1002/ejic.201200394

The following article has been deleted due to publisher copyright policy.

Bünzli, A. M., Bolink, H. J., Constable, E. C., Housecroft, C. E., Neuburger, M., Ortí, E., Pertegás, A. and Zampese, J. A. (2012), Fine-Tuning of Photophysical and Electronic Properties of Materials for Photonic Devices Through Remote Functionalization. Eur. J. Inorg. Chem., 2012: 3780–3788.

doi: 10.1002/ejic.201200394

The following article has been deleted due to publisher copyright policy.

Bünzli, A. M., Bolink, H. J., Constable, E. C., Housecroft, C. E., Neuburger, M., Ortí, E., Pertegás, A. and Zampese, J. A. (2012), Fine-Tuning of Photophysical and Electronic Properties of Materials for Photonic Devices Through Remote Functionalization. Eur. J. Inorg. Chem., 2012: 3780–3788.

doi: 10.1002/ejic.201200394

The following article has been deleted due to publisher copyright policy.

Bünzli, A. M., Bolink, H. J., Constable, E. C., Housecroft, C. E., Neuburger, M., Ortí, E., Pertegás, A. and Zampese, J. A. (2012), Fine-Tuning of Photophysical and Electronic Properties of Materials for Photonic Devices Through Remote Functionalization. Eur. J. Inorg. Chem., 2012: 3780–3788.

doi: 10.1002/ejic.201200394

Journal of Materials Chemistry C

PAPER

View Article Online
View Journal | View Issue

Cite this: *J. Mater. Chem. C*, 2014, **2**, 7047

Bright and stable light-emitting electrochemical cells based on an intramolecularly π-stacked, 2-naphthyl-substituted iridium complex†

Gabriel E. Schneider,[a] Antonio Pertegás,[b] Edwin C. Constable,[a] Catherine E. Housecroft,*[a] Nik Hostettler,[a] Collin D. Morris,[a] Jennifer A. Zampese,[a] Henk J. Bolink,[b] José M. Junquera-Hernández,[b] Enrique Ortí*[b] and Michele Sessolo[b]

Received 4th June 2014
Accepted 9th July 2014

DOI: 10.1039/c4tc01171f

www.rsc.org/MaterialsC

The synthesis and characterization of a new cationic bis-cyclometallated iridium(III) complex and its use in solid-state light-emitting electrochemical cells (LECs) are described. The complex $[Ir(ppy)_2(Naphbpy)][PF_6]$, where Hppy = 2-phenylpyridine and Naphbpy = 6-(2-naphthyl)-2,2′-bipyridine, incorporates a pendant 2-naphthyl unit that π-stacks face-to-face with the adjacent ppy^- ligand and acts as a peripheral bulky group. The complex presents a structureless emission centred around 595–600 nm both in solution and in thin film with relatively low photoluminescence quantum yields compared with analogous systems. Density functional theory calculations support the charge transfer character of the emitting triplet state and rationalize the low quantum yields in terms of a ligand-centred triplet localized on the 2-naphthyl unit that lies close in energy to the emitting state. LECs incorporating the $[Ir(ppy)_2(Naphbpy)][PF_6]$ complex as the electroluminescent material are driven using a pulsed current operation mode and show high luminance, exceeding 300 cd m^{-2}, and exceptional stabilities.

Introduction

The successful market entry of displays based on organic light-emitting diodes (OLEDs) testifies the maturity of the technology in terms of both stability and efficiency. The latter is achieved through the use of different materials designed to comply with specific functions, such as hole/electron injection and transport, exciton formation and light emission.[1–3] These materials are stacked in multilayer structures obtained through vacuum deposition, and use low work function cathodes that have to be protected from the environment through rigorous encapsulation to avoid fast degradation.[4] The corresponding costs are compatible with the display market but need to be substantially reduced for lighting applications. For this reason, simple solution-processed OLEDs are still the focus of considerable attention.[5–7] Light-emitting electrochemical cells (LECs) are also solution processed and consist of a single electroactive layer of an ionic organic semiconductor placed between two electrodes.[8] The high concentration of ions assists both charge injection and transport, allowing the use of stable metal electrodes and thus paving the way to a new generation of low-cost lighting sources.[9,10]

Ionic transition-metal complexes (iTMCs) are among the most studied active species for LECs.[11] They exhibit high photoluminescence quantum yield (PLQY) and the emission can be easily tuned through ligand design. iTMCs can be deposited as pure layers in electroluminescent devices since the complex by itself assists charge injection and transport and is the active luminescent species.[12] The simplest LEC consists of a single active layer composed entirely of an iTMC balanced by small mobile counter anions such as $[PF_6]^-$ or $[BF_4]^-$.

Cationic heteroleptic iridium(III) complexes with the structure $[Ir(C^N)_2(N^N)]^+$, where C^N is an anionic cyclometallated ligand and N^N a neutral diimine ancillary ligand, represent the most promising candidates for long-living, stable LECs. While the optoelectronic properties can be directly tuned by varying the type of ligands and the electron affinity of their substituents, the performances in devices (*i.e.*, the stability, efficiency and turn-on time) cannot be straightforwardly predicted. Some trends, however, exist and a few general design rules have been proposed. The introduction of bulky substituents on the periphery of the iTMC allows for an increased spatial separation between the emissive centers in a pure film and thereby for a reduction of the exciton quenching.[13,14] This effect enhances the PLQY of the film and therefore the overall device efficiency. On

[a]*Department of Chemistry, University of Basel, Spitalstrasse 51, CH–4056 Basel, Switzerland. E-mail: catherine.housecroft@unibas.ch*

[b]*Instituto de Ciencia Molecular, Universidad de Valencia, ES–46980 Paterna, Valencia, Spain. E-mail: enrique.orti@uv.es*

† Electronic supplementary information (ESI) available: Fig. S1 CV of $[Ir(ppy)_2(Naphbpy)][PF_6]$; Table S1 experimental and calculated bond parameters of $[Ir(ppy)_2(Naphbpy)]^+$; Fig. S2 optimized structure of the transition state connecting conformers 1 and 2; Fig. S3 optimized bond lengths calculated for the pendant 2-naphthyl group. CCDC 972526. For ESI and crystallographic data in CIF or other electronic format see DOI: 10.1039/c4tc01171f

the other hand, the device lifetime has been correlated with the reactivity of the complex in the excited state, where nucleophilic molecules are able to react with the iTMCs leading to the formation of quenching species and to fast device degradation.[15,16] This phenomena can be limited by introducing intramolecular π–π interactions within the ligands, which close the structure of the complex and protect the metal center from nucleophilic substitution with water or residual solvent molecules in the film.[17] An illustrative example is the incorporation of a pendant phenyl ring adjacent to one N-donor of the chelating N^N ligand, which results in a face-to-face π-stacking with one of the cyclometallating C^N ligands.[18] This structural feature has an enormous impact on the device lifetime, which increases from a few hours to several months. The control of both inter- and intramolecular interactions in iTMCs has led to a new generation of LECs with enhanced lifetime and efficiency, with potential practical application in solid-state lighting.[19]

Within this perspective, we have synthesized and characterized the hexafluoridophosphate $[PF_6]^-$ salt of a heteroleptic iridium(III) complex with the formula $[Ir(ppy)_2(Naphbpy)][PF_6]$, where Hppy is 2-phenylpyridine and Naphbpy is the 6-(2-naphthyl)-2,2′-bipyridine ancillary ligand. The purpose of the 2-naphthyl substituent on the bpy ligand is twofold: (i) to π-stack with the ppy^- ligands, stabilizing the geometry of the complex in the excited state, and (ii) to act as a bulky group on the periphery of the complex thus reducing the intermolecular interactions. The $[Ir(ppy)_2(Naphbpy)][PF_6]$ complex was used to prepare single-layer LECs and its structural features resulted in a high device stability and efficiency.

Experimental section

General

A Bruker Avance III-500 NMR spectrometer was used to record ^1H and ^{13}C NMR spectra; chemical shifts are referenced to residual solvent peaks with respect to δ(TMS) = 0 ppm. Electrospray ionization (ESI) mass spectra were recorded using a Bruker esquire 3000^{plus} instrument. Solution electronic absorption spectra were recorded on an Agilent 8453 spectrophotometer, emission spectra using a Shimadzu RF-5301 PC spectrofluorometer and FT-IR spectra with a Shimadzu 8400S instrument with Golden Gate accessory (solid samples). Solution quantum yields were measured using a Hamamatsu absolute PL quantum yield spectrometer C11347 Quantaurus-QY, and lifetimes were measured using a Hamamatsu Compact Fluorescence Lifetime Spectrometer C11367 Quantaurus-Tau; an LED light source with excitation wavelength of 280 nm was used. Microwave reactions were carried out in a Biotage Initiator 8 reactor.

Electrochemical measurements were recorded using a CH Instruments 900B potentiostat using glassy carbon, a platinum wire and a silver wire as the working, counter and reference electrodes, respectively. Samples were dissolved in HPLC grade MeCN ($\approx 10^{-4}$ mol dm^{-3}) containing 0.1 mol dm^{-3} [^{n}Bu$_4$N][PF$_6$] as the supporting electrolyte; all solutions were degassed with argon. Cp_2Fe was used as an internal reference.

1-(2-Naphthyl)-3-dimethylamino propan-1-one was prepared according to a literature method.[20]

6-(2-Naphthyl)-2,2′-bipyridine (Naphbpy)

The synthesis of Naphbpy has previously been described.[21] However, we find the following method convenient although the yield is lower than that reported. 1-(2-Naphthyl)-3-dimethylaminopropan-1-one (425 mg, 1.61 mmol), 1-(2-oxo-2-(2-pyridyl) ethyl)pyridine-1-ium iodide (525 mg, 1.61 mmol) and NH_4OAc (10 eq.) were combined in EtOH (20 mL) and the mixture was heated overnight at reflux. The resulting brown oily liquid was reduced in volume, dissolved in water and extracted into CH_2Cl_2 (3 × 25 mL). The organic solvent was evaporated and the crude material was purified twice by column chromatography (silica, CH_2Cl_2 changing to CH_2Cl_2 : MeOH 100 : 1.5 and CH_2Cl_2 : MeOH 100 : 0.5). Naphbpy was isolated as a white solid (65.1 mg, 0.231 mmol, 14.3%). The ^1H NMR spectrum has previously been reported in DMSO-d_6.[21] ^1H NMR (500 MHz, CD_2Cl_2, 295 K, atom labelling as in Scheme 1) δ/ppm 8.71 (m, 2H, H^{E3+E6}), 8.64 (d, J = 1.2 Hz, 1H, H^{G1}), 8.42 (dd, J = 6.5, 2.3 Hz, 1H, H^{F3}), 8.36 (dd, J = 8.6, 1.8 Hz, 1H, H^{G3}), 8.04–7.88 (overlapping m, 6H, $H^{E4+F4+F5+G4+G5+G8}$), 7.54 (m, 2H, H^{G6+G7}), 7.37 (ddd, J = 7.5, 4.7, 1.2 Hz, 1H, H^{E5}). $^{13}C\{^1H\}$ NMR (126 MHz, CD_2Cl_2, 295 K) δ/ppm 156.6 (C^{E2}), 156.4 (C^{F6}), 156.2 (C^{F2}), 149.6 (C^{E6}), 138.3 (C^{F4}), 137.2 (C^{E4}), 136.8 ($C^{G4a+G8a}$), 134.0 (C^{G2}), 128.9 (C^{G8}), 128.1 (C^{G4+G5}), 126.9 (C^{G6+G7}), 125.1 (C^{G3}), 124.3 (C^{E5}), 121.5 (C^{E3}), 120.9 (C^{F5}).

[Ir(ppy)$_2$(Naphbpy)][PF$_6$]

A yellow suspension of $[Ir_2(ppy)_4(\mu\text{-}Cl)_2]$ (107 mg, 0.100 mmol) and Naphbpy (56.8 mg, 0.201 mmol) in MeOH (15 mL) was heated in a microwave reactor at 120 °C for 2 h (P = 8 bar). The yellow solution was allowed to cool to room temperature, and then an excess of NH_4PF_6 (326 mg, 2.00 mmol) was added. The mixture was stirred for 30 min at room temperature and then evaporated to dryness. The crude yellow material was purified twice by column chromatography (Fluka Silica 60; CH_2Cl_2 changing to CH_2Cl_2 : MeOH 100 : 2). $[Ir(ppy)_2(Naphbpy)][PF_6]$ was isolated as a yellow solid (92.3 mg, 0.099 mmol, 49.6%). Addition of $[Bu_4N][PF_6]$ to a CD_2Cl_2 solution of the complex resulted in no shift of the signals arising from protons H^{E3} and H^{F3} confirming the lack of chloride impurity.[22] ^1H NMR (500 MHz, CD_2Cl_2, 295 K) δ/ppm 8.56 (dd, J = 8.1, 1.3 Hz, 1H, H^{F3}), 8.52 (d, J = 8.2 Hz, 1H, H^{F3}), 8.26 (t, J = 7.9 Hz, 1H, H^{F4}), 8.12 (m, 1H, H^{E4}), 7.91 (m, 1H, H^{E6}) overlapping with 7.88

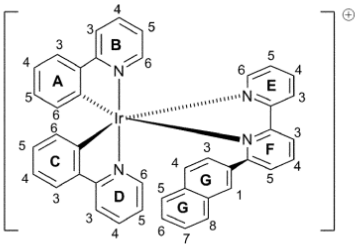

Scheme 1 Structure of the $[Ir(ppy)_2(Naphbpy)]^+$ cation and atom numbering for NMR assignments.

(m, 1H, $H^{B4/D4}$), 7.80 (m, 1H, $H^{B3/D3}$) overlapping with 7.77 (m, 1H, $H^{B4/D4}$), 7.73 (d, J = 5.7 Hz, 1H, H^{D6}), 7.66 (br, H^{D3}) overlapping with 7.64 (dd, J = 7.8, 1.2 Hz, 1H, H^{G7}), 7.60 (dd, J = 7.7, 1.2 Hz, 1H, H^{F5}), 7.50 (dd, J = 7.7, 1.4 Hz, 1H, H^{A3}), 7.48–7.37 (overlapping m, 3H, $H^{B6+E5+G6}$), 7.32 (v. br, $H^{G1/G3/G4/G5/G8}$), 7.23 (v. br, $H^{G1/G3/G4/G5/G8}$), 7.11 (m, 1H, $H^{B5/D5}$), 7.08 (m, 1H, $H^{B5/D5}$), 6.92 (m, 1H, H^{A4}), 6.78 (m, 1H, H^{A5}), 6.53 (v. br, H^{C3}), 6.03 (v. br, H^{C5}), 5.98 (br t, J = 7.5 Hz, 1H, H^{C4}), 5.89 (m, 1H, H^{A6}), 5.49 (br d, 1H, H^{C6}); not all signals for $H^{G1/G3/G4/G5/G8}$ observed. ^{13}C NMR (126 MHz, CD_2Cl_2, 295 K) δ/ppm 169.1 (C^{D2}), 167.5 (C^{B2}), 166.2 (C^{F6}), 157.2 (C^{E2}), 150.8 (C^{E6}), 149.3 ($C^{B6/D6}$), 149.2 ($C^{B6/D6}$), 146.9 (C^{A1}), 143.3 (C^{A2}), 140.0 (C^{F4}), 139.7 (C^{E4}), 138.6 ($C^{B4/D4}$), 138.3 ($C^{B4/D4}$), 131.2 (C^{C6}), 131.1 (C^{A5}), 130.5 (C^{A6}), 130.4 (C^{F5}), 128.1 (C^{E5}), 127.9 (C^{G7}), 127.0 (C^{G6}), 125.4 (C^{E3}), 125.0 (C^{A3}), 123.7 ($C^{B5/D5}$), 124.0 (C^{F3}), 123.1 (C^{A4}), 122.7 ($C^{B5/D5}$), 120.5 (C^{C4}), 120.4 ($C^{B3/D3}$), 120.2 ($C^{B3/D3}$); $C^{C1/C2/C3/C5/G1/G2/G3/G4G4a/G5/G8/G8a}$ not resolved. IR (solid, ν/cm^{-1}) 3998 (m), 3043 (w), 1667 (w), 1607 (s), 1582 (m), 1558 (m), 1551 (m), 1477 (s), 1447 (m), 1440 (m), 1419 (m), 1317 (w), 1269 (w), 1230 (m), 1164 (m), 1161 (m), 1124 (w), 1063 (w), 1031 (m), 1010 (w), 949 (w), 885 (w), 830 (s), 777 (m), 754 (s), 746 (s), 735 (s), 728 (s), 697 (w), 668 (m), 631 (m), 603 (s). ESI-MS m/z 783.2 $[M - PF_6]^+$ (calc. 783.2). UV-Vis λ/nm (ε/dm^3 mol^{-1} cm^{-1}) (CH_2Cl_2, 1.00 × 10^{-5} mol dm^{-3}) 271 (44200), 313 (22100, sh), 387 (4800). Emission (CH_2Cl_2, 1.00 × 10^{-5} mol dm^{-3}, λ_{ex} = 275 nm) λ_{em} = 598 nm. Found: C 53.96, H 3.39, N 6.44; $C_{42}H_{30}IrN_4PF_6$ requires C 54.37, H 3.26, N 6.04%.

Crystallography

Data were collected on a Bruker-Nonius KappaAPEX diffractometer with data reduction, solution and refinement using APEX2[23] and SHELXL97.[24] The ORTEP-style diagram was generated using Mercury v. 3.0, and this program was also used for structural analysis.[25,26]

[Ir(ppy)$_2$(Naphbpy)][PF$_6$]

$C_{42}H_{30}F_2IrN_4P$, M = 927.89, yellow block, orthorhombic, space group $Ccca$, a = 23.8655(10), b = 34.2298(10), c = 17.5645(5) Å, U = 14348.6(8) Å^3, Z = 16, D_c = 1.718 Mg m^{-3}, μ(Cu-Kα) = 8.224 mm^{-1}, T = 123 K. Total 108787 reflections, 6518 unique, R_{int} = 0.0482. Refinement of 5227 reflections (510 parameters) with $I > 2\sigma(I)$ converged at final R_1 = 0.0439 (R_1 all data = 0.0556), wR_2 = 0.1084 (wR_2 all data = 0.1222), gof = 1.083, CCDC 972526.†

Computational details

Density functional calculations (DFT) were carried out with the D.01 revision of the Gaussian 09 program package[27] using Becke's three-parameter B3LYP exchange-correlation functional[28,29] together with the 6-31G** basis set for C, H, and N,[30] and the "double-ζ" quality LANL2DZ basis set for the Ir element.[31] The geometries of the singlet ground state and of the lowest-energy triplet states were fully optimized without imposing any symmetry restriction. All the calculations were performed in the presence of the solvent (CH_2Cl_2). Solvent effects were considered within the self-consistent reaction field (SCRF) theory using the polarized continuum model (PCM) approach.[32–34] Time-dependent DFT (TD-DFT) calculations of the lowest-lying 20 triplets were performed in the presence of the solvent at the minimum-energy geometry optimized for the ground state. The geometries of the two lowest-energy triplets (T_1 and T_2) were first optimized at the spin-unrestricted UB3LYP level and afterwards reoptimized at the more accurate TD-DFT level.

Results and discussion

Synthesis and single crystal structure of [Ir(ppy)$_2$(Naphbpy)][PF$_6$]

The ligand Naphbpy was prepared by Kröhnke methodology,[35] rather than by the Jameson literature procedure.[21] [Ir(ppy)$_2$(Naphbpy)][PF$_6$] was prepared using the proven methodology of treating the [Ir$_2$(ppy)$_4$(μ-Cl)$_2$] dimer with two equivalents of Naphbpy.[36] After work-up, [Ir(ppy)$_2$(Naphbpy)][PF$_6$] was isolated in 49.6% yield. The base peak in the electrospray mass spectrum (m/z 783.2) arose from the $[M - PF_6]^+$ ion, and exhibited the characteristic isotope pattern of iridium. Single crystals of [Ir(ppy)$_2$(Naphbpy)][PF$_6$] grew upon slow evaporation of solvent from a CH_2Cl_2 solution of the compound. The complex crystallizes in the orthorhombic space group $Ccca$ and the structure of the Λ-[Ir(ppy)$_2$(Naphbpy)]$^+$ ion present in the asymmetric unit is shown in Fig. 1. The chirality arises from the presence of the three chelating ligands bound to the octahedral Ir1 atom, and both enantiomers are present in the lattice. As is typical of a [Ir(C^N)$_2$(N^N)]$^+$ complex, the N-donors of the two cyclometalled ppy$^-$ ligands are *trans* to one another. Each ppy$^-$ ligand is close to planar (angles between the least squares planes of the phenyl and pyridine rings are 4.2 and 7.0°). The bpy domain is distorted (angle between the two pyridine rings = 18.5°) and the 2-naphthyl unit is twisted through 60.3° with respect to the pyridine ring to which it is connected. The

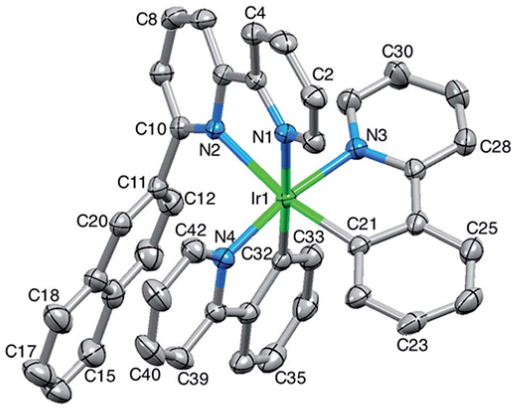

Fig. 1 Structure of the Λ-[Ir(ppy)$_2$(Naphbpy)]$^+$ cation in [Ir(ppy)$_2$(Naphbpy)][PF$_6$] (ellipsoids plotted at 30% probability level and H atoms omitted). Selected bond parameters: Ir1–C21 = 2.007(6), Ir1–C32 = 2.019(6), Ir1–N4 = 2.037(5), Ir1–N3 = 2.064(5), Ir1–N1 = 2.150(5), Ir1–N2 = 2.215(5) Å; N1–Ir1–N2 = 75.60(18), C21–Ir1–N3 = 79.9(2), C32–Ir1–N4 = 80.4(2)°.

deformation is associated with a face-to-face π-interaction between the 2-naphthyl unit and the phenyl ring of one of the cyclometallated ligands (Fig. 2).

Dynamic behaviour of $[Ir(ppy)_2(Naphbpy)]^+$ in solution

In $[Ir(C^N)_2(N^N)]^+$ derivatives in which the N^N ligand is a 6-phenyl-substituted bipyridine (Phbpy), the phenyl group undergoes hindered rotation at room temperature on the NMR timescale.[37–40] In these complexes, the ^{1}H NMR spectra at 295 K show broad signals only for the *ortho*- and *meta*-protons of the 6-phenyl substituent and, upon cooling, only these signals are affected. At 295 K, the ^{1}H NMR spectrum of a CD_2Cl_2 solution of $[Ir(ppy)_2(Naphbpy)][PF_6]$ exhibits very broad signals for the 2-naphthyl protons (not all are observed) and broadened signals for the protons of the orthometallated ring C (top spectrum in Fig. 3). This is consistent with dynamic behaviour involving the ring C and G domains (see Scheme 1 for ring labels). Rings C and G correspond to those involved in the intra-cation face-to-face π-stacking (Fig. 1 and 2), and their resonances for most of the ^{13}C nuclei are not resolved in the ^{13}C NMR spectrum at 295 K, but are resolved at 210 K. In contrast, at 295 K, the signals for protons in the bipyridine (rings E and F) and phenylpyridine rings A, B and D are well resolved.

On cooling from 295 K to 210 K, signals for the protons in bpy rings E and F and orthometallated ring A remain largely unaffected, with the exception of the effects of signal overlap (Fig. 3). The broad signals for orthometallated ring C are resolved at 210 K into two sets of signals with relative integrals 2 : 1. This is illustrated in Fig. 4; the signal for the minor component of H^{C6} coincides with the signal at δ 5.32 ppm for residual $CDHCl_2$. Fig. 3 reveals that the two multiplets for H^{B5} and H^{D5} initially broaden upon cooling. Analysis of the COSY, HMQC and HMBC spectra recorded at 295 K and 210 K reveals that each of the signals for H^{B6}, H^{D6} and H^{D3} splits into two doublets (relative integrals 2 : 1).

The spectroscopic data are consistent with the $[Ir(ppy)_2(Naphbpy)]^+$ cation existing in two conformations at low temperature by virtue of the position of the 2-naphthyl substituent with respect to the cyclometallated ring C. The 2D VT-NMR spectra were not consistent with rotation of the 2-naphthyl group, and we propose that the dynamic behaviour involves a change in conformation by internal rotation of the bpy ligand. Conformer 1 in Fig. 5a corresponds to the crystallographically determined structure, with the 2-naphthyl unit (rings G) lying over the cyclometallated ring C. Twisting around the inter-ring bond of the bpy ligand generates conformer 2 in which the 2-naphthyl unit retains the stacking interaction over ring C but adopts a different relative π-stacked arrangement. Fig. 5b shows the optimized geometry calculated for conformer 2 using DFT calculations (see below).

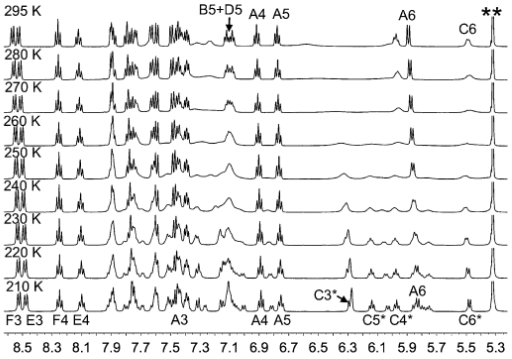

Fig. 3 Variable temperature ^{1}H NMR (500 MHz, CD_2Cl_2) spectra of $[Ir(ppy)_2(Naphbpy)][PF_6]$ (** = residual $CDHCl_2$). See Scheme 1 and Fig. 5 for atom labelling. Chemical shifts in ∂/ppm.

Electrochemical and photophysical properties

The electrochemical behaviour of $[Ir(ppy)_2(Naphbpy)][PF_6]$ in CH_2Cl_2 solution was investigated by cyclic voltammetry. A quasi-reversible oxidation, assigned to an iridium-centred process, occurs at +0.83 V (with respect to Fc/Fc^+), which is similar to those reported for $[Ir(ppy)_2(bpy)][PF_6]$ (+0.84 V)[39] and $[Ir(ppy)_2(Phbpy)][PF_6]$ (+0.81 V)[14] in DMF. A second unidentified species is observed after oxidation of the metal complex, the

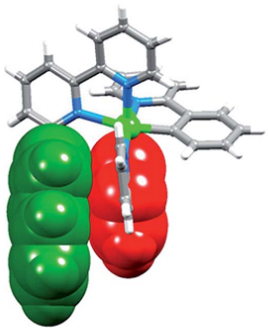

Fig. 2 Intra-cation face-to-face π-stacking of the 2-naphthyl unit (green) with the phenyl ring (red) of one ppy^- ligand in Λ-$[Ir(ppy)_2(Naphbpy)]^+$.

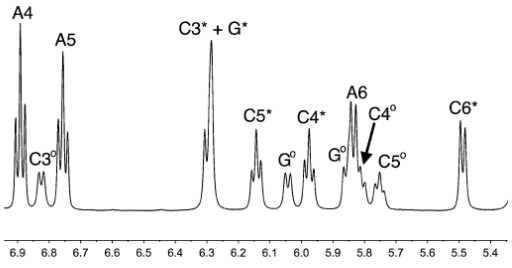

Fig. 4 Part of the ^{1}H NMR (500 MHz, CD_2Cl_2) spectrum of $[Ir(ppy)_2(Naphbpy)][PF_6]$ at 210 K (expansion of lowest trace in Fig. 3). See Scheme 1 and Fig. 5 for atom labelling. * = major conformer; ° = minor conformer. Chemical shifts in ∂/ppm.

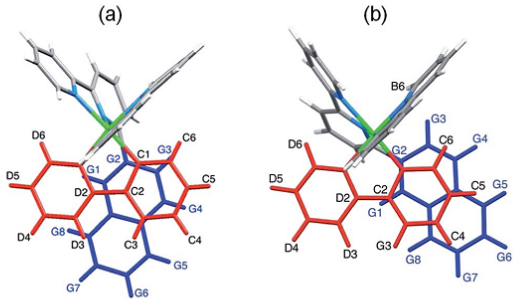

Fig. 5 Ring orientations and phenyl ring carbon atom labelling in (a) conformer 1 (X-ray structure) and (b) conformer 2 (DFT-optimized geometry) of $[Ir(ppy)_2(Naphbpy)]^+$.

origins of which are unknown (see Fig. S1 in the ESI†). On the other hand, the quasi-reversible reduction wave at −1.85 V is assigned to a ligand-based process. The electrochemical band gap ($E^{ox}_{1/2} - E^{red}_{1/2}$) of 2.68 V compares with 2.61 V for $[Ir(ppy)_2(bpy)][PF_6]$[39] and 2.60 V for $[Ir(ppy)_2(Phbpy)][PF_6]$.[14]

The absorption spectrum of $[Ir(ppy)_2(Naphbpy)][PF_6]$ (Fig. 6a) is dominated by a broad and intense, ligand-centred (LC) band at 264 nm assigned to spin-allowed $\pi \rightarrow \pi^*$ transitions involving both the cyclometallating and the ancillary ligands. The less intense broad absorption at 387 nm is attributed to transitions with mixed metal-to-ligand (MLCT) and ligand-to-ligand (LLCT) charge transfer character. Finally, the weak band observed in the spectra above 450 nm is due to direct spin-forbidden transitions from the singlet ground state (S_0) to the first triplet excited states of the complex, enabled by the high spin–orbit coupling constant of the iridium metal core ($\zeta_{Ir} = 3909\ cm^{-1}$).[19]

Excitation at 275 nm produces a broad, structureless emission centred at 598 nm (Fig. 6b). The band shape is consistent with there being significant MLCT character in the emitting state.[19] The emission maximum recorded for $[Ir(ppy)_2(Naphbpy)][PF_6]$ is almost identical to those reported for $[Ir(ppy)_2(bpy)][PF_6]$ ($\lambda^{em}_{max} = 594$ nm, MeCN)[39] and $[Ir(ppy)_2(Phbpy)][PF_6]$ ($\lambda^{em}_{max} = 595$ nm, MeCN).[18] The PLQY and the emission lifetime (τ) were determined in argon-degassed CH_2Cl_2 solutions of $[Ir(ppy)_2(Naphbpy)][PF_6]$. The PLQY and τ values recorded for $[Ir(ppy)_2(Naphbpy)][PF_6]$ (7.7% and 148 ns, respectively) are lower than those reported in de-aerated MeCN solution for $[Ir(ppy)_2(bpy)][PF_6]$ (14% and 430 ns).[39]

Photoluminescence in the solid state was measured on a 100 nm thick film (Fig. 7b) obtained by spin coating a solution of the complex mixed with the ionic liquid (IL) 1-butyl-3-methylimidazolium hexafluoridophosphate $[BMIM][PF_6]$ on a quartz substrate (the molar ratio complex:IL was 4 : 1). The IL was added to mimic the formulation of the active layer in a LEC (see below). The emission spectrum in thin film consists of a broad emission centred at 596 nm that mostly matches the band observed in solution, thus confirming the charge transfer nature of the luminescence. The measured PLQY was 10.2%, a value smaller than those obtained for the analogous complexes $[Ir(ppy)_2(bpy)][PF_6]$ (34%)[39] and $[Ir(ppy)_2(Phbpy)][PF_6]$ (21%).[14] The origin of this reduction in PLQY is commented upon in the next section.

Theoretical calculations

To gain further insight into the structural, electrochemical and photophysical properties, the molecular and electronic structures of the $[Ir(ppy)_2(Naphbpy)]^+$ cation, in both ground and excited states, were investigated by performing DFT calculations at the B3LYP/(6-31G**+LANL2DZ) level in the presence of the solvent (CH_2Cl_2).

Geometry optimization of $[Ir(ppy)_2(Naphbpy)]^+$ in the ground electronic state (S_0) leads to the two conformers depicted in Fig. 5. Conformer 1 corresponds to that observed in the crystal structure (Fig. 1). Even considering the differences to be expected between the calculated geometry (in CH_2Cl_2 solution) and the crystal structure due to the different media, calculations

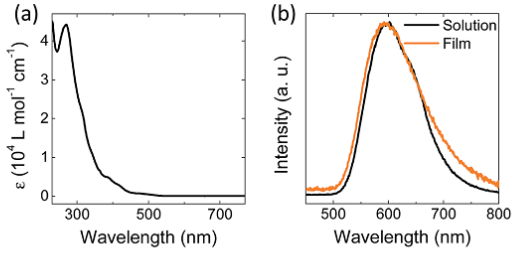

Fig. 6 (a) Absorption spectrum of $[Ir(ppy)_2(Naphbpy)][PF_6]$ (CH_2Cl_2, 5×10^{-5} mol dm^{-3}), and (b) emission spectrum in solution (CH_2Cl_2, 1.00×10^{-5} mol dm^{-3}, $\lambda_{exc} = 275$ nm) and in solid film (100 nm thick film on quartz, $\lambda_{exc} = 310$ nm).

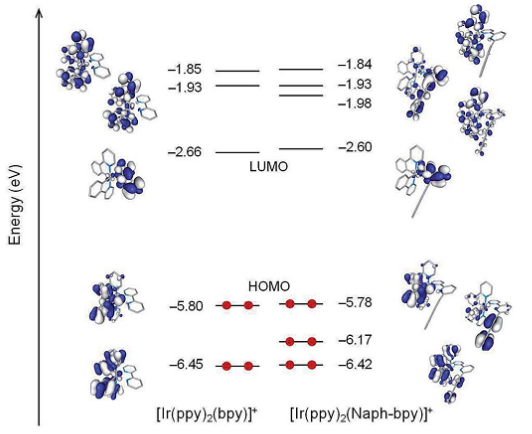

Fig. 7 Schematic diagram showing the electron density contours (0.03 a.u.) and energies calculated for the highest-occupied and lowest-unoccupied molecular orbitals of $[Ir(ppy)_2(bpy)]^+$ and $[Ir(ppy)_2(Naphbpy)]^+$. Hydrogen atoms are omitted.

predict geometric parameters in good accord with the experimental X-ray data (see Table S1 in the ESI†). For instance, the values computed for the bite angle of the ancillary (73.9°) and the cyclometallating (80.1 and 80.0°) ligands agree well with the X-ray values (75.60(18), 79.9(2) and 80.4(2)°, respectively). In agreement with experiment, the ppy$^-$ ligands are close to planar whereas the bpy ligand presents a dihedral N(1)–C(5)–C(6)–N(2) angle of 17.5° (X-ray value = 14.4°) to accommodate the pendant 2-naphthyl group. The 2-naphthyl unit is twisted around the C(10)–C(11) bond by 57.5° (N(2)–C(10)–C(11)–C(20) dihedral angle) slightly underestimating the X-ray value (61.1°). Calculations correctly reproduce the face-to-face π-stacking between the 2-naphthyl group and the phenyl ring of the adjacent ppy$^-$ ligand. The influence of the crystal packing could explain the difference between the value calculated for the bond distance Ir–N(2) (2.356 Å) and the X-ray value (2.215(5) Å), as N(2) belongs to the pyridine to which the pendant 2-naphthyl group is attached.

Conformer 2 is mostly isoenergetic with conformer 1, the energy difference being only 0.09 kcal mol^{-1}. It mainly differs from conformer 1 in the negative value (−20.8°) of the N(1)–C(5)–C(6)–N(2) dihedral angle, which leads to a different π-stacked arrangement of the 2-naphthyl group (Fig. 5). The interconversion between conformers 1 and 2 implies the internal rotation of the bpy ligand around the inter-ring C(5)–C(6) bond and is limited by a barrier of only 1.12 kcal mol^{-1} through a transition state in which the bpy ligand is mostly planar (N(1)–C(5)–C(6)–N(2) = −1.1°, Fig. S2†). The small interconversion barrier justifies the dynamic behavior observed in solution from the NMR data for [Ir(ppy)$_2$(Naphbpy)]$^+$ (see above).

Fig. 7 displays the atomic orbital compositions calculated for the highest-occupied (HOMO−2 to HOMO) and lowest-unoccupied (LUMO to LUMO+3) molecular orbitals of the [Ir(ppy)$_2$(Naphbpy)]$^+$ cation, together with those obtained for the [Ir(ppy)$_2$(bpy)]$^+$ archetype. The MOs sketched for [Ir(ppy)$_2$(Naphbpy)]$^+$ correspond to those computed for conformer 1. Identical compositions and energies that differ by less than 0.02 eV are obtained for conformer 2. As expected, the MOs calculated for [Ir(ppy)$_2$(Naphbpy)]$^+$ and [Ir(ppy)$_2$(bpy)]$^+$ present similar topologies and appear at close energies (Fig. 7).

The almost identical HOMO energies are in good agreement with the oxidation potentials measured for [Ir(ppy)$_2$(Naphbpy)]$^+$ (+0.83 V) and [Ir(ppy)$_2$(bpy)]$^+$ (+0.84 V), and the slightly higher (0.04 eV) HOMO–LUMO gap predicted for the former is in accord with the slightly greater (0.07 V) electrochemical gap reported for this complex. For both cations, the HOMO is composed of a mixture of Ir(III) d_π orbitals (t_{2g}) and phenyl π orbitals with some contribution from the pyridine rings of the cyclometallating ligands, whereas the LUMO corresponds to the π* LUMO of the bpy ligand. Therefore, if emission originates from the triplet state associated with the HOMO → LUMO excitation, similar wavelengths and photophysical properties are to be expected for both complexes. However, it is worth mentioning the presence in [Ir(ppy)$_2$(Naphbpy)]$^+$ of two MOs, the HOMO−1 and the LUMO+2, that are mainly localized on the pendant 2-naphthyl group. Transitions originating from the HOMO−1 of [Ir(ppy)$_2$(Naphbpy)]$^+$ have no equivalence in [Ir(ppy)$_2$(bpy)]$^+$ and may appear at lower energies than those resulting from the HOMO−1 in the latter.

The nature of the low-lying triplet states was first investigated by performing time-dependent DFT (TD-DFT) calculations at the optimized geometry of the ground state (S_0). Table 1 lists the vertical excitation energies and electronic descriptions computed for the four lowest-lying triplet excited states of [Ir(ppy)$_2$(Naphbpy)]$^+$. A close correspondence, both in energy and electronic nature, can be made between states T_1 (2.46 eV), T_3 (2.71 eV) and T_4 (2.78 eV) of [Ir(ppy)$_2$(Naphbpy)]$^+$ and the T_1, T_2 and T_3 states of [Ir(ppy)$_2$(bpy)]$^+$ calculated at 2.43, 2.75 and 2.80 eV, respectively. For both systems, the lowest-lying triplet state (T_1) is mainly defined by the HOMO → LUMO excitation, which has a mixture of metal-to-ligand and ligand-to-ligand charge transfer (^{3}MLCT/^{3}LLCT) character. States T_3 and T_4 of [Ir(ppy)$_2$(Naphbpy)]$^+$ are defined by transitions from the HOMO to the LUMO+1 and LUMO+2 and have ligand-centred (^{3}LC) character involving the C^N ligands as it is also the case for the T_2 and T_3 states of [Ir(ppy)$_2$(bpy)]$^+$.

The T_2 state of [Ir(ppy)$_2$(Naphbpy)]$^+$ is singular as it has no correspondence in the archetype [Ir(ppy)$_2$(bpy)]$^+$ cation. Despite its large multiconfigurational character, it mainly involves electron excitations between MOs centred on the pendant 2-naphthyl group. It therefore has a ^{3}LC character largely localized on the 2-naphthyl substituent of the ancillary ligand. The presence of this singular T_2 state reduces the energy difference between the first and second triplet states to 0.17 eV in [Ir(ppy)$_2$(Naphbpy)]$^+$. As the energy of both states will decrease after geometrical relaxation, the small gap between them opens the possibility that T_2 becomes competitive with T_1.

To study this possibility, the two lowest triplet states of [Ir(ppy)$_2$(Naphbpy)]$^+$ were reexamined by optimizing their geometries at the TD-DFT level. The optimized structure of T_1 presents small but noticeable differences compared with that obtained for the ground state (Table S1†). The Ir–N(2) bond shortens from 2.356 to 2.249 Å in passing from S_0 to T_1 and the bpy domain becomes more planar (the N(1)–C(5)–C(6)–N(2) dihedral angle changes from 17.5 to 11.0°). These changes point to a stronger interaction between the Ir core and the ancillary ligand in T_1. For the T_2 state, the coordination sphere of the iridium center remains mostly unaffected compared to S_0 (Table S1†), and the most important changes concern the pendant 2-naphthyl group (Fig. S3†). The intramolecular π-stacking between the 2-naphthyl group and the phenyl ring of the adjacent ppy$^-$ ligand is preserved in both excited states.

Fig. 8 displays the unpaired-electron spin density distributions calculated for the T_1 and T_2 states after full-geometry relaxation. For T_1, the spin density distribution (Ir: 0.48, ppy: 0.49, bpy: 1.01, Naph: 0.02 e) perfectly matches the topology of the HOMO → LUMO excitation (Fig. 7) and indicates an electron transfer from the Ir(ppy)$_2$ moiety to the bpy ligand. It therefore corroborates the mixed ^{3}MLCT/^{3}LLCT character of the T_1 state. For T_2, the spin density distribution (Ir: 0.01, ppy: 0.03, bpy: 0.15, Naph: 1.81 e) is mostly localized over the 2-naphthyl unit and confirms the ^{3}LC (2-naphthyl) character predicted above for this triplet (Table 1). The different electronic nature

Table 1 Lowest triplet excited states calculated at the TD-DFT B3LYP/(6-31G**+LANL2DZ) level for complex $[Ir(ppy)_2(Naphbpy)]^+$ in CH_2Cl_2 solution. Vertical excitation energies (E), dominant monoexcitations with contributions (within parentheses) greater than 15%, nature of the electronic transition and description of the excited state are summarized. H and L denote HOMO and LUMO, respectively

State	E (eV)	Monoexcitations	Nature	Description
T_1	2.46	H → L (96)	$d_\pi(Ir) + \pi_{C^\wedge N} \rightarrow \pi^*_{N^\wedge N}$	^{3}MLCT/^{3}LLCT
T_2	2.63	H−1 → L+2 (28)	$\pi_{naph} \rightarrow \pi^*_{naph}$	^{3}LC (Naph)
		H−1 → L+5 (16)	$\pi_{naph} \rightarrow \pi^*_{naph}$	
T_3	2.71	H → L+1 (40)	$d_\pi(Ir) + \pi_{C^\wedge N} \rightarrow \pi^*_{C^\wedge N}$	^{3}LC (C^N)
		H → L+3 (15)	$d_\pi(Ir) + \pi_{C^\wedge N} \rightarrow \pi^*_{C^\wedge N}$	
T_4	2.78	H → L+3 (36)	$d_\pi(Ir) + \pi_{C^\wedge N} \rightarrow \pi^*_{C^\wedge N}$	^{3}LC (C^N)
		H−2 → L+1 (17)	$d_\pi(Ir) + \pi_{C^\wedge N} \rightarrow \pi^*_{C^\wedge N}$	

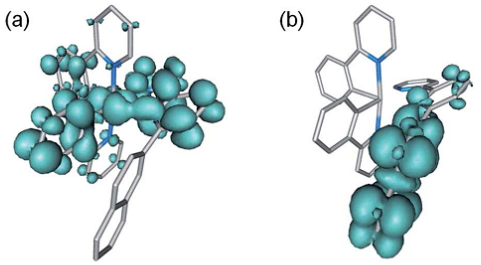

Fig. 8 Unpaired-electron spin-density contours (0.002 a.u.) calculated for the fully-relaxed T_1 (a) and T_2 (b) triplet states of $[Ir(ppy)_2(Naphbpy)]^+$.

obtained for T_1 and T_2 justifies the changes computed for their respective geometries. The important point is that, after full-geometry relaxation at the TD-DFT level, the ^{3}MLCT/^{3}LLCT T_1 state continues to be the lowest-lying triplet, although it is only 0.09 eV below the T_2 state (adiabatic energy difference = electronic energy difference between the excited states at their respective minimum-energy equilibrium geometries).

Calculations therefore suggest that the emitting T_1 state of $[Ir(ppy)_2(Naphbpy)]^+$ has a mixed ^{3}MLCT/^{3}LLCT nature in good agreement with the broad and unstructured aspect of the emission band (Fig. 6b). However, the ^{3}LC T_2 triplet resides at energies low enough to compete with T_1 during the population process. This could be the reason for the lower PLQY measured for $[Ir(ppy)_2(Naphbpy)]^+$ compared to $[Ir(ppy)_2(bpy)]^+$, for which no low-energy state equivalent to T_2 state is available. The vertical emission energy calculated for T_1 at its optimized minimum-energy geometry (621 nm) is in reasonably good accord with the emission maximum observed experimentally (598 nm).

Electroluminescent devices

The electroluminescence (EL) of the $[Ir(ppy)_2(Naphbpy)][PF_6]$ complex was investigated in double layer LECs consisting of a 100 nm thick layer of the complex spin-coated from acetonitrile (2 wt%) onto an 80 nm thick film of poly(3,4-ethylenedioxythiophene):poly(styrenesulfonate) (PEDOT:PSS). The PEDOT:PSS layer was deposited on a pre-patterned indium–tin-oxide (ITO)-coated glass substrate with the twofold purpose of flattening the ITO anode surface and enhancing hole injection from the ITO to the HOMO of the complex. Prior to spin-coating, the IL $[BMIM][PF_6]$ was added to the $[Ir(ppy)_2(Naphbpy)][PF_6]$ solution (the molar ratio complex : IL was 4 : 1), in order to enhance the ionic mobility of the emitting layer and thus reducing the turn-on time of the device.[41] Finally, an aluminum cathode (100 nm) was vacuum-deposited onto the emitting layer through a shadow mask. Spin-coating was done in ambient atmosphere; the base pressure during the cathode evaporation was 10^{-6} mbar. The thickness of the films was determined with an Ambios XP-1 profilometer. Thin film photoluminescence spectra and quantum yields were measured with a Hamamatsu C9920-02 absolute pl quantum yield measurement system. Lifetime data were obtained by applying pulsed currents and monitoring the voltage and simultaneously the luminance by a true colour sensor MAZeT (MTCSICT Sensor) using a lifetime test system designed by Botest (Botest OLT OLED Lifetime-Test System). The photocurrent was calibrated using a Minolta LS-100 luminance meter. Electroluminescence spectra were recorded using an Avantis fiber optics photospectrometer. Devices were not encapsulated and were characterized inside a glovebox. The LECs were driven using a pulsed current (block wave, 1000 Hz; duty cycle 50%; peak current per pulse 100 A m^{-2}; average current 50 A m^{-2}) and their performances were recorded continuously over time (Fig. 9a–b).

Due to the pulsed current driving, the LECs turn on instantly delivering more than 100 cd m^{-2} after being biased for 1 s. In the first measured hour the device luminance reaches 200 cd m^{-2} and then grows steadily until reaching ~330 cd m^{-2} where it remains stable for the duration of the experiment (350 hours) (Fig. 9a). The average voltage follows the opposite trend, starting from values above 5 V at the beginning of the measurements, and progressively decaying and subsequently stabilizing at about 2.7 V (Fig. 9a). This indicates a reduction of the device resistance, which is consistent with the formation of doped zones in the emitting layer near the electrodes.[42] As mentioned above, the device lifetime was monitored for more than 350 hours, showing high luminance and essentially no degradation. Accelerated lifetime testing in LECs is unfortunately not trivial as higher temperature testing would influence the ionic motion and therefore the local distribution of ions, which alters the device performance. Testing at higher luminance levels can also

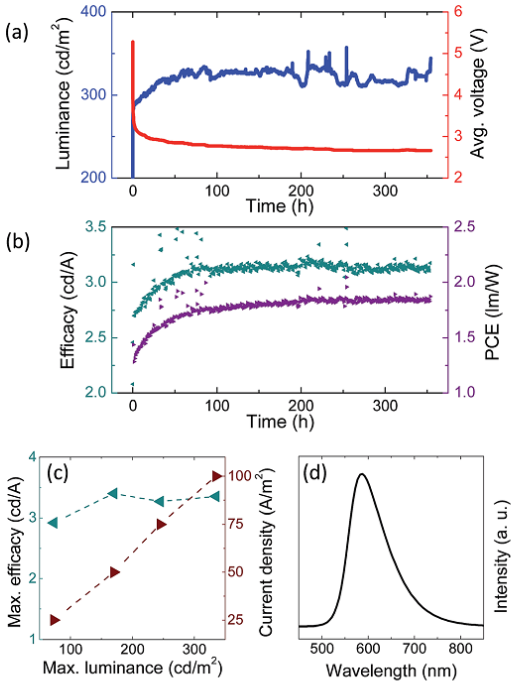

Fig. 9 Typical device performance data. (a) Luminance (blue)/voltage (red) and (b) efficacy (green)/power (purple) conversion efficiency *vs.* time for a LEC biased with a pulsed current using a block wave at a frequency of 1000 Hz, a duty cycle of 50% and a peak current density of 100 A m^{-2}. (c) Maximum efficacy (green) and correspondent current density (red) as a function of the peak luminance measured. (d) Electroluminescent spectra of the [Ir(ppy)$_2$(Naphbpy)][PF$_6$] complex in the LEC.

not be easily modeled to lower luminance driving conditions because with higher luminance the current density is increased and leads to an increase in the doped region and, as a result, to an increase in the luminescence quenching. Due to this we were not able to extrapolate the lifetime but it is expected to be at least 10 times this initial phase leading to a stability of 3000 hours. Such a very good stability is consistent with an efficient intramolecular interaction able to stabilize the excited state of the complex and thus enhancing the device lifetime.[14] The corresponding efficacy was stable at an average value of 3.2 cd A^{-1} and a power conversion efficiency of 1.8 lm W^{-1} when considering the measured potential drop at the device contacts (Fig. 9b). A series of devices was prepared and measured at different peak current density, from 25 to 100 A m^{-2}. The device efficacy is essentially independent of the luminance level and scales linearly with the applied current density over this range, meaning that the LEC can be used at the desired light output without altering its efficiency (Fig. 9c). The electroluminescent spectra appears as a broad peak centered at 588 nm (Fig. 9d), very similar to what is observed in the photoluminescence spectra (Fig. 6b) and in analogous complexes reported previously.[14]

Conclusions

A new charged bis-cyclometallated iridium(III) complex, [Ir(ppy)$_2$(Naphbpy)][PF$_6$], incorporating a 2-naphthyl substituent in the 6-position of the ancillary 2,2′-bipyridine ligand has been presented. The pendant 2-naphthyl group π-stacks with the adjacent cyclometallating ligand and protects the complex from undesirable degradation reactions. The complex presents a broad, structureless emission band centred around 595–600 nm both in solution and in thin film that points to an emission from a triplet state with a large charge transfer character. Theoretical calculations confirm the MLCT/LLCT nature of the lowest-energy emitting triplet and predict a second low-lying triplet state of LC nature associated with the 2-naphthyl unit. The presence of this triplet is invoked as a plausible reason for the relatively low photoluminescence quantum yields displayed by the complex. Despite this shortcoming, the complex gives rise to bright and very stable solid-state light-emitting electrochemical cells. Instantaneous light turn-on and luminances above 300 cd m^{-2} are obtained for LECs using this complex. Furthermore, no decay in luminance is observed for more than 350 hours, demonstrating their extraordinary stability.

Acknowledgements

We thank the Swiss National Science Foundation, the University of Basel, the European Union (CELLO, STRP 248043), the European Research Council (Advanced Grant 267816 LiLo), the Spanish Ministry of Economy and Competitiveness MINECO (MAT2011-24594 and CTQ2012-31914), the Generalitat Valenciana (PROMETEO/2012/053) and European Feder funds (CTQ2012-31914) for financial support. A.P. acknowledges the MINECO for a FPI grant.

Notes and references

1 Y. Shirota and H. Kageyama, *Chem. Rev.*, 2007, **107**, 953–1010.
2 S. O. Jeon, S. E. Jang, H. S. Son and J. Y. Lee, *Adv. Mater.*, 2011, **23**, 1436–1441.
3 H. Sasabe and J. Kido, *Eur. J. Org. Chem.*, 2013, 7653–7663.
4 M. Stössel, J. Staudigel, F. Steuber, J. Simmerer and A. Winnacker, *Appl. Phys. A: Mater. Sci. Process.*, 1999, **68**, 387–390.
5 C. D. Muller, A. Falcou, N. Reckefuss, M. Rojahn, V. Wiederhirn, P. Rudati, H. Frohne, O. Nuyken, H. Becker and K. Meerholz, *Nature*, 2003, **421**, 829–833.
6 L. Duan, L. Hou, T.-W. Lee, J. Qiao, D. Zhang, G. Dong, L. Wang and Y. Qiu, *J. Mater. Chem.*, 2010, **20**, 6392–6407.
7 C. Zhong, C. Duan, F. Huang, H. Wu and Y. Cao, *Chem. Mater.*, 2010, **23**, 326–340.
8 Q. B. Pei, G. Yu, C. Zhang, Y. Yang and A. J. Heeger, *Science*, 1995, **269**, 1086–1088.

9 J. C. deMello, N. Tessler, S. C. Graham and R. H. Friend, *Phys. Rev. B: Condens. Matter Mater. Phys.*, 1998, **57**, 12951–12963.
10 J. D. Slinker, J. A. DeFranco, M. J. Jaquith, W. R. Silveira, Y. W. Zhong, J. M. Moran-Mirabal, H. G. Craighead, H. D. Abrũa, J. A. Marohn and G. G. Malliaras, *Nat. Mater.*, 2007, **6**, 894–899.
11 J. K. Lee, D. S. Yoo, E. S. Handy and M. F. Rubner, *Appl. Phys. Lett.*, 1996, **69**, 1686–1688.
12 J. D. Slinker, J. Rivnay, J. S. Moskowitz, J. B. Parker, S. Bernhard, H. D. Abruna and G. G. Malliaras, *J. Mater. Chem.*, 2007, **17**, 2976–2988.
13 C. Rothe, C.-J. Chiang, V. Jankus, K. Abdullah, X. Zeng, R. Jitchati, A. S. Batsanov, M. R. Bryce and A. P. Monkman, *Adv. Funct. Mater.*, 2009, **19**, 2038–2044.
14 R. D. Costa, E. Ortí, H. J. Bolink, S. Graber, C. E. Housecroft and E. C. Constable, *Adv. Funct. Mater.*, 2010, **20**, 1511–1520.
15 L. J. Soltzberg, J. D. Slinker, S. Flores-Torres, D. A. Bernards, G. G. Malliaras, H. D. Abruña, J.-S. Kim, R. H. Friend, M. D. Kaplan and V. Goldberg, *J. Am. Chem. Soc.*, 2006, **128**, 7761–7764.
16 J. D. Slinker, J.-S. Kim, S. Flores-Torres, J. H. Delcamp, H. D. Abruna, R. H. Friend and G. G. Malliaras, *J. Mater. Chem.*, 2007, **17**, 76–81.
17 R. D. Costa, E. Ortí, H. J. Bolink, S. Graber, C. E. Housecroft and E. C. Constable, *J. Am. Chem. Soc.*, 2010, **132**, 5978–5980.
18 H. J. Bolink, E. Coronado, R. D. Costa, E. Ortí, M. Sessolo, S. Graber, K. Doyle, M. Neuburger, C. E. Housecroft and E. C. Constable, *Adv. Mater.*, 2008, **20**, 3910–3913.
19 R. D. Costa, E. Ortí, H. J. Bolink, F. Monti, G. Accorsi and N. Armaroli, *Angew. Chem., Int. Ed.*, 2012, **51**, 8178–8211.
20 F. Chung, C. Tisné, T. Lecourt, F. Dardel and L. Micouin, *Angew. Chem., Int. Ed.*, 2007, **46**, 4489–4491.
21 J. G. Park and Y. Jahng, *Bull. Korean Chem. Soc.*, 1998, **19**, 436–439.
22 G. E. Schneider, H. J. Bolink, E. C. Constable, C. D. Ertl, C. E. Housecroft, A. Pertegas, J. A. Zampese, A. Kanitz, F. Kessler and S. B. Meier, *Dalton Trans.*, 2014, 1961–1964.
23 I. Bruker Analytical X-ray Systems, APEX2, version 2 User Manual, M86-E01078, Madison, WI, 2006.
24 G. M. Sheldrick, *Acta Crystallogr., Sect. A: Found. Crystallogr.*, 2007, **64**, 112–122.
25 C. F. Macrae, I. J. Bruno, J. A. Chisholm, P. R. Edgington, P. McCabe, E. Pidcock, L. Rodriguez-Monge, R. Taylor, J. Van De Streek and P. A. Wood, *J. Appl. Crystallogr.*, 2008, **41**, 466–470.
26 I. J. Bruno, J. C. Cole, P. R. Edgington, M. Kessler, C. F. Macrae, P. McCabe, J. Pearson and R. Taylor, *Acta Crystallogr., Sect. B: Struct. Sci.*, 2002, **58**, 389–397.
27 M. J. Frisch, G. W. Trucks, H. B. Schlegel, G. E. Scuseria, M. A. Robb, J. R. Cheeseman, G. Scalmani, V. Barone, B. Mennucci, G. A. Petersson, H. Nakatsuji, M. Caricato, X. Li, H. P. Hratchian, A. F. Izmaylov, J. Bloino, G. Zheng, J. L. Sonnenberg, M. Hada, M. Ehara, K. Toyota, R. Fukuda, J. Hasegawa, M. Ishida, T. Nakajima, Y. Honda, O. Kitao, H. Nakai, T. Vreven, J. A. Montgomery, Jr, J. E. Peralta, F. Ogliaro, M. Bearpark, J. J. Heyd, E. Brothers, K. N. Kudin, V. N. Staroverov, R. Kobayashi, J. Normand, K. Raghavachari, A. Rendell, J. C. Burant, S. S. Iyengar, J. Tomasi, M. Cossi, N. Rega, N. J. Millam, M. Klene, J. E. Knox, J. B. Cross, V. Bakken, C. Adamo, J. Jaramillo, R. Gomperts, R. E. Stratmann, O. Yazyev, A. J. Austin, R. Cammi, C. Pomelli, J. W. Ochterski, R. L. Martin, K. Morokuma, V. G. Zakrzewski, G. A. Voth, P. Salvador, J. J. Dannenberg, S. Dapprich, A. D. Daniels, Ö. Farkas, J. B. Foresman, J. V. Ortiz, J. Cioslowski and D. J. Fox, *Gaussian 09, Revision D.01*, Gaussian, Inc., Wallingford, CT, 2009.
28 C. Lee, W. Yang and R. G. Parr, *Phys. Rev. B: Condens. Matter Mater. Phys.*, 1988, **37**, 785–789.
29 A. D. Becke, *J. Chem. Phys.*, 1993, **98**, 5648–5652.
30 M. M. Francl, W. J. Pietro, W. J. Hehre, J. S. Binkley, M. S. Gordon, D. J. DeFrees and J. A. Pople, *J. Chem. Phys.*, 1982, **77**, 3654–3665.
31 P. J. Hay and W. R. Wadt, *J. Chem. Phys.*, 1985, **82**, 299–310.
32 J. Tomasi and M. Persico, *Chem. Rev.*, 1994, **94**, 2027–2094.
33 C. S. Cramer and D. G. Truhlar, *Solvent Effects and Chemical Reactivity*, Kluwer, 1996, pp. 1–80.
34 J. Tomasi, B. Mennucci and R. Cammi, *Chem. Rev.*, 2005, **105**, 2999–3094.
35 F. Kröhnke, *Synthesis*, 1976, 1.
36 F. Neve, A. Crispini, S. Campagna and S. Serroni, *Inorg. Chem.*, 1999, **38**, 2250–2258.
37 E. Baranoff, H. J. Bolink, E. C. Constable, M. Delgado, D. Haussinger, C. E. Housecroft, M. K. Nazeeruddin, M. Neuburger, E. Orti, G. E. Schneider, D. Tordera, R. M. Walliser and J. A. Zampese, *Dalton Trans.*, 2013, 1073–1087.
38 A. M. Bünzli, H. J. Bolink, E. C. Constable, C. E. Housecroft, M. Neuburger, E. Ortí, A. Pertegás and J. A. Zampese, *Eur. J. Inorg. Chem.*, 2012, **2012**, 3780–3788.
39 R. D. Costa, E. Ortí, D. Tordera, A. Pertegás, H. J. Bolink, S. Graber, C. E. Housecroft, L. Sachno, M. Neuburger and E. C. Constable, *Adv. Energy Mater.*, 2011, **1**, 282–290.
40 D. Tordera, A. M. Bünzli, A. Pertegás, J. M. Junquera-Hernández, E. C. Constable, J. A. Zampese, C. E. Housecroft, E. Ortí and H. J. Bolink, *Chem.–Eur. J.*, 2013, **19**, 8597–8609.
41 S. T. Parker, J. D. Slinker, M. S. Lowry, M. P. Cox, S. Bernhard and G. G. Malliaras, *Chem. Mater.*, 2005, **17**, 3187–3190.
42 S. B. Meier, S. van Reenen, B. Lefevre, D. Hartmann, H. J. Bolink, A. Winnacker, W. Sarfert and M. Kemerink, *Adv. Funct. Mater.*, 2013, **23**, 3531–3538.

4. iTMCs purity

4.1. Introduction

Impurities in luminescent materials are undesired as often they lead to quenching of the excited state, which reduces the radiative recombination paths. One well-established method for the straightforward separation of impurities in luminescent organic small-molecules is via thermal gradient sublimation.[90-92] This technique has been widely employed to purify materials for organic light emitting diodes (OLEDs). In contrast to OLEDs based on neutral organic molecules, light emitting electrochemical cells (LECs) use ionic transition-metal complexes (iTMCs) as active material, which are not amenable to a sublimation procedure for their purification. Column chromatography[89,93] or recrystallization[94,95] is used instead. There is no report available on the effectiveness of these techniques with regard to the final material quality and its evaluation in LECs. This is especially important since it has been demonstrated that the presence of nucleophilic molecules leads to the degradation of iTMC-based LECs.[96-99]

In LECs, typical impurities present in the final iTMCs arise from undesired contaminants in the precursor materials used in the synthesis. Typically, the synthesis of the Ir-iTMCs used in LECs involves $IrCl_3$ as a chemical precursor together with the cyclometallating and ancillary ligands leading to the chloride salt. However, chloride-based Ir(III)-iTMCs are not usefull for LECs due to the small size of the counter-anion, that leads to short lifetimes. In fact, most relevant achievements have been obtained using hexafluorophosphate-based Ir(III)-iTMCs. The preparation of the complexes incorporating the hexafluorophosphate ($[PF_6]$) counter-anions involves an anion exchange reaction typically done by adding an excess of a $[PF_6]$ salt, which precipitates with the iTMC (Figure 13). From this point of view, it is logical to think that a typical impurity present in the iTMCs is chloride.

In this chapter, the effect of chloride as impurity in complex B1 $[iTMC][PF_6]$ has been evaluated in order to show how the presence of small amounts of chloride affects the performance of LECs.

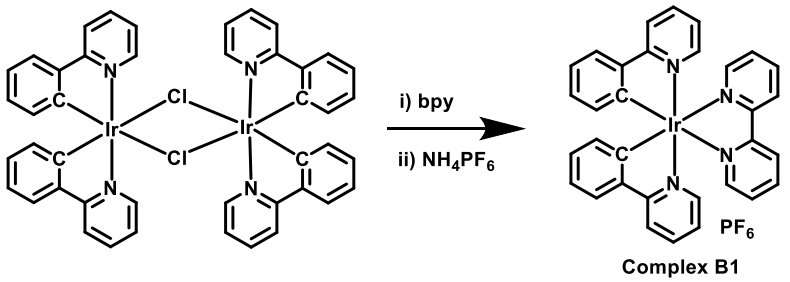

Figure 13. Schematic synthesis route for complex **B1**. The presence of chloride in the starting dimer increase the possibility of chloride impurities.

4.2. Results and discussion.

The device characteristics of two different batches of the archetype complex B1 $[Ir(ppy)_2(bpy)][PF_6]$ with different chloride content were evaluated. The batches are name as A (chloride free) and B (1% chloride as counter-anion).

LECs were prepared in order to evaluate the performance of each batch. The devices were characterized using an average pulsed current of 100 A m^{-2} (1000 Hz, 50% duty cycle and block wave). The device characteristics are depicted in Figure 14. The LECs showed no significant difference in the turn-on and voltage behavior. This shows that the device operation is similar, as the ionic mobility was not affected by the presence of small amounts of chloride impurities. However, a different performance was observed between batches. Specifically, LECs prepared using batch B suffered a reduction of one-half of its luminance respect with batch A when using the same driving conditions described above. As a consequence, significantly different maximum efficacies of 8.8 and 5.0 $cd \cdot A^{-1}$ were reached for LECs prepared with batch A and B, respectively. As the devices showed comparable device operation characteristics, the reason of this enormous disparity was attributed to the presence of chloride impurity.

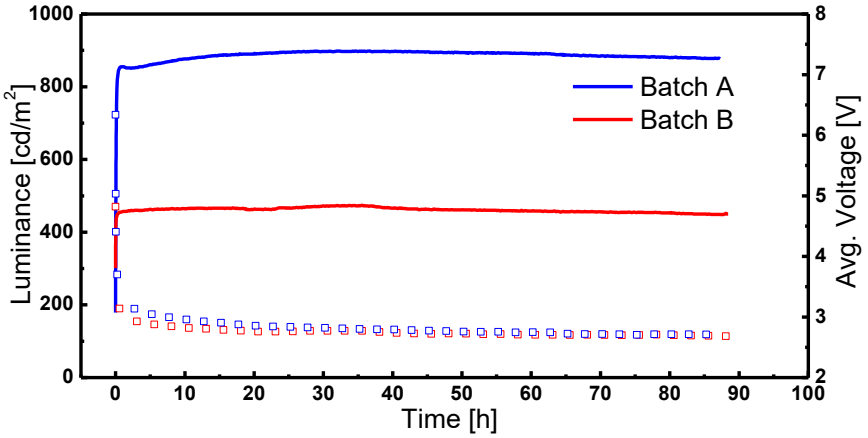

Figure 14. Performance of batch A and B of $[Ir(ppy)_2(bpy)][PF_6]$ incorporated in: ITO/PEDOT:PSS/$[Ir(ppy)_2(bpy)][PF_6]$:$[Bmim][PF_6]$ 4:1/Al LEC driven using a pulsed current of 100 $A{\cdot}m^{-2}$ (1000 Hz, 50% duty cycle, block wave).

The effect of the presence of small amounts of chloride was first investigated by NMR. Several ^1H NMR titrations of $[^nBu_4N]Cl$ were performed into CD_2Cl_2 solutions of batch A. The signal due to proton E3 (Figure 15) exhibited dramatic shifts to higher frequency upon the addition of $[^nBu_4N]Cl$ from 8.505 to 9.326 ppm. Among the remaning protons, only the resonance of proton E4 showed a small shift. The sensitivity of E3 protons to the presence of chloride ion suggests a highly specific interaction of chloride ion with these protons of the 2,2-bipyridine rings. It has been previously observed a deuterium exchange in $[Ru(bpy)_3]^{2+}$ in basic media due to the relatively acidic of these protons.[100]

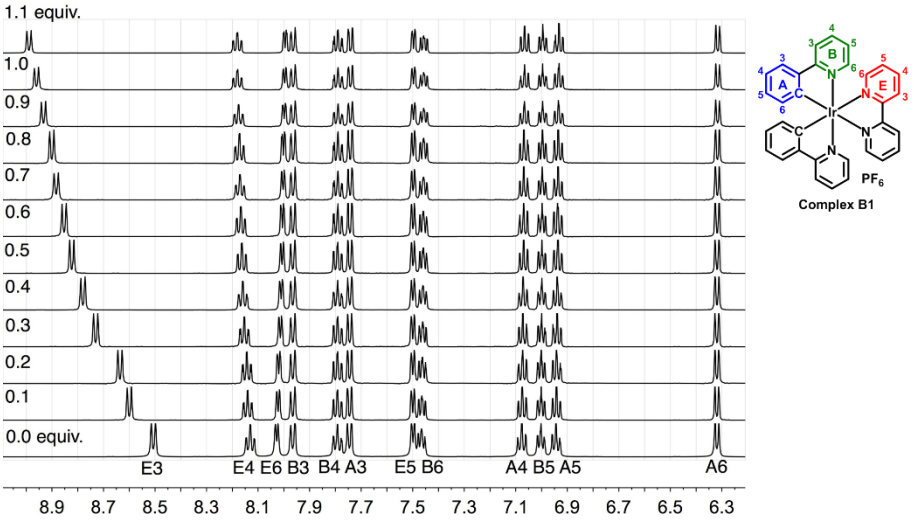

Figure 15. ^{1}H NMR spectra of $[Ir(ppy)_2(bpy)][PF_6]$ in CD_2Cl_2 upon adding different amounts of $[^nBu_4N]Cl$.

For further understanding of the specific chloride-E3 proton interaction, single crystals were obtained from solutions containing $[Ir(ppy)_2(bpy)]Cl$. The X-ray structure analysis showed that the chloride anion was chelated to the 2,2′-bipyridine protons labeled as E3 by hydrogen bond formation. This was consistent with solution NMR spectra what confirms the specific interaction of chloride ions with E3 protons.

Finally, the effect of chloride on the photoluminescent properties of $[Ir(ppy)_2(bpy)]$ was investigated. The experiments consisted on the measurement of the ϕ_{PL} in thin film for: a) $[Ir(ppy)_2(bpy)][PF_6]$, b) $[Ir(ppy)_2(bpy)][PF_6]$ mixed with different quantities, 0.5 and 1 equivalents of tetraethylammonium chloride ($[Et_4N][Cl]$) and c) $[Ir(ppy)_2(bpy)][Cl]$. It was found that upon adding up to 0.5 equivalents of $[Et_4N][Cl]$, ϕ_{PL} was practically unvaried (32.6%) with respect to the pure $[Ir(ppy)_2(bpy)][PF_6]$, which showed 33.2%. However, with increasing the amount of chloride to 1 equivalent, ϕ_{PL} was substantially lower (24.6%). Furthermore, the ϕ_{PL} for the complex $[Ir(ppy)_2(bpy)][Cl]$ was even lower (20.9%). This fact must be related with the drop in device performance by the presence of chloride impurities.

4.2. Conclusions

The presence of chloride as counter-anion leads to the formation of a strong chelating hydrogen bond with bypyridine protons in position E3, forming ion-paired $[Ir(C^N)_2(N^N)]$-Cl species at low quantities of chloride. Photoluminescence studies have showed that the ϕ_{PL} of $[Ir(ppy)_2(bpy)][PF_6]$ decreases when the chloride content in thin films increases. This must be related with the batch-to-batch variability observed in Ir(III)-iTMC-based LECs where significant differences in device efficiency were observed in the particular study done here. This observation could be one of the reasons for the superiority of $[PF_6]^-$ salts in LEC applications.

4.3. Contributions of the author

Article 3: ***Chloride ion impact on materials for light-emitting electrochemical cells***. *Dalton Transactions* **2014**, *43*, 1961-1964

Dalton Transactions

COMMUNICATION

View Article Online
View Journal | View Issue

Cite this: *Dalton Trans.*, 2014, **43**, 1961

Received 15th November 2013,
Accepted 27th November 2013

DOI: 10.1039/c3dt53229a

www.rsc.org/dalton

Chloride ion impact on materials for light-emitting electrochemical cells†

Gabriel E. Schneider,[a] Henk J. Bolink,[b,c] Edwin C. Constable,*[a] Cathrin D. Ertl,[a] Catherine E. Housecroft,[a] Antonio Pertegàs,[b,c] Jennifer A. Zampese,[a] Andreas Kanitz,[d] Florian Kessler[d] and Sebastian B. Meier[d]

Small quantities of Cl^- ions result in dramatic reductions in the performance of ionic transition metal complexes in light-emitting electrochemical cells. Strong ion-pairing between aromatic protons and chloride has been established in both the solid state and solution. X-ray structural determination of $2\{[Ir(ppy)_2(bpy)][Cl]\}\cdot 2CH_2Cl_2\cdot[H_3O]\cdot Cl$ reveals the unusual nature of an impurity encountered in the preparation of $[Ir(ppy)_2(bpy)][PF_6]$.

High performance electronic devices have traditionally been prepared by vapour deposition methods involving reactions of ultrapure volatile compounds to generate solid state materials.[1] Solution casting offers an alternative fabrication method in which preformed materials are deposited from the solution phase.[2] Materials of interest are usually refined to chemical, but not electronic, standards of purity. In this communication we report the dramatic effect of trace components on the device performance of ionic iridium emitters in light-emitting electrochemical cells (LECs) and describe an unusual interaction of chloride with such complexes.

We routinely prepare the complex $[Ir(ppy)_2(bpy)][PF_6]$ (Hppy = 2-phenylpyridine, bpy = 2,2′-bipyridine), which gives long-lived LECs,[3] by the reaction of $[Ir_2(ppy)_4Cl_2]$ with bpy in MeOH under microwave heating, followed by precipitation with excess $[NH_4][PF_6]$ and multiple chromatographic purification (Scheme 1). The preparation is readily upscaled to gram quantities, but we have found batch-to-batch variability between materials of apparently similar chemical constitution and purity when evaluated in a solid-state LEC (see Fig. 1).[4] The device configuration is similar to that previously reported.[3] A layer of poly(3,4-ethylenedioxythiophene): polystyrenesulfonate (PEDOT:PSS) (100 nm) was deposited on top of a patterned indium tin oxide (ITO) substrate to increase the device preparation yield. The complex $[Ir(ppy)_2(bpy)][PF_6]$ together with 1-butyl-3-methylimidazolium hexafluorophosphate [BMIM][PF_6] at a molar ratio of 4 : 1 was then spin-coated from MeCN solution to yield an 80 nm thick layer. The ionic liquid was added to reduce the turn-on time of the device.[5] The device was completed by the deposition of 80 nm aluminium as the top electrode contact.

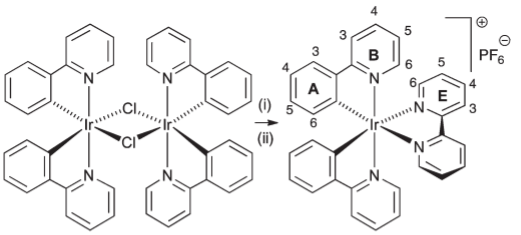

Scheme 1 Synthesis of $[Ir(ppy)_2(bpy)][PF_6]$ with labelling for NMR spectroscopic assignments: (i) bpy, MeOH, microwave, 2 h, 120 °C; (ii) $[NH_4][PF_6]$.

The ^{1}H NMR spectra of the materials used for the two devices in Fig. 1 were at first sight identical, but a detailed analysis revealed that the signal assigned to proton E3 was shifted by about 0.5 Hz between the two samples (Fig. S1†). Subsequent elemental analysis indicated that the poorly performing materials had typically 1% Cl^- and 99% $[PF_6]^-$ as counter-ion. Further purification of the poorly performing material by precipitation with $[NH_4][PF_6]$ and $Ag[PF_6]$ (to precipitate any Cl^- present as AgCl) followed by chromatography gave material with optimal performance, confirming that the presence of small amounts of Cl^- has a profound effect on the device properties as

[a]*Department of Chemistry, University of Basel, Spitalstrasse 51, CH-4056 Basel, Switzerland. E-mail: edwin.constable@unibas.ch*
[b]*Instituto de Ciencia Molecular, Universidad de Valencia, Catedrático José Beltrán 2, Paterna, E-46980, Spain. E-mail: henk.bolink@uv.es*
[c]*Fundació General de la Universitat de Valencia (FGUV), PO Box 22085, Valencia, Spain*
[d]*Siemens AG, Corporate Technology CT RTC MAT IEC-DE, Günther-Scharowsky-Str. 1, 91058 Erlangen, Germany*

†Electronic supplementary information (ESI) available: Fig. S1: ^{1}H NMR signals for H^{E3} and H^{B3} in batches 1 and 2 of materials; Fig. S2: ^{19}F NMR spectra for addition of $[^nBu_4N]Cl$ to $[Ir(ppy)_2(bpy)][PF_6]$. Synthesis of chloride-free $[Ir(ppy)_2(bpy)][PF_6]$ and of $[Ir(msppy)_2(6\text{-}Phbpy)][PF_6]$ and $[Ir(msppy)_2(6\text{-}Phbpy)][Cl]$. Crystallographic data for $2\{[Ir(ppy)_2(bpy)][Cl]\}\cdot 2CH_2Cl_2\cdot[H_3O]\cdot Cl$ and $[Ir(msppy)_2(6\text{-}Phbpy)][Cl]$. CCDC 959828 and 971737. For ESI and crystallographic data in CIF or other electronic format see DOI: 10.1039/c3dt53229a

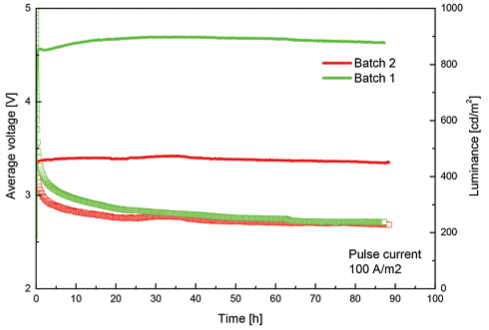

Fig. 1 Performance of two batches of $[Ir(ppy)_2(bpy)][PF_6]$ with a similar chemical history incorporated in a LEC device (ITO/PEDOT:PSS/ $[Ir(ppy)_2(bpy)][PF_6]$ + [BMIM][PF_6] (4 : 1)/Al). The performance of batch 2 is significantly inferior due to the presence of small amounts of chloride as counterion.

smaller counter-ions have been shown to alter the LEC dynamics.[6,7] The ESI† provides a protocol for the preparation of chloride-free material with reproducible device performance.

In order to understand the effect of chloride ion, we have performed ^{1}H NMR titrations of $[^nBu_4N]Cl$ into CD_2Cl_2 solutions of pure $[Ir(ppy)_2(bpy)][PF_6]$ (Fig. 2). The signal due to proton E3 (the 3 and 3′ protons of the 2,2′-bipyridine ligand) exhibited dramatic shifts to higher frequency upon the addition of $[^nBu_4N]Cl$, from δ 8.505 to 9.326 ppm after the addition of >10 equivalents. Of the remaining protons, only the resonance for proton E4 showed a shift and this was very much less than that observed for proton E3.

Dichloromethane is a poorly solvating solvent in which relatively tight ion-pairing between cation and anion is expected and we have analysed the data according to the equilibrium:

$$\{[Ir(ppy)_2(bpy)][PF_6]\} + Cl^- \rightleftharpoons \{[Ir(ppy)_2(bpy)]Cl\} + [PF_6]^-$$

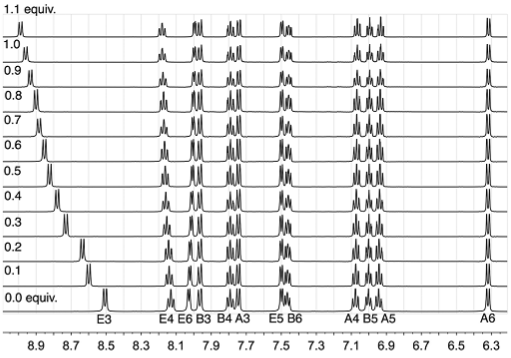

Fig. 2 The effect of adding 1.1 equivalents of $[^nBu_4N]Cl$ in 0.1 aliquots to a CD_2Cl_2 solution of $[Ir(ppy)_2(bpy)][PF_6]$ (0.02 mmol of complex in 0.75 mL CD_2Cl_2). Only the resonance assigned to proton E3 is significantly affected and a limiting shift of δ 9.326 ppm is observed after adding >10 equivalents of $[^nBu_4N]Cl$. See Scheme 1 for labelling.

Non-linear least-squares fitting of the ^{1}H chemical shift of E3 using WinEQNMR2[8] yielded a log K value of 2.24 (R = 0.001789) for this equilibrium, favouring the formation of the chloride ion-pair. Similar small shifts, of the order of δ 0.7 ppm are also observed in the ^{19}F NMR spectrum upon the addition of $[^nBu_4N]Cl$ to $[Ir(ppy)_2(bpy)][PF_6]$ (Fig. S2†); the ^{31}P NMR spectrum is unchanged. As expected, the equilibrium is also affected by the addition of additional $[PF_6]^-$ (Fig. 3) and on this basis, the chemical shift of the E3 proton can be used as a sensitive qualitative and quantitative probe for the presence of Cl^- in supposedly pure samples of $[Ir(ppy)_2(bpy)][PF_6]$. For a CD_2Cl_2 solution, the value of δ_{E3} as a function of the percentage of $[Ir(ppy)_2(bpy)]Cl$ *versus* $[Ir(ppy)_2(bpy)][PF_6]$ is given by:

$$\delta_{E3} = 8.505 + \{(-0.3289 \times 10^{-5})(\%Cl)^2 + 0.007843(\%Cl)\}$$

Not unexpectedly, the photophysical properties of the complex depend on the counterion and pure samples of $[Ir(ppy)_2(bpy)][PF_6]$ and $[Ir(ppy)_2(bpy)][Cl]$ were studied in the solid state and in MeCN solution (to avoid CH_2Cl_2 as a potential source of Cl^-). In solution, the pure complexes and those with mixed counter-ions exhibited the same properties (λ_{em} = 600 nm, ϕ = 0.13), whereas in the solid state, $[Ir(ppy)_2(bpy)][PF_6]$ and $[Ir(ppy)_2(bpy)]Cl$ exhibited different emission maxima (λ_{em} = 510 nm and 540 nm respectively) although the quantum yields were similar (ϕ = 0.16).

The sensitivity of the E3 protons to the presence of Cl^- suggests a highly specific interaction of chloride ion with these positions of the 2,2′-bipyridine rings. This position is relatively acidic and has previously been observed to undergo deuterium exchange in the complex $[Ru(bpy)_3]^{2+}$ in basic conditions[9] and is also the site of orthometallation in iridium[10] as well as nickel, palladium and platinum[11] 2,2′-bipyridine complexes. As this manuscript was being prepared, related observations for specific interactions of chloride with the 3- and 3′-protons in $[Ru(bpy)_3]^{2+}$ derivatives were described.[12] We have observed analogous shifting of the E3 proton signals in a wide range of $[Ir(C^N)_2(N^N)]^+$ complexes, both in CD_2Cl_2 and CD_3CN solutions. For example, in CD_3CN, protons E3 and F3† in $[Ir(msppy)_2(6\text{-}Phbpy)][PF_6]$ resonate at δ 8.56 and 8.60 ppm, compared to δ 8.65 and 8.68 ppm in $[Ir(msppy)_2(6\text{-}Phbpy)]Cl$

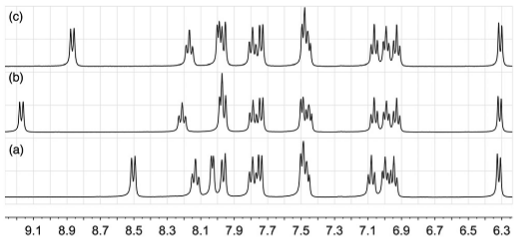

Fig. 3 Room temperature 400 MHz ^{1}H NMR spectra of CD_2Cl_2 solutions of (a) pure $[Ir(ppy)_2(bpy)][PF_6]$, (b) $[Ir(ppy)_2(bpy)][PF_6]$ with added $[^nBu_4N]Cl$, and (c) after the addition of $[^nBu_4N][PF_6]$ to solution (b).

(Hmsppy = 2-(4-methylsulfonylphenyl)pyridine, 6-Phbpy = 6-phenyl-2,2′-bipyridine).† While significant, the shift in signals is less dramatic in CD_3CN than in the less polar CD_2Cl_2. The ^{13}C NMR spectra† of [Ir(msppy)$_2$(6-Phbpy)][PF_6] and [Ir(msppy)$_2$(6-Phbpy)][Cl] show no significant differences. To understand the origin of the NMR spectroscopic changes, we determined the solid state structures of [Ir(msppy)$_2$(6-Phbpy)]Cl (as a representative bulk-sample chloride salt) and of the chloride-containing material present in gram-scale syntheses of [Ir(ppy)$_2$(bpy)][PF_6].

Single crystals† of 2{[Ir(ppy)$_2$(bpy)][Cl]}·2CH_2Cl_2·[H_3O]·Cl were obtained from solutions containing [Ir(ppy)$_2$(bpy)][PF_6] and [Ir(ppy)$_2$(bpy)]Cl. The structure of one of the two enantiomeric {[Ir(ppy)$_2$(bpy)]Cl} units in the lattice is shown in Fig. 4. The [Ir(ppy)$_2$(bpy)]$^+$ cation closely resembles that in [Ir(ppy)$_2$(bpy)][PF_6][3] with the metal ion in a slightly distorted octahedral environment and with the expected *trans*-arrangement of ppy$^-$ N-donor atoms. The ppy$^-$ ligands are near-planar with angles between the least squares planes of the phenyl and pyridine rings of 4.8 and 5.0°. The bpy ligand is more distorted with an interannular angle of 8.7°. The Cl$^-$ anion is chelated to the bpy 3- and 3′-protons (crystallographic ally labelled H4a and H7a, Fig. 4a), consistent with solution NMR spectra, and forms hydrogen bonds[13] to H4a and H7a with CH···Cl distances of 2.79 and 2.87 Å, respectively, (C4···Cl1 = 3.627(4) and C7···Cl1 = 3.794(4) Å) and the angle H4a–Cl1–H7a = 45.6°. This chloride ion is also hydrogen bonded to the 4-proton of one bpy and the 5-proton of a ppy$^-$ (see Scheme 1) of two different {[Ir(ppy)$_2$(bpy)][Cl]} moieties (CH···Cl, 2.86 and 2.68 Å, respectively). The [H_3O]$^+$Cl$^-$ unit is disordered and has been modelled with the O and Cl atoms (O10 and Cl10) in symmetry related sites, each of fractional occupancy 0.5. The O···Cl separation of 2.818(6) Å is similar to, but shorter than, that observed in the crystal structure of [H_3O]Cl (2.95(1) Å).[14] Single crystals of [Ir(msppy)$_2$(6-Phbpy)][Cl] grew after diffusion of Et_2O into a MeCN solution of the complex. Fig. 4b shows the structure of the ion pair containing the Δ-[Ir(msppy)$_2$(6-Phbpy)]$^+$ cation; both enantiomers are present in the lattice. The octahedral coordination environment of atom Ir1 is similar to that in [Ir(ppy)$_2$(bpy)]$^+$, and bond parameters are given in the caption to Fig. 4b. The Cl$^-$ anion is again bound by the bpy 3- and 3′-protons (H4a and H7a in Fig. 4b) with CH···Cl distances of 2.62 and 2.80 Å, respectively, with an H4a–Cl1–H7a angle of 46.0°. Although the CSD (v. 5.34 with three updates, Conquest v. 1.15[15]) contains 429 examples of metal-bound 2,2′-bipyridine with Cl (either Cl$^-$ or covalently bonded Cl) hydrogen-bonded between the 3- and 3′-protons, only nine of these are iridium complexes; of these, only two involve Cl$^-$ ion[16,17] as opposed to, for example, a Cl–M unit of an adjacent molecule.

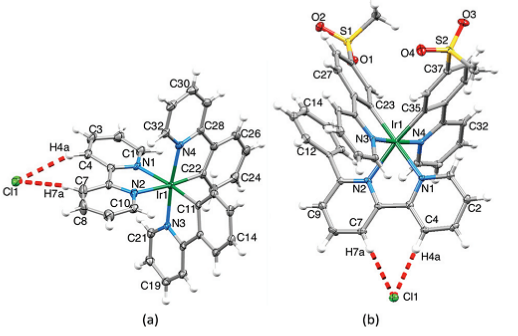

Fig. 4 (a) The Δ-cation–Cl$^-$ ion pair of 2{[Ir(ppy)$_2$(bpy)][Cl]}·2CH_2Cl_2·[H_3O]·[Cl] Selected bond parameters: Ir1–C11 = 2.011(3), Ir1–C22 = 2.012(3), Ir1–N4 = 2.042(3), Ir1–N3 = 2.050(3), Ir1–N2 = 2.135(3), Ir1–N1 = 2.142(3) Å; N1–Ir1–N2 = 76.5(1), N3–Ir1–C11 = 80.2(1), N4–Ir1–C22 = 80.4(1)°. (b) The Δ-cation–Cl$^-$ ion pair in [Ir(msppy)$_2$(6-Phbpy)]Cl. Selected bond parameters: Ir1–C35 = 2.005(4), Ir1–C23 = 2.034(4), Ir1–N1 = 2.119(3), Ir1–N2 = 2.207(3), Ir1–N3 = 2.050(3), Ir1–N4 = 2.050(3) Å; N1–Ir1–N2 = 76.14(12), C23–Ir1–N3 = 80.33(14), C35–Ir1–N4 = 80.43(14)°. Both are shown with 40% probability level ellipsoids.

Conclusions

The presence of chloride can result in a dramatic reduction in the performance of the ionic transition metal complex [Ir(ppy)$_2$(bpy)][PF_6] used as the emissive component in LECs. The solution ^1H NMR chemical shift of the bpy 3- and 3′-protons is very sensitive to the presence of Cl$^-$ (both in CD_2Cl_2 and more polar CD_3CN), and in the solid state, Cl$^-$ forms a strong chelating hydrogen bond with this position. The tight ion-pairing in [Ir(C^N)$_2$(N^N)][Cl] means that Cl$^-$ is easily carried through synthetic steps which start with [Ir$_2$(C^N)$_4$Cl$_2$] dimers. An HCl adduct of the salt [Ir(ppy)$_2$(bpy)]Cl was structurally characterized allowing clarification of the nature of side-products isolated in gram-scale preparations of [Ir(ppy)$_2$(Xbpy)][PF_6] materials.

Acknowledgements

We thank the Swiss National Science Foundation, University of Basel, European Union (CELLO, STRP 248043) and European Research Council (Advanced Grant 267816 LiLo) for financial support. A.P. acknowledges the Spanish Ministry of Economy and Competitiveness (MINECO) for an FPI grant. Liselotte Siegfried, Dr Colin J. Martin and Dr Collin Morris (University of Basel) are thanked for initial NMR titrations, help with WinEQNMR2, and ESI-MS measurements, respectively.

Notes and references

1 D. M. Dobkin and M. K. Zuraw, *Principles of Chemical Vapor Deposition*, Springer, 2010.
2 R. H. Friend, J. H. Burroughes and T. Shimoda, *Phys. World*, 1999, **12**(June), 35.

3 R. D. Costa, E. Ortí, H. J. Bolink, S. Graber, S. Schaffner, M. Neuburger, C. E. Housecroft and E. C. Constable, *Adv. Funct. Mater.*, 2009, **19**, 3456.
4 R. D. Costa, E. Ortí, H. J. Bolink, F. Monti, G. Accorsi and N. Armaroli, *Angew. Chem., Int. Ed.*, 2012, **51**, 8178.
5 S. T. Parker, J. D. Slinker, M. S. Lowry, M. P. Cox, S. Bernhard and G. G. Malliaras, *Chem. Mater.*, 2005, **17**, 3187.
6 M. Buda, G. Kalyuzhny and A. J. Bard, *J. Am. Chem. Soc.*, 2002, **124**, 6090.
7 H. Rudmann, S. Shimada and M. F. Rubner, *J. Am. Chem. Soc.*, 2002, **124**, 4918.
8 M. J. Hynes, *J. Chem. Soc., Dalton Trans.*, 1993, 311.
9 E. C. Constable and K. R. Seddon, *J. Chem. Soc., Chem. Commun.*, 1982, 34.
10 P. S. Braterman, G. A. Heath, A. J. MacKenzie, B. C. Noble, R. D. Peacock and L. J. Yellowlees, *Inorg. Chem.*, 1984, **23**, 3425; A. C. Hazell and R. G. Hazell, *Acta Crystallogr., Sect. C: Cryst. Struct. Commun.*, 1984, **40**, 806; P. J. Spellane, R. J. Watts and C. J. Curtis, *Inorg. Chem.*, 1983, **22**, 4060; G. Nord, A. C. Hazell, R. G. Hazell and O. Farver, *Inorg. Chem.*, 1983, **22**, 3429.
11 B. Butschke and H. Schwarz, *Organometallics*, 2010, **29**, 6002–6011; B. Butschke, M. Schlangen, D. Schroeder and H. Schwarz, *Chem.–Eur. J.*, 2008, **14**, 11050–11060.
12 W. M. Ward, B. H. Farnum, M. Siegler and G. J. Meyer, *J. Phys. Chem. A*, 2013, **117**, 8883.
13 J. Emsley, *Chem. Soc. Rev.*, 1980, **9**, 91.
14 Y. K. Yoon and G. B. Carpenter, *Acta Crystallogr.*, 1959, **12**, 17.
15 F. H. Allen, *Acta Crystallogr., Sect. B: Struct. Sci.*, 2002, **58**, 380; I. J. Bruno, J. C. Cole, P. R. Edgington, M. Kessler, C. F. Macrae, P. McCabe, J. Pearson and R. Taylor, *Acta Crystallogr., Sect. B: Struct. Sci.*, 2002, **58**, 389.
16 T. Moriuchi, C. Katano and T. Hirao, *Chem. Lett.*, 2012, **41**, 310.
17 M.-T. Youinou and R. Ziessel, *J. Organomet. Chem.*, 1989, **363**, 197.

5. Host-Guest systems

5.1. Introduction

The highest efficient light emitting electrochemical cell (LEC) reported up to date showed an efficiency of 38 cd A^{-1} and employed a green iridium material.[71] As explained in chapter 1, ionic transition metal complexes (iTMCs) are extensively used in electroluminescent devices as they are highly phosphorescent due to their high spin-orbit coupling constants. They can harvest both singlet and triplet excitons leading to electroluminescent devices that can reach internal quantum efficiency close to 100%. However, in solid state, most of luminescent materials suffer quenching processes such as self-quenching or triplet-triplet annihilation that especially depends on the concentration of the luminescent material in the film. In this way, there is a strong dependency of the photoluminescent quantum yield ϕ_{PL} with the concentration of the emitter in the solid film. Hence, the ϕ_{PL} increases by diluting the luminiscent material in the solid film using, for example, an inert polymer as polymethylmethacrylate (PMMA) as a matrix.

In general, as described in chapter 1, most iTMC-LECs are based on single component layers where ϕ_{PL} is severally restricted by the high concentration of the active material in the film, where quenching processes can gain strong importance. This high concentration is needed to maintain the electronic transport in the active layer.

An interesting approach consists in the preparation of the active layer by mixing the emitter, in diluted conditions, together with a matrix. This strategy is known as the host-guest approach and has been widely employed in OLEDs.[101] The approach requires: a) a good mixing compatibility between the matrix (host) and the emitter (guest) in the solid state, b) the organic host must show electronic transport properties in order to allow the charge carriers to move though the device and c) the system has to be composed of the appropriate materials in order to allow energy transfer from the host to the guest. This concept allows to decouple the transport, carried by the host, and the light emission processes, performed by the emitter, and, as a consequence, to strongly reduce the self-quenching processes. Therefore, a host-

guest system provides, on the one hand, a way to increase the ϕ_{PL} by reducing the concentration of the emitter in the active layer, what is particularly interesting in LECs. On the other hand, it reduces considerably the amount of iridium required for device preparation as the typically emitter concentration is only 1-10% wt. This is also important because of the low abundance of iridium in the Earth´s Crust that restricts the practical applications of LECs in global scale.

The strategy has been scarcely employed in LECs using Ir-iTMCs[102,103] and polymers[104] as host. The maximum efficacy reported was 29.3 cd A^{-1}, although at low luminance (<80 cd m^{-2}), for a system composed of $[Ir(F_2ppy)_2(dasb)][PF_6]$ as host and $[Ir(ppy)_2(dasb)][PF_6]$ as guest (where F_2ppy is 2-(2,4-difluorophenyl)pyridine, dasb is 4,5-diaza-9,9'-spirobifluorene and ppy is 2-phenylpyridine). Furthermore, the same group reported $[Ir(ppy)_2(dasb)][PF_6]$ as a host for small molecules (SMs) cyanine dyes as emitters in infrared LECs.[105]

In this chapter, we propose three different host-guest systems (Figure 16) for LEC applications. The first system (A) has an active layer consisting of three components: a) a novel ionic organic small molecule based on carbazole (NMS25), b) an electron transport material (SPPO13) and c) a neutral Ir-TMC as the emitter (FIrPic). The second system (B) was prepared using a two-component active layer consisting of a cyanine dye host (Dye H) and a cyanine dye emitter (Dye G). The third system is also based on a mix of two conjugated small molecules, where the host is a non-cyanine system (MYW2), which shows a thermal activated delayed fluorescence (TADF) and the guest was the a cyanine (Dye H).

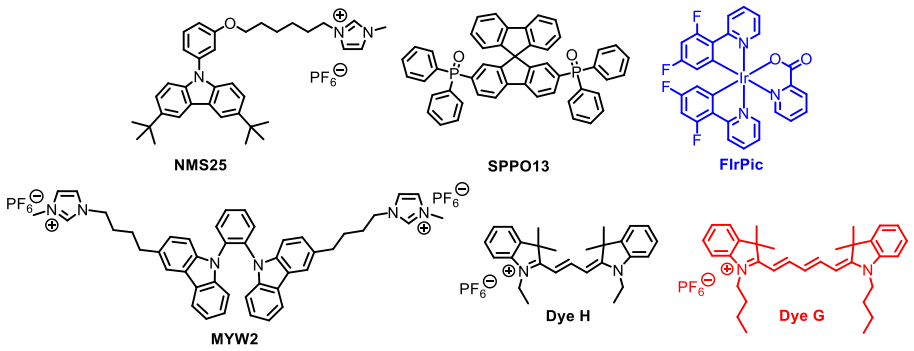

Figure 16. Chemical structure of the components used in the two host-guest systems studied in LECs: a) NMS25, SPPO13 and FIrPic (guest) and b) Dye H and Dye G (guest).

5.2. Results and discussion

Carbazole is a commonly used hole-transporter for blue organic light emitting diodes (OLEDs). After assuming that the suitability of the carbazole host is not affected by its ionic remote functionalization, the ionic carbazole NMS25 was considered an appropriate matrix element for blue LECs and it was prepared. SPPO13 is also a well-known electron transport material in blue OLEDs based on FIrPic as emitter. In this way, the combination of all three materials was considered as an adequate host-guest system for LECs.

In order to find the optimum ratio of the matrix elements, several LECs with the device configuration: ITO/PEDOT:PSS/matrix:FIrPic with the ionic liquid (IL) 1-butyl-3-methylimidazolium tetrafluoroborate in 4:1 molar ratio of matrix:IL/Al were prepared. All the devices exhibited blue electroluminescence (EL) from FIrPic with a maximum at 474 nm and with the typical characteristics of LECs. The devices exhibited a rapid decrease of the initially high driving voltage to lower steady-state values, which depend on the amount of NMS25. The higher the amount of NMS25 the lower was the steady-state voltage, owing to the higher ionic density. The device characteristics at 100 A m^{-2} pulsed current are summarized in Table 3.

Table 3. Performance of ITO/PEDOT:PSS/Matrix + 10wt% of FIrPic : IL/Al LECs at a pulsed current of 100 A m^{-2}. The matrix was composed with NMS25:SPPO13 mixtures.

NMS25:SPPO13 (mass)	t_{max} [min]	Lum_{max} [cd m^{-2}]	$t_{1/2}$ [h]	E_{tot} [J]	Efficacy [cd A^{-1}]
0:1	0.4	176	0.1	0.01	1.7
0.5:9.5	6.6	165	0.6	0.02	1.6
2.5:7.5	4.2	205	1.1	0.03	1.9
3.5:6.5	14	124	3.9	0.07	1.2
1:1	41	67	14	0.13	0.6

The LEC with the longest lifetime and the highest total emitted energy had an emitting layer with a 1:1 mass ratio of NMS25:SPPO13. Its steady-state driving voltage was the lowest, indicating optimized charge-injection/transport. Further optimizations were required as the LEC performance was affected by: a) the active layer thickness, b) the presence of the ionic liquid, c) the driving operation and d) the thermal annealing process. The best characteristics were found for: a) an active layer thickness of 80 nm, b) a device without IL, c) an operation at 75 A m^{-2} using a pulsed current driving and d) an annealing process of 100 ºC for 1 hour prior the evaporation of the top contact. By combining all these parameters, the LEC reached an efficacy of 5.1 cd A^{-1} at a luminance of 420 cd m^{-2}. These values are remarkably good compared with previously reported host-guest LECs where the best efficiencies were reported at luminances below 100 cd m^{-2}.[102,103]

On the other hand, cyanine dyes are well-known by their fluorescent properties. However, their emission properties are severally affected in the solid state due to their tendency to aggregate, which promotes self-quenching processes. This was confirmed by the preparation of a LEC based on a one-component active layer of Dye H. Using a constant voltage driving, the ITO/PEDOT:PSS/Dye H/Al showed a typical LEC behavior, although the performance was very poor. The preparation of LECs based on cyanine dyes required a host-guest system in order to increase the ϕ_{PL} in the active layer.

The host-guest system was designed as the emission of Dye H overlaps with the absorption of Dye G in order to guarantee an efficient energy transfer. To determine the optimum concentration of Dye G in the matrix of Dye H, the photoluminescence spectrum and the ϕ_{PL} were measured for different blends while exciting at a fixed wavelength of 526 nm (Figure 17), which corresponds to one of the absorption bands of Dye H. All the films showed strong emission at 700 nm originating from the emission of Dye G. The maximum ϕ_{PL} (27%) was observed for the film with the lowest amount of Dye G (0.1% wt).

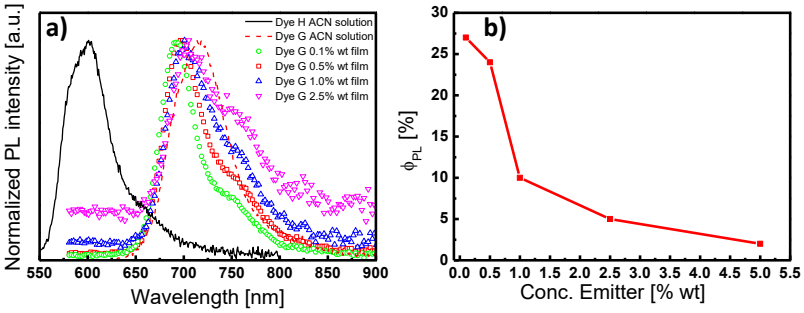

Figure 17. (a) Photoluminescent (PL) spectra of dyes H and G in acetonitrile solution and mixtures of Dye H:Dye G at different concentrations of Dye G (0.1%-2.5% wt) in solid state. (b) PL quantum yield (ϕ_{PL}) concentration dependence for the different mixtures characterized.

To evaluate the EL properties, we selected the host-guest thin film with 0.1% wt of Dye G to prepare a LEC in order to strengthen the device efficiency. The EL spectrum of these LECs shows a maximum emission at 706 nm, which corresponds with the emission of Dye G. No residual emission from the host was detected in accordance with the PL studies described above. The time response of the cyanine-based host-guest LECs under a pulsed current driving is depicted in Figure 18 for LECs with and without IL into the active layer. In both cases, the average voltage required to apply 100 A m^{-2} rapidly decreases with time, which is an indication that no additional ions are required to operate the LECs. However, the LECs that contain extra ions (coming from the IL) showed

slightly higher light-output and external quantum efficiencies (EQE). Considering that the ϕ_{PL} was increased to 27% by using this Host-Guest film, and that the light outcoupling is typically of 20%, the theoretical maximum EQE for a LEC based on this fluorescent host-guest emitting system is 1.3% when all injected electrons and holes recombine. We observed an EQE of 0.32% using a pulsed current driving and an EQE of 0.44% under a constant voltage driving, which is not a bad result but implies that some further optimization is possible.

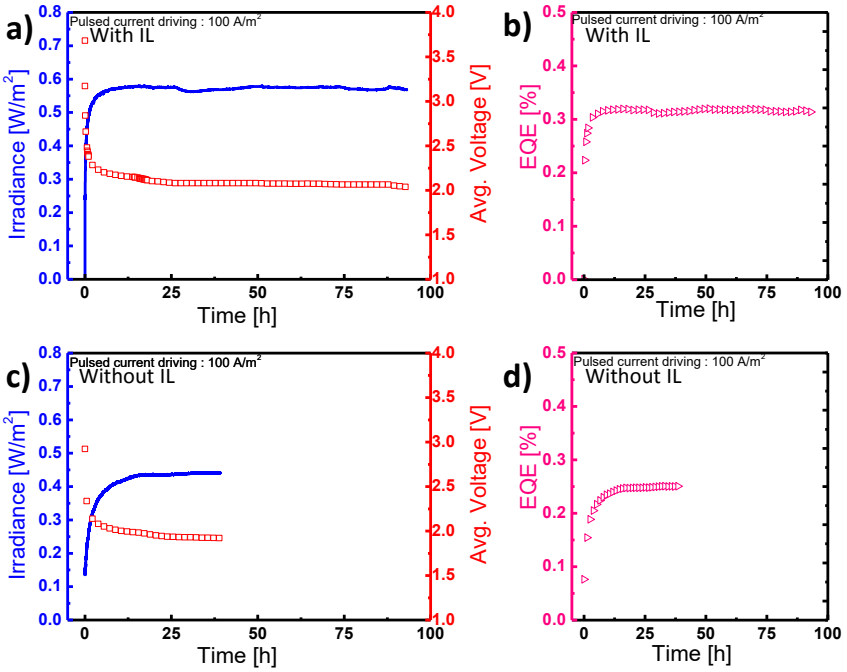

Figure 18. Irradiance (blue line), average voltage (red open squares) and external quantum efficiency (open triangles) for ITO/PEDOT:PSS/Active layer/Al LECs operated under an average pulsed current of 100 A m^{-2} using a block-wave at 1000 Hz and a duty cycle of 50 A m^{-2}. The composition of the active layer was: (a) Dye H + 0.1% wt of Dye G and (b) Dye H + 0.1% wt of Dye G + 16.7% wt of (1-butyl-3-ethylimidazolium hexafluorophosphate). (c) and (d) Dye H + 0.1% wt of Dye G.

Finally, a third host-guest system was designed based on conjugated small molecules as active components. The selected molecules were MYW2 and Dye H as host and guest respectively. Before the incorporation into electroluminescent devices, their optical properties were evaluated by photoluminescence studies. The absorption spectrum of Dye H was complementary to that of the MYW2. The well separated absorption spectra of the two species is advantageous for determining if any charge transfer occurs in blends of the two materials (Figure 19a). While exciting the MYW2 at 320 nm leads to an intense photoluminescence (PL) peak centered at 532 nm (Figure 19b), with ϕ_{PL} of 16.2%, we were not able to detect any luminescence originating from Dye H when exciting at the same wavelength. On the other hand, an intense, well-resolved PL spectra was obtained when exciting the cyanine (1wt% in PMMA) at 510 nm, with a resulting ϕ_{PL} of 30.2% with a photoluminescence spectrum centered at 574 nm. More interesting is the photoluminescence of MYW2 thin films doped with small amount (0.1 wt%) of Dye H. When exciting the MYW2 host (at 320 nm), the PL spectrum of the host-guest system is dominated by the guest emission, which peaks at 568 nm with only a small contribution from the MYW2 fluorescence. This clearly shows that following optical excitation of the host, charge transfer occurs to the cyanine guest. The ϕ_{PL} of the mixed film is also enhanced compared to that of its component, and was found to be as high as 43.1%.

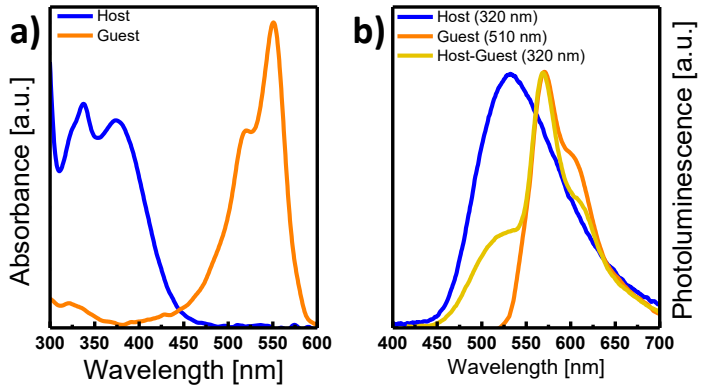

Figure 19. Thin film absorption (a) and photoluminescence spectra (b) of the host, guest compounds and host-guest mixture (0.1wt%). To enable the recording of both spectra, dye H was dispersed in PMMA (1wt%). The numbers in parenthesis in (b) indicates the excitation wavelength.

After assessing that indeed charge transfer takes place among the two molecules, their thin films were assembled into electroluminescent devices. A typical LEC architecture ITO/PEDOT:PSS/active layer/Al, was employed. Devices were driven by applying a pulsed current at a frequency of 1 kHz and with a 50% duty cycle. LECs were prepared using the host-guest system with 0.1 wt% of the cyanine dye into the MYW2 matrix. Yellow electroluminescence was observed immediately after biasing the LEC, independently on the current density applied. The device biased at 10 A m^{-2} showed a maximum luminance of 65 cd m^{-2} within a minute of operation (Figure 20a). This is a modest brightness but still represents a five-fold increase when compared to the pure host. With increasing the current density (25 A m^{-2}) the electroluminescence changed substantially, with a maximum luminance of 165 cd m^{-2} immediately after biasing the device. In terms of efficiency, LECs employing the host-guest system as the active layer showed a maximum EQE of 1.90 % (Figure 20b), independently on the excitation intensity. Taking into account the thin-film PLQY of the S2108 dye doped into the MYW2 host (43.1%), and considering the singlet generation yield and out-coupling efficiency, the maximum theoretical value is only slightly higher

than the measured EQE, about 2.16%. This result is of great interest for future applications of LECs, since it confirms that the host-guest approach widely applied to OLEDs would also be valid in the case of much simpler devices such LECs.

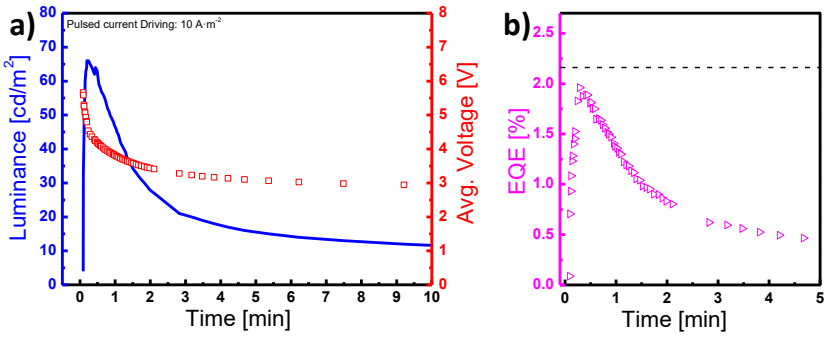

Figure 20. Dynamic behavior of ITO/PEDOT:PSS/Active Layer/Al employing the host-guest (MYW2 doped with Dye H at 0.1 wt%) system as the active layer. (a) Average voltage (open red squares) and luminance (solid blue line). (b) External quantum efficiency (open pink triangles) reported as a function of time driven at 10 A m^{-2} (1KHz, 50% duty cycle, block wave). In (b), the dashed line represents the theoretical limit of the EQE for this particular system and device.

5.3. Conclusions

Host-Guest systems have been successfully applied as electroluminescent active layers in LECs. Using this approach, the following features have been demonstrated: a) the device efficiency can be considerably enhanced via the increase of the ϕ_{PL} in the solid film, b) the possibility to reduce the amount of low-abundant iridium-based emitters and c) the possibility to expand LECs to other class of ionic materials, such as cyanine dyes. Furthermore, cyanine dyes are easily adjusted and prepared in large quantities, they constitute and interesting class of ionic materials to develop low cost applications. Therefore, the host-guest approach is easily compatible with solution-processed light-emitting devices based on low iridium content.

5.4. Contributions of the author

Article 4: ***Host-guest blue light-emitting electrochemical cells.*** *Journal of Materials Chemistry C* **2014**, *2*, 1605-1611

Article 5: ***Light-emitting electrochemical cells using cyanine dyes as the active components.*** *Journal of the American Chemical Society* **2013**, *135*, 18008-18011.

Article 6: **Efficient light-emitting electrochemical cells using small molecular weight, ionic, host-guest systems.** *ECS Journal of Solid State Science and Technology* **2016**, *5,* R3160-R3163.

Journal of Materials Chemistry C

PAPER

View Article Online
View Journal | View Issue

Host–guest blue light-emitting electrochemical cells†

Cite this: J. Mater. Chem. C, 2014, 2, 1605

Antonio Pertegás,[a] Nail M. Shavaleev,*[b] Daniel Tordera,[a] Enrique Ortí,[a] Mohammad K. Nazeeruddin[b] and Henk J. Bolink*[a]

Received 8th October 2013
Accepted 25th November 2013

DOI: 10.1039/c3tc31983k

www.rsc.org/MaterialsC

Carbazole, a commonly used hole-transporter for organic electronics, has been modified with an imidazolium cation and a hexafluorophosphate counter-anion to give an ionic hole-transporter. It has been applied as one of the hosts in a host–guest blue light-emitting electrochemical cell (LEC) with the neutral blue emitter FIrPic. We have obtained efficient and bright blue LECs with an electroluminescence maximum at 474 nm and efficacy of 5 cd A^{-1} at a luminance of 420 cd m^{-2}, thereby demonstrating the potential of the ionic organic charge-transporters and of the host–guest architecture for LECs.

Introduction

Electroluminescent devices using organic semiconductors are becoming a serious alternative to conventional inorganic technology as their efficiencies and stabilities have improved significantly over the last few years.[1] The most efficient and stable organic light-emitting devices (OLEDs) are based on a multi-stack of low molecular-weight components that use air-sensitive charge-injection layers.[2] The multi-layer architecture is obtained by sequentially evaporating the active species under vacuum. OLEDs require rigorous encapsulation to prevent degradation of the charge-injection layers.[3,4]

Another type of electroluminescent device, referred to as the light-emitting electrochemical cell (LEC), has a simpler architecture and does not rely on air-sensitive charge-injection layers,[5–10] which simplifies its preparation and makes it more cost-efficient. In its simplest form, the LEC consists of a single emitting layer of either an ionic transition-metal complex (iTMC)[9] or a neutral light-emitting material (usually a polymer) mixed with an ionic transporter and a salt.[8,10] The presence of mobile ions facilitates the formation of ionic junctions that lower the barrier for charge injection and make the LEC independent of the work function of the electrode material.[11–17]

Despite these advances, the lack of efficient blue LECs remains a problem. Although several blue LECs have been reported, they exhibit low efficiency, luminance and lifetime.[18–23] Efficacies of up to 18.3 cd A^{-1} at a luminance of 14.5 cd m^{-2} have been reported for blue-green LECs.[22] For deeper-blue emission, the performances are worse: 2.6 cd A^{-1} at 5.3 cd m^{-2} for a sky-blue LEC[23] and 0.65 cd A^{-1} at 39 cd m^{-2} for the bluest LEC reported so far.[19] With polymers as the active material in a tri-layer structure, an efficient LEC was made (5.3 cd A^{-1}).[24] However, in general, the stability of blue LECs is low, from minutes to a few hours; moreover, their colour stability is rarely discussed.

In iTMC–LECs, the iTMC is the only component involved both in charge transport and in emission. With blue LECs, these processes are challenging, because they involve high-energy excitons (blue emitters have a large energy gap between the lowest unoccupied and the highest occupied molecular orbitals). The same problem occurs in OLEDs, which is a reason for the continued search for stable and efficient blue emitters. In OLEDs, charge transport is usually not performed by the emitter but by the specially designed electron- and hole-transporters.[25] In contrast, in LECs, charge transport occurs *via* the emitter and involves its reduction and oxidation. Because charge transport in blue LECs forms high-energy species, efficient blue LECs are hard-to-make. Hence, in LECs, it is of interest to decouple the charge transport and the emission by using different molecules for these processes. LECs rely on ionic movement to reduce the charge injection barriers; therefore, in the LEC, the charge-transporter must be mixed with the emitter and, more importantly, the ionic movement must be maintained; for example, host–guest orange and red LECs have been made with moderate band-gap iTMCs as the host.[26–29]

Here, we report a wide band-gap ionic hole-transporter **NMS25** suitable for blue light-emitting guests. **NMS25** is an arylcarbazole modified with an imidazolium cation and a hexafluorophosphate counter-anion (Scheme 1). **NMS25** was mixed with a neutral polar electron-transporter **SPPO13** and a neutral blue-phosphorescent iridium(III) emitter **FIrPic** (Scheme 1). We show that the combination of these low molecular weight compounds, when they are sandwiched between two air-stable

[a]Instituto de Ciencia Molecular, Universidad de Valencia, C/Catedrático J. Beltrán 2, ES-46980 Paterna, Valencia, Spain. E-mail: henk.bolink@uv.es

[b]Laboratory of Photonics and Interfaces, Institute of Chemical Sciences and Engineering, École Polytechnique Fédérale de Lausanne, CH-1015 Lausanne, Switzerland. E-mail: shava@mail.ru; Fax: +41 21 693 4111; Tel: +41 21 693 6124

† Electronic supplementary information (ESI) available: Spectroscopy and electrochemistry of **NMS25**. See DOI: 10.1039/c3tc31983k

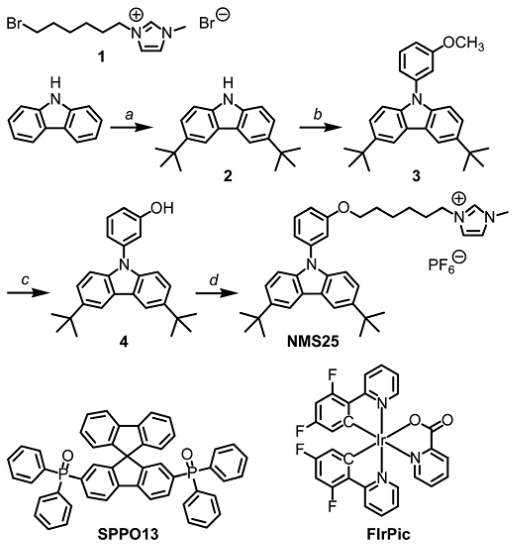

Scheme 1 Synthesis of **NMS25**: (a) $AlCl_3$, *tert*-butyl chloride, CH_2Cl_2, under Ar, 0 °C to RT; (b) 3-iodoanisole, Cs_2CO_3, Cu_2O, DMF, under Ar, 120 °C; (c) pyridine hydrochloride, under Ar, 200 °C; (d) **1**, K_2CO_3, DMF, under Ar, 60 °C. Structures of **SPPO13** and **FIrPic**.

electrodes, gives efficient blue-electroluminescent devices that function as LECs, with a slow turn-on determined by the movement of ions, and that reach an efficacy of 5 cd A^{-1} at a luminance of 420 cd m^{-2}.

Results and discussion

Synthesis and characterization

NMS25 was prepared in a multi-step procedure, which was upscaled to give up to 4 g of the product (Scheme 1). In **NMS25**, the *tert*-butyl groups were added to improve the solubility and to block electrochemically-reactive C3 and C6 positions of the carbazole; a long hexyloxy-chain was introduced to prevent interaction of the imidazolium cation with the carbazole. Imidazolium was chosen because it is optically-transparent and electrochemically-inert. **NMS25** is a white solid that is soluble in polar organic solvents; it exhibits electronic absorption with a cut-off at 365 nm in dichloromethane solution (Fig. S1, ESI†). The redox potentials for **NMS25** were measured by cyclic voltammetry. In acetonitrile, **NMS25** undergoes reversible oxidation of the carbazole at 0.77 V (against ferrocene couple), confirming its hole-transport properties, but no reduction down to −2.7 V (Fig. S2, ESI†).

Electroluminescence devices

Two-layer LECs were prepared by spin-coating from solution. An 80 nm layer of PEDOT:PSS was spin-coated on ITO-glass to increase the reproducibility of the devices. Then, an 80 nm layer of **NMS25**, **SPPO13** and **FIrPic** was deposited from an anisole solution. Aluminium was used as the top electrode.

To find the optimum ratio of hole- and electron-transporters, we evaluated devices with various mass ratios of **NMS25**:**SPPO13** (matrix; Fig. 1). The device configuration was: ITO/PEDOT:PSS (80 nm)/matrix:**FIrPic** (80 nm; with 10 wt% **FIrPic**) with the ionic liquid (IL) 1-butyl-3-methylimidazolium tetrafluoroborate added in a 4 : 1 molar ratio of matrix:IL/Al. The LECs were run with a block-wave pulsed current at a frequency of 1000 Hz and a duty cycle of 50% at an average density of 100 A m^{-2}.

All of the devices exhibit blue electroluminescence from **FIrPic** with a maximum at 474 nm and with the typical characteristics of LECs (Fig. 1–4). In pulsed-current mode, the LECs exhibit a rapid decrease of the initially high driving voltage to a lower steady-state value (Fig. 1–4). This is caused by the decrease in injection barriers for electrons and holes as ions migrate to the electrodes. The maximum luminance (L_{max}) and the time when it is reached (t_{max}) vary significantly for the different LECs, thereby complicating the lifetime comparison (as lifetime, for example, defined by the time it takes for the luminance to decrease to half of its maximum value, $t_{1/2}$, counted from $t = 0$, depends on the luminance). Kalyuzhny *et al.* suggested[30] to characterize the LEC by the total emitted energy (E_{tot}) up to the time when the luminance decreases to the 1/5 of its maximum.

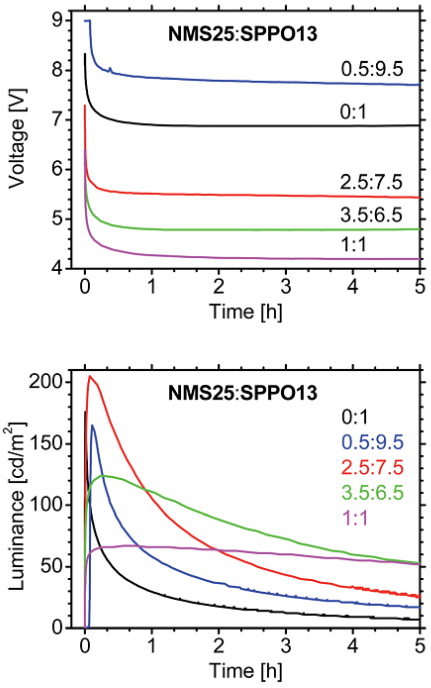

Fig. 1 Time-dependence of voltage and luminance for LECs with various mass ratios of **NMS25**:**SPPO13** (matrix) with 10 wt% **FIrPic** and with a 4 : 1 molar ratio matrix:IL 80 nm emitting layer (block-wave pulsed current; 1000 Hz; 50% duty cycle; average density 100 A m^{-2}).

Table 1 Performance of LECs at a pulsed current of 100 A m^{-2} (Fig. 1)

NMS25:SPPO13 (mass)	t_{max} (min)	L_{max} (cd m^{-2})	$t_{1/2}$ (h)	E_{tot} (J)	Eff_{max} (cd A^{-1})	EQE_{max} (%)
0 : 1	0.4	176	0.1	0.01	1.7	0.6
0.5 : 9.5	6.6	165	0.6	0.02	1.6	0.6
2.5 : 7.5	4.2	205	1.1	0.03	1.9	0.8
3.5 : 6.5	14	124	3.9	0.07	1.2	0.5
1 : 1	41	67	14	0.13	0.6	0.3

Table 1 summarizes the performance of LECs. The LEC with the longest lifetime and the highest total emitted energy had an emitting layer with a 1 : 1 mass ratio of **NMS25:SPPO13** (Table 1); its steady-state driving voltage was the lowest, indicating optimized charge-injection/transport (Fig. 1). Hence, this LEC was chosen for optimization.

The thickness of the emitting layer changes the LEC performance;[20] therefore, we varied it from 40 to 80 and to 100 nm (Fig. 2). Although the driving voltage increases for thicker layers, the highest luminance was achieved with an 80 nm layer (Fig. 2). The driving conditions were evaluated by changing the average current density[31] from 25 to 100 A m^{-2}, with the optimum determined to be 75 A m^{-2}.

There are two salts in the optimized LEC: the ionic hole-transporter and the IL. A device was also prepared without IL to confirm that it can function as a LEC by using only the ions from **NMS25** (Fig. 3). The LEC without the IL exhibits a higher maximum luminance and efficiency, but a higher driving voltage and a lower stability of the luminance than does the LEC with the IL (Fig. 3).

Here, we demonstrate the potential of the host–guest LECs in terms of efficiency and luminance (in previous reports,[19,23] the stability of blue LECs was low and the focus was on the efficiency). The LEC (without the IL) was optimized by annealing the emitting layer for 1 h at 100 °C prior to the evaporation of the top contact (the annealing changes the morphology and increases the photoluminescence quantum yield of the active layer[32]); the thus manufactured blue LEC exhibits a current efficacy of 5 cd A^{-1} at a luminance of 420 cd m^{-2} (Fig. 4). These values are significantly higher than are those previously reported for blue LECs.[19,21,23] The lifetime of the optimized LEC (without the IL) is short (Fig. 4); however, it is possible to increase it by adding the IL (Fig. 3 and Table 1).

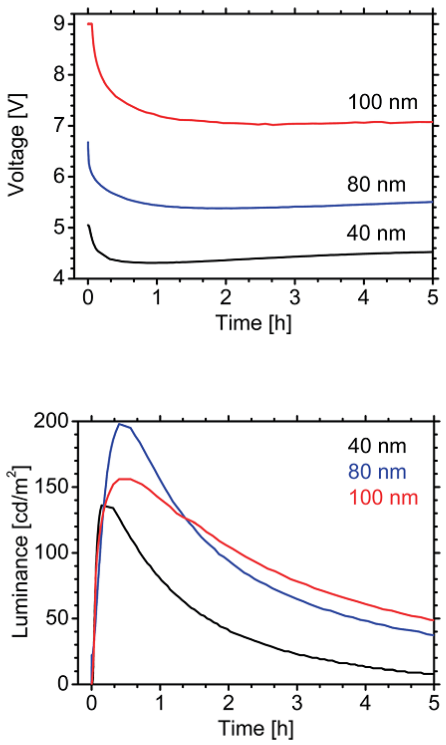

Fig. 2 Time-dependence of voltage and luminance for LECs with various thicknesses of the emitting layer: **NMS25**:**SPPO13** (1 : 1 by mass) with 10 wt% **FIrPic** (without IL); pulsed current (1000 Hz; 50% duty cycle; average density 100 A m^{-2}).

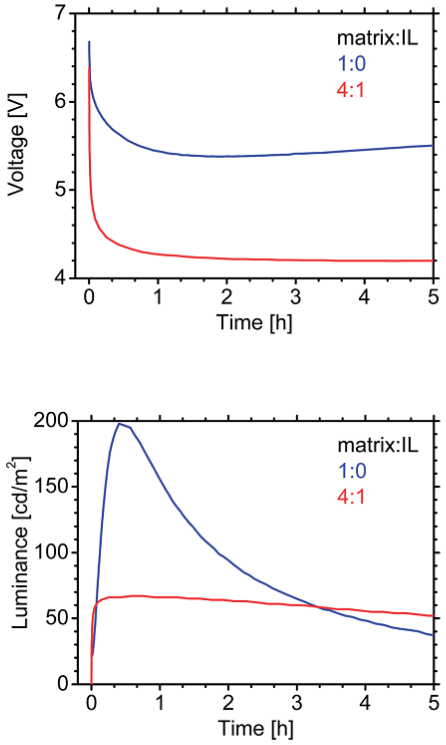

Fig. 3 Time-dependence of voltage and luminance for LECs with and without an ionic liquid (IL; in molar ratio): 80 nm emitting layer; **NMS25**:**SPPO13** (matrix; 1 : 1 by mass) with 10 wt% **FIrPic**; pulsed current (1000 Hz; 50% duty cycle; average density 100 A m^{-2}).

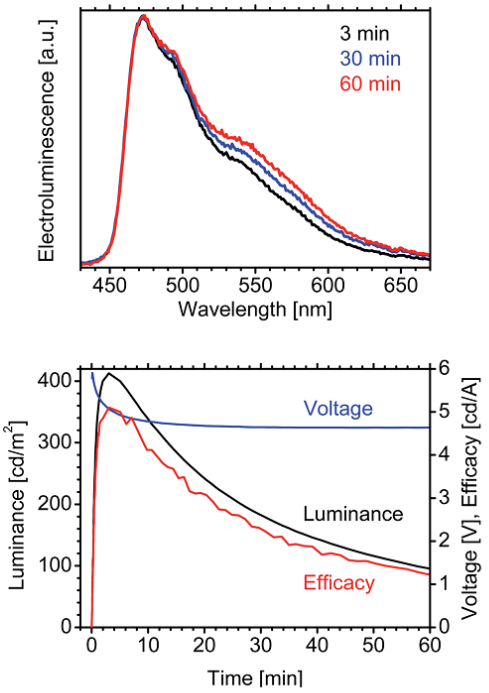

Fig. 4 Time-dependence of electroluminescence spectrum, luminance, voltage and efficacy of optimized LEC (1 : 1 by mass of **NMS25**:**SPPO13** with 10 wt% **FIrPic**; 80 nm emitting layer; annealed at 100 °C for 1 h; without IL; block-wave pulsed current; 1000 Hz; 50% duty cycle; average density 75 A m^{-2}).

Table 2 CIE coordinates for optimized LEC (Fig. 4)

t (min)	CIE (x)	CIE (y)	λ_{max} (nm)
3	0.214	0.377	473
5	0.217	0.379	474
10	0.219	0.380	474
30	0.230	0.389	473
60	0.242	0.400	474

In the optimized device, **FIrPic** exhibits only small red-shift of electroluminescence, that is, the host–guest LEC gives stable blue electroluminescence during the 60 min of work (Fig. 4 and Table 2). In contrast, in previous reports, the electroluminescence of blue iTMC–LECs underwent significant red-shift.[33,34]

Conclusions

Ionic derivatives of charge-transport hosts are successfully applied in host–guest LECs. The performance of these LECs depends on the amount and type of the ions. For a blue LEC, we achieve high colour stability and a maximum efficacy of 5 cd A^{-1} at a luminance of 420 cd m^{-2}. One can modify neutral charge-transporters with a suitable ionic group to optimize their performance in organic electronics.

Experimental

Materials and methods

Purification and handling of all compounds were carried out under air. All products were stored in the dark. Chemicals from commercial suppliers were used without purification. Chromatography was performed on a column with an i.d. of 30 mm on silica gel 60 (Fluka, Nr 60752). The progress of reactions and the elution of products were followed on TLC plates (silica gel 60 F_{254} on aluminum sheets, Merck).

Elemental analyses were performed by Dr E. Solari, Service for Elemental Analysis, Institute of Chemical Sciences and Engineering (ISIC EPFL). ^{1}H and ^{13}C NMR spectra were recorded with Bruker AV400 (400 MHz) and AVIII-400 (400 MHz) spectrometers. Mass spectra were recorded with Q-TOF Ultima (Waters) and TSQ7000 (Thermo Fisher) spectrometers (Mass-Spectroscopy Service, ISIC EPFL).

Synthesis of NMS25

Imidazolium salt, 1. The reaction was performed under air while protected from the moisture with a $CaCl_2$-filled tube. 1,6-Dibromohexane (5 mL, 7.9 g, 32 mmol, excess, Fluka) was added to a solution of 1-methylimidazole (1 mL, 1.03 g, 12.5 mmol, Fluka) in acetone (10 mL) at RT. The mixture was stirred at 40 °C overnight to give a white suspension. It was filtered to remove white solid, which is the bis-substituted by-product. The solid was washed with acetone and discarded. The combined filtrates were rotor-evaporated to remove the acetone. Chromatography was performed on silica (20 g) with CH_2Cl_2 to remove the starting material and with 5–10% of CH_3OH in CH_2Cl_2 to recover the product (TLC were developed with I_2; the bis-substituted imidazolium salt follows the product). Viscous pale yellow oil: 2.56 g (7.85 mmol, 63%; $C_{10}H_{18}Br_2N_2$; M_W 326.07). ^{1}H NMR (400 MHz, DMSO-d_6): δ = 9.12 (s, 1H), 7.79–7.75 (m, 1H), 7.72–7.68 (m, 1H), 4.15 (t, J = 7.2 Hz, 2H), 3.84 (s, 3H), 3.52 (t, J = 6.8 Hz, 2H), 1.83–1.73 (m, 4H), 1.45–1.35 (m, 2H), 1.30–1.20 (m, 2H) ppm. ESI$^+$ MS: m/z 245.3 ({M − Br}$^+$, 100%).

Scaled-up synthesis. 1-Methylimidazole (2 mL, 2.06 g, 25 mmol) and 1,6-dibromohexane (15 mL, 24 g, 97 mmol, excess) in acetone (25 mL) gave 6 g (18.4 mmol, 74%) of the product. Chromatography was performed on silica (30 g) with 0–1% CH_3OH in CH_2Cl_2 to remove the starting material and with 7.5% CH_3OH in CH_2Cl_2 to recover **1**.

Di-*tert*-butyl carbazole, 2. The reaction was performed under argon in dry solvents. Carbazole (5 g, 29.9 mmol) was suspended in CH_2Cl_2 (100 mL) at RT. $AlCl_3$ (4 g, 29.9 mmol, Sigma-Aldrich) was added to give a brown suspension. It was cooled to 0 °C and a solution of *tert*-butyl chloride (6.51 mL, 5.53 g, 59.8 mmol, Aldrich) in CH_2Cl_2 (20 mL) was added drop-wise over 10 min to give a dark yellow suspension. It was allowed to warm to RT, and it was stirred overnight to give brown solution. It was cooled in an ice bath and very cautiously quenched with ice [**Caution**: the quenching is highly exothermic and has an

induction period (!); external cooling (ice bath) is recommended]. Extraction with water and CH_2Cl_2 provided at first an orange cloudy organic layer that after multiple washings with water became pale yellow and clear. Hexane (100 mL) was added and CH_2Cl_2 was rotor-evaporated to provide a suspension of the product in hexane. It was cooled to RT. The solid was filtered (the filtrate was yellow) and washed with a small volume of hexane. White crystalline solid: 2.90 g (10.4 mmol, 35%). Anal. calcd for $C_{20}H_{25}N$ (M_W 279.42): C, 85.97; H, 9.02; N, 5.01. Found: C, 86.06; H, 8.94; N, 4.98. ^{1}H NMR (400 MHz, DMSO-d_6): δ = 10.90 (s, 1H), 8.12 (d, J = 1.2 Hz, 2H), 7.41 (dd, J = 8.4, 1.6 Hz, 2H), 7.34 (d, J = 8.4 Hz, 2H), 1.39 (s, 18H) ppm. ^{13}C NMR (100 MHz, $CDCl_3$): δ = 142.5, 138.3, 123.8, 123.5, 116.4, 110.3, 35.0, 32.3 ppm. ESI$^+$ MS: m/z 280.3 ($\{M + H\}^+$, 100%).

Aryl carbazole, 3. The reaction was performed under argon in dry solvents.[35] 3-Iodoanisole (0.45 mL, 0.88 g, 3.77 mmol, small excess, Aldrich), di-*tert*-butyl carbazole **2** (1 g, 3.58 mmol), Cs_2CO_3 (3.7 g, 11 mmol, excess, Aldrich), Cu_2O powder (<5 μm, 74 mg, 0.52 mmol, catalyst, Aldrich) in DMF (4.5 mL; 99.8%, extra dry over molecular sieve, AcroSeal, Acros) were stirred at 120 °C for 24 h to give a brownish-green suspension. It was cooled to RT, and it was extracted with water and ether (dark brown solid remains at the phase interface, and the aqueous phase remains a brown suspension). The organic layer was washed with water and evaporated. Chromatography was performed on silica (15 g) with hexane–CH_2Cl_2 (6/1) to provide the crude product as colourless oil (the starting carbazole is one of the main impurities). It was dissolved in a minimum volume (5 mL) of CH_2Cl_2. Ethanol (15 mL) was added and CH_2Cl_2 was rotor-evaporated leaving a suspension of the product in ethanol (the compound easily forms oversaturated ethanol solution; sonication, scratching and seeding may be required to induce the precipitation). The suspension was cooled to 0 °C, filtered, and washed with a small volume of cold (−15 °C) ethanol. White solid: 927 mg (2.40 mmol, 67%; $C_{27}H_{31}NO$; M_W 385.54). ^{1}H NMR (400 MHz, $CDCl_3$): δ = 8.16 (d, J = 2.0 Hz, 2H), 7.56–7.46 (m, 3H), 7.41 (d, J = 8.8 Hz, 2H), 7.20–7.16 (m, 1H), 7.13 (t, J = 2.0 Hz, 1H), 7.00 (dd, J = 8.4, 2.4 Hz, 1H), 3.88 (s, 3H), 1.50 (s, 18H) ppm. **3** is soluble in hexane.

Scaled-up synthesis. 3-Iodoanisole (1.8 mL, 3.53 g, 15.1 mmol), di-*tert*-butyl carbazole **2** (4 g, 14.3 mmol), Cs_2CO_3 (17 g, 52 mmol), Cu_2O powder (296 mg, 1.55 mmol) in DMF (12 mL; 99.8%, extra dry over molecular sieve, AcroSeal, Acros) were stirred at 120 °C for 24 h. Chromatography on silica (20 g) and re-crystallization from CH_2Cl_2 and ethanol (20 mL) gave 4.6 g (11.9 mmol, 83%) of **3**.

Phenol-carbazole, 4. The reaction was performed under argon. Aryl carbazole **3** (450 mg, 1.17 mmol) and pyridine hydrochloride (Py·HCl, 15 g, 0.13 mol, excess, used as a reagent and as a solvent, Aldrich) were stirred at 200 °C for 6 h to give pale green solution. It was cooled to RT. The solid reaction mixture was extracted with CH_2Cl_2–water. The organic layer was thoroughly washed with water to remove Py·HCl. Evaporation provided pale-violet foam. Chromatography was performed on silica (12 g) with hexane–CH_2Cl_2 (3/1) to remove the starting material and with hexane–CH_2Cl_2 (1/2) to recover the product as a colourless fraction (the fraction may look pale yellow on the column; a yellow impurity follows the product; intensely coloured by-products remain at the top of the column). Colourless or pale yellow oil which easily foams and slowly solidifies to white or pale green solid: 256 mg (0.69 mmol, 59%; $C_{26}H_{29}NO$; M_W 371.51). The yield can be improved by extending the reaction time. ^{1}H NMR (400 MHz, DMSO-d_6): δ = 9.9 (s, br, 1H, OH), 8.27 (d, J = 1.6 Hz, 2H), 7.47 (dd, J = 8.8, 2.0 Hz, 2H), 7.43 (t, J = 8.0 Hz, 1H), 7.32 (dd, J = 8.8, 0.4 Hz, 2H), 6.99 (ddd, J = 8.0, 2.0, 0.8 Hz, 1H), 6.93 (t, J = 2.0 Hz, 1H), 6.88 (ddd, J = 8.0, 2.4, 0.8 Hz, 1H), 1.41 (s, 18H) ppm. Solid **4** turns green upon long exposure to air at RT, but it can be safely stored for indefinite time in a freezer.

Scaled-up synthesis. Aryl carbazole **3** (2.12 g, 5.49 mmol) and Py·HCl (40 g, 0.35 mol) were stirred at 200 °C for 7.5 h. Chromatography on silica (30 g) gave 1.25 g (3.36 mmol, 61%) of **4**.

Scaled-up synthesis. Aryl carbazole **3** (4.6 g, 11.9 mmol) and Py·HCl (80 g, 0.69 mol) were stirred at 200 °C for 8 h. Chromatography on silica (30 g) gave 3.18 g (8.56 mmol, 72%) of **4**.

Carbazole host, NMS25

Batch 1. The reaction was performed under argon in dry solvents. Phenol-carbazole **4** (241 mg, 0.65 mmol), imidazolium salt **1** (212 mg, 0.65 mmol), and K_2CO_3 (90 mg, 0.65 mmol) were stirred in DMF (4 mL; 99.8%, extra dry over molecular sieve, AcroSeal, Acros) at 60 °C for 24 h to give a white suspension. It was diluted with water (100 mL) containing KPF_6 (for anion exchange; 0.55 g, 2.99 mmol, excess). The resulting suspension was stirred for 30 min and filtered. The solid was washed with water and hexane. It was extracted with water–CH_2Cl_2. The organic layer was washed with water and evaporated. Chromatography was performed on silica (15 g) with 0.5% CH_3OH in CH_2Cl_2 to remove impurities and with 2% CH_3OH in CH_2Cl_2 to recover the pure product. The product may separate as thick and easily foaming oil; in this case, mixing with ether and sonication followed by evaporation of the solvent converts the oil to a solid. White solid: 300 mg (0.44 mmol, 68%). Anal. calcd for $C_{36}H_{46}F_6N_3OP$ (M_W 681.73): C, 63.42; H, 6.80; N, 6.16. Found: C, 63.66; H, 6.84; N, 6.24. ^{1}H NMR (400 MHz, CD_2Cl_2): δ = 8.55 (s, 1H), 8.18 (d, J = 2.0 Hz, 2H), 7.55–7.47 (m, 3H), 7.40 (d, J = 8.4 Hz, 2H), 7.25 (s, br, 1H), 7.22 (s, br, 1H), 7.17 (dd, J = 7.6, 1.2 Hz, 1H), 7.09 (t, J = 2.4 Hz, 1H), 7.00 (dd, J = 8.0, 2.0 Hz, 1H), 4.20 (t, J = 7.2 Hz, 2H), 4.04 (t, J = 6.0 Hz, 2H), 3.94 (s, 3H), 2.01–1.91 (m, 2H), 1.90–1.80 (m, 2H), 1.65–1.40 (m, 4H, obscured by signal of water protons), 1.48 (s, 18H) ppm. ^{1}H NMR (400 MHz, DMSO-d_6): δ = 9.08 (s, 1H), 8.28 (d, J = 2.0 Hz, 2H), 7.76 (t, J = 1.6 Hz, 1H), 7.67 (t, J = 1.6 Hz, 1H), 7.54 (t, J = 8.0 Hz, 1H), 7.47 (dd, J = 8.4, 1.6 Hz, 2H), 7.32 (d, J = 8.4 Hz, 2H), 7.15 (d, J = 7.6 Hz, 1H), 7.10 (t, J = 2.0 Hz, 1H), 7.04 (dd, J = 8.4, 2.4 Hz, 1H), 4.15 (t, J = 6.8 Hz, 2H), 4.04 (t, J = 6.4 Hz, 2H), 3.82 (s, 3H), 1.86–1.69 (m, 4H), 1.41 (s, 18H), 1.52–1.20 (m, 2H), 1.37–1.26 (m, 2H) ppm. ^{13}C NMR (100 MHz, DMSO-d_6): δ = 160.6, 143.2, 139.2, 139.2, 137.2, 131.5, 124.3, 124.3, 123.6, 122.9, 118.9, 117.3, 114.3, 112.7, 109.8, 68.3, 49.4, 36.4, 35.1, 32.5, 30.0, 29.1, 26.0, 25.6 ppm. ESI$^+$ TOF MS: m/z 536.36 ($\{M - PF_6\}^+$, 100%).

Batch 2, scaled-up synthesis. Phenol-carbazole **4** (1.25 g, 3.36 mmol), imidazolium salt **1** (1.10 g, 3.37 mmol), and K_2CO_3 (0.47 g, 3.40 mmol) in DMF (8 mL; 99.8%, extra dry over molecular sieve, AcroSeal, Acros) at 60 °C for 24 h gave a pale orange

suspension. Work-up with KPF_6 (for anion exchange; 4 g, 22 mmol) and chromatography on silica (35 g) with 0.5–2.0% CH_3OH in CH_2Cl_2 (pale green impurity precedes the product) gave 1.45 g of the product that contained a small amount of impurity. The product was dissolved in CH_2Cl_2 (5 mL) and poured into ether (>200 mL). A solution formed at first, but a fine dense precipitate appeared after 1 min of stirring. It was filtered and washed with ether to provide the pure product: 1.38 g (2.03 mmol, 60%).

Batch 3, scaled-up synthesis. Phenol-carbazole **4** (3.18 g, 8.56 mmol), imidazolium salt **1** (2.79 g, 8.56 mmol), and K_2CO_3 (1.20 g, 8.68 mmol) in DMF (9 mL; 99.8%, Extra Dry over Molecular Sieve, AcroSeal, Acros) at 60 °C for 24 h gave a pale orange suspension. Work-up was performed with KPF_6 (for anion exchange; 13 g, 71 mmol) and by chromatography on silica (30 g) with 0.5–2.0% CH_3OH in CH_2Cl_2. The product was dissolved in CH_2Cl_2 (15 mL) and poured into ether (>350 mL). A solution formed at first, but a fine dense precipitate appeared after 1 min of stirring. It was filtered and washed with ether to provide the pure product: 4.17 g (6.12 mmol, 71%).

Electroluminescence devices. All commercial materials were used as received: aqueous dispersion of poly(3,4-ethylenedioxythiophene):poly(styrenesulfonate) (PEDOT:PSS, CLEVIOS™ P VP Al 4083; Heraeus); ionic liquid (IL) 1-butyl-3-methyl-imidazolium tetrafluoroborate [Bmim][BF_4] (Aldrich); **SPPO13** and **FIrPic** (Luminescence Technology Corp.).

The LEC devices were made as follows. Indium tin oxide ITO-coated glass plates were patterned by conventional photolithography (Naranjo Substrates). The substrates were cleaned ultrasonically in water-soap, water and 2-propanol baths. After drying, the substrates were placed in a UV–ozone cleaner (Jelight 42-220) for 20 min. An 80 nm layer of PEDOT:PSS was spin-coated on the ITO-glass substrate. For the emitting layer preparation, the devices were spin-coated at 1000 rpm for 30 s from an anisole solution containing hosts (with 10% wt of **FIrPic**). To find the optimum ratio of **NMS25**:**SPPO13** (matrix), we employed solutions with mass ratios of 1 : 0, 0.5 : 9.5, 2.5 : 7.5, 3.5 : 6.5, 1 : 1 (matrix + **FIrPic**; 30 mg mL^{-1}) for each device and we added [Bmim][BF_4] to give a 4 : 1 molar ratio of matrix:IL. The effect of the IL was checked by preparing the emitting layer from a solution with a 1 : 1 mass ratio **NMS25**:**SPPO13** (matrix + **FIrPic**; 30 mg mL^{-1}), without adding any IL. To test the effect of thickness, the solutions of 20, 30 and 40 mg mL^{-1} with a 1 : 1 mass ratio **NMS25**:**SPPO13** without IL were spin-coated to give a film thickness of 40, 80 and 100 nm, respectively. After deposition of the emitting layer, the devices were transferred into an inert atmosphere glovebox, where the aluminium electrode was thermally evaporated using a shadow mask. The size of the LEC was 6.5 mm^2.

The thickness of the films was determined with an Ambios XP-1 profilometer. Thin film photoluminescence spectra and quantum yields were measured with a Hamamatsu C9920-02 Absolute PL Quantum Yield Measurement System. It consists of an excitation light source (a xenon lamp linked to a monochromator), an integration sphere and a multi-channel spectrometer. Time dependence of luminance and voltage was measured by applying pulsed current and by monitoring the voltage and the luminance simultaneously by a True Colour Sensor MAZeT (MTCSICT Sensor) using a Lifetime Test System designed by BoTEST (Botest OLT OLED Lifetime-Test System). Electroluminescence spectra were recorded with an Avantes fiber-optics photo-spectrometer. The devices were not encapsulated and were characterized inside the glovebox.

Acknowledgements

This work is supported by the European Union (CELLO, STRP 248043; http://www.cello-project.eu/) and the Spanish Ministry of Economy and Competitiveness (MINECO) (MAT2011-24594, CSD2007-00010, and CTQ2009-08790). A.P. and D.T. acknowledge the support of a FPI and FPU grant of the MINECO and MECD, respectively.

References

1 S. Reineke, F. Lindner, G. Schwartz, N. Seidler, K. Walzer, B. Lüssem and K. Leo, *Nature*, 2009, **459**, 234.
2 K. Walzer, B. Maennig, M. Pfeiffer and K. Leo, *Chem. Rev.*, 2007, **107**, 1233.
3 L. Xiao, S.-J. Su, Y. Agata, H. Lan and J. Kido, *Adv. Mater.*, 2009, **21**, 1271.
4 C. Rothe, C.-J. Chiang, V. Jankus, K. Abdullah, X. Zeng, R. Jitchati, A. S. Batsanov, M. R. Bryce and A. P. Monkman, *Adv. Funct. Mater.*, 2009, **19**, 2038.
5 Q. B. Pei, G. Yu, C. Zhang, Y. Yang and A. J. Heeger, *Science*, 1995, **269**, 1086.
6 K. M. Maness, R. H. Terrill, T. J. Meyer, R. W. Murray and R. M. Wightman, *J. Am. Chem. Soc.*, 1996, **118**, 10609.
7 J. D. Slinker, A. A. Gorodetsky, M. S. Lowry, J. J. Wang, S. Parker, R. Rohl, S. Bernhard and G. G. Malliaras, *J. Am. Chem. Soc.*, 2004, **126**, 2763.
8 Q. J. Sun, Y. F. Li and Q. B. Pei, *J. Disp. Technol.*, 2007, **3**, 211.
9 R. D. Costa, E. Ortí, H. J. Bolink, F. Monti, G. Accorsi and N. Armaroli, *Angew. Chem., Int. Ed.*, 2012, **51**, 8178.
10 S. Tang, W.-Y. Tan, X.-H. Zhu and L. Edman, *Chem. Commun.*, 2013, **49**, 4926.
11 D. J. Dick, A. J. Heeger, Y. Yang and Q. B. Pei, *Adv. Mater.*, 1996, **8**, 985.
12 J. D. Slinker, J. A. DeFranco, M. J. Jaquith, W. R. Silveira, Y. W. Zhong, J. M. Moran-Mirabal, H. G. Craighead, H. D. Abruña, J. A. Marohn and G. G. Malliaras, *Nat. Mater.*, 2007, **6**, 894.
13 P. Matyba, K. Maturova, M. Kemerink, N. D. Robinson and L. Edman, *Nat. Mater.*, 2009, **8**, 672.
14 S. van Reenen, P. Matyba, A. Dzwilewski, R. A. J. Janssen, L. Edman and M. Kemerink, *J. Am. Chem. Soc.*, 2010, **132**, 13776.
15 M. Lenes, G. García-Belmonte, D. Tordera, A. Pertegás, J. Bisquert and H. J. Bolink, *Adv. Funct. Mater.*, 2011, **21**, 1581.
16 P. Zalar, Z. B. Henson, G. C. Welch, G. C. Bazan and T. Q. Nguyen, *Angew. Chem., Int. Ed.*, 2012, **51**, 7495.
17 E. Zysman-Colman, J. D. Slinker, J. B. Parker, G. G. Malliaras and S. Bernhard, *Chem. Mater.*, 2008, **20**, 388.

18 A. B. Tamayo, S. Garon, T. Sajoto, P. I. Djurovich, I. M. Tsyba, R. Bau and M. E. Thompson, *Inorg. Chem.*, 2005, **44**, 8723.
19 L. He, L. Duan, J. Qiao, R. J. Wang, P. Wei, L. D. Wang and Y. Qiu, *Adv. Funct. Mater.*, 2008, **18**, 2123.
20 M. K. Nazeeruddin, R. T. Wegh, Z. Zhou, C. Klein, Q. Wang, F. De Angelis, S. Fantacci and M. Grätzel, *Inorg. Chem.*, 2006, **45**, 9245.
21 M. Mydlak, C. Bizzarri, D. Hartmann, W. Sarfert, G. Schmid and L. De Cola, *Adv. Funct. Mater.*, 2010, **20**, 1812.
22 L. He, L. A. Duan, J. A. Qiao, G. F. Dong, L. D. Wang and Y. Qiu, *Chem. Mater.*, 2010, **22**, 3535.
23 B. Chen, Y. H. Li, W. Yang, W. Luo and H. B. Wu, *Org. Electron.*, 2011, **12**, 766.
24 S. Tang, A. Sandström, J. F. Fang and L. Edman, *J. Am. Chem. Soc.*, 2012, **134**, 14050.
25 A. Chaskar, H.-F. Chen and K.-T. Wong, *Adv. Mater.*, 2011, **23**, 3876.
26 A. R. Hosseini, C. Y. Koh, J. D. Slinker, S. Flores-Torres, H. D. Abruña and G. G. Malliaras, *Chem. Mater.*, 2005, **17**, 6114.
27 H. C. Su, C. C. Wu, F. C. Fang and K. T. Wong, *Appl. Phys. Lett.*, 2006, **89**, 26118.
28 H. C. Su, H. F. Chen, Y. C. Shen, C. T. Liao and K. T. Wong, *J. Mater. Chem.*, 2011, **21**, 9653.
29 C.-T. Liao, H.-F. Chen, H.-C. Su and K.-T. Wong, *Phys. Chem. Chem. Phys.*, 2012, **14**, 1262.
30 G. Kalyuzhny, M. Buda, J. McNeill, P. Barbara and A. J. Bard, *J. Am. Chem. Soc.*, 2003, **125**, 6272.
31 D. Tordera, J. Frey, D. Vonlanthen, E. C. Constable, A. Pertegás, E. Ortí, H. J. Bolink, E. Baranoff and M. K. Nazeeruddin, *Adv. Energy Mater.*, 2013, **3**, 1338.
32 C. Y. Liu and A. J. Bard, *Appl. Phys. Lett.*, 2003, **83**, 5431.
33 H. J. Bolink, L. Cappelli, S. Cheylan, E. Coronado, R. D. Costa, N. Lardies, M. K. Nazeeruddin and E. Orti, *J. Mater. Chem.*, 2007, **17**, 5032.
34 S. B. Meier, W. Sarfert, J. M. Junquera-Hernandez, M. Delgado, D. Tordera, E. Orti, H. J. Bolink, F. Kessler, R. Scopelliti, M. Gratzel, M. K. Nazeeruddin and E. Baranoff, *J. Mater. Chem. C*, 2013, **1**, 58.
35 A. Correa and C. Bolm, *Adv. Synth. Catal.*, 2007, **349**, 2673.

The following article has been deleted due to publisher copyright policy.

Antonio Pertegás, Daniel Tordera, Juan J. Serrano-Pérez, Enrique Ortí, and Henk J. Bolink, Light-Emitting Electrochemical Cells Using Cyanine Dyes as the Active Components. *J. Am. Chem. Soc.*, 2013, 135 (48), pp 18008−18011

DOI: 10.1021/ja407515w

The following article has been deleted due to publisher copyright policy.

Antonio Pertegás, Daniel Tordera, Juan J. Serrano-Pérez, Enrique Ortí, and Henk J. Bolink, Light-Emitting Electrochemical Cells Using Cyanine Dyes as the Active Components. *J. Am. Chem. Soc.*, 2013, 135 (48), pp 18008−18011

DOI: 10.1021/ja407515w

The following article has been deleted due to publisher copyright policy.

Antonio Pertegás, Daniel Tordera, Juan J. Serrano-Pérez, Enrique Ortí, and Henk J. Bolink, Light-Emitting Electrochemical Cells Using Cyanine Dyes as the Active Components. *J. Am. Chem. Soc.*, 2013, 135 (48), pp 18008−18011

DOI: 10.1021/ja407515w

The following article has been deleted due to publisher copyright policy.

Antonio Pertegás, Daniel Tordera, Juan J. Serrano-Pérez, Enrique Ortí, and Henk J. Bolink, Light-Emitting Electrochemical Cells Using Cyanine Dyes as the Active Components. *J. Am. Chem. Soc.*, 2013, 135 (48), pp 18008−18011

DOI: 10.1021/ja407515w

The following article has been deleted due to publisher copyright policy.

Antonio Pertegas, Michael Yin Wong, Michele Sessolo, Eli Zysman-Colman and Henk J. Bolink, Efficient Light-Emitting Electrochemical Cells Using Small Molecular Weight, Ionic, Host-Guest Systems. *ECS J. Solid State Sci. Technol. 2016 volume 5, issue 1, R3160-R3163*

doi: 10.1149/2.0201601jss

The following article has been deleted due to publisher copyright policy.

Antonio Pertegas, Michael Yin Wong, Michele Sessolo, Eli Zysman-Colman and Henk J. Bolink, Efficient Light-Emitting Electrochemical Cells Using Small Molecular Weight, Ionic, Host-Guest Systems. *ECS J. Solid State Sci. Technol. 2016 volume 5, issue 1, R3160-R3163*

doi: 10.1149/2.0201601jss

6. Resumen de la tesis doctoral

6.1. Introducción

Debido al continuo aumento del consumo energético a escala global, el acceso a la energía podría verse comprometido en un periodo de 20-30 años como consecuencia del aumento poblacional. Además, este consumo, pone en riesgo el medio natural mediante las emisiones de gases de efecto invernadero. El consumo eléctrico destinado a iluminación supone actualmente cerca del 20% de la producción energética a nivel mundial, de modo que es posible alcanzar un importante ahorro energético mediante el uso de sistemas de iluminación más eficientes.

Concretamente, la generación de luz mediante uso de corriente eléctrica ha evolucionado durante cerca de un siglo, desde las tradicionales bombillas incandescentes hasta la aplicación de diodos emisores de luz basados en semiconductores inorgánicos (LEDs). De forma paralela, el campo de la electrónica orgánica ha experimentado un desarrollo espectacular en las últimas dos décadas dando lugar, entre otras aplicaciones, a los diodos orgánicos emisores de luz (OLEDs). El procesado de materiales orgánicos se adapta más fácilmente a nuevos diseños de dispositivos emisores de luz y es, a día de hoy, una realidad en pequeñas pantallas para dispositivos móviles o similares. Sin embargo, los OLEDs, presentan serias limitaciones que dificultan su aplicación en el mercado de la iluminación. Por una parte, requieren una estructura de multicapa orgánica, procesada(s) mediante técnicas de ultra alto vacío. Por otra, precisan del uso de electrodos sensibles al oxígeno y agua atmosféricos, por lo que es necesaria una encapsulación rigurosa del dispositivo. Estos requerimientos aumentan el coste de producción y, por tanto, dificultan el acceso a esta tecnología a escala global.

Sin embargo, existen otros tipos de dispositivos emisores de luz basados en compuestos orgánicos. Las células electroquímicas emisoras de luz (LECs) son dispositivos electroluminiscentes que presentan múltiples ventajas respecto a los OLEDs. Los LECs pueden ser fabricados mediante una única capa orgánica depositada a partir de la disolución entre dos electrodos estables al aire (cátodo de Au, Ag, Al). El

uso de estos electrodos, unido a la simple arquitectura de los LECs y su procesado desde la disolución, les hace compatibles con técnicas de fabricación de bajo coste. Además los LECs operan a bajos voltajes (bajo consumo) debido a la presencia de compuestos iónicos en la capa activa

Al aplicar una diferencia de potencial, los iones presentes en la capa activa, se disocian y se mueven hacia los correspondientes electrodos, reduciendo la energía necesaria para producir la inyección de cargas eléctricas (electrones y huecos) en la capa activa. La presencia de electrones y huecos en la capa activa da lugar a la formación de excitones que se pueden recombinar radiativamente emitiendo luz. Para que todos estos procesos tengan lugar en la capa activa de los LECs, es necesario que el material presente propiedades de transporte electrónico, además de un alto rendimiento cuántico de emisión (ϕ_{PL}).

Existe un amplio rango de materiales orgánicos que pueden emplearse en la fabricación de LECs. Sin embargo, desde su descubrimiento en 1995, los materiales más empleados han sido, por un lado, polímeros semiconductores neutros dopados con sales inorgánicas (p-LECs) y complejos de metales de transición iónicos (iTMC-LECs). En general, ambos tipos de materiales han alcanzado un funcionamiento óptimo, con buenos resultados en cuanto a estabilidad, eficiencia y altos valores de luminancia. Concretamente, los mejores resultados, en términos de eficiencia eléctrica, se han dado en iTMC-LECs basados en complejos de iridio(III) (Ir-iTMCs). En estos materiales, la emisión de luz se produce desde un estado triplete. La presencia de átomos pesados en la estructura molecular aumenta el acoplamiento spín-órbita y permite recolectar todos los excitones singlete y triplete generados mediante excitación eléctrica, alcanzando un alto rendimiento de emisión.

Desde los inicios de la tecnología LEC, ha existido un controvertido debate sobre el mecanismo de operación de los LECs. Después de una década de investigación, se ha resuelto como el mecanismo predominante: el *modelo de dopado electroquímico*. Este mecanismo ha permitido comprender, las principales limitaciones iniciales presentes la tecnología LEC y que pueden enumerarse como: a) largos tiempos de

encendido del dispositivo b) bajas eficiencias y c) baja estabilidad de operación. Multitud de científicos a nivel mundial han desarrollado soluciones a cada uno de estos problemas mediante diversas estrategias. Sin embargo, no ha sido posible obtener una solución conjunta a todos estos problemas, existiendo todavía como principales limitaciones:

1) Bajas eficiencias en comparación con los sistemas de iluminación actual (LEDs).
2) Obtención de emisión de luz azul que permita la fabricación de sistemas de iluminación con luz blanca.

6.2. Objetivos

La presente tesis se centra~~,~~ en el diseño y preparación de LECs con el fin de optimizar su máxima eficiencia mediante diferentes estrategias al modificar el ϕ_{PL}. En concreto, se ha trabajado sobre tres estrategias diferentes:

1) Modificación química del ligando auxiliar.
2) Estudio de la influencia de la presencia de impurezas cloruro en LECs.
3) Uso de sistemas matriz-dopante.

6.3. Metodología

Para llevar a cabo los objetivos de la tesis, la metodología general de trabajo comprende: a) el estudio de las propiedades fotofísicas de los materiales en estado sólido y/o disolución y b) optimización de las variables (grosor, composición y modo de operación) más relevantes que componen el dispositivo LEC.

La preparación de los dispositivos LEC se llevó a cabo en una sala limpia clase 10000 siguiendo el procedimiento siguiente: a) limpieza de los sustratos recubiertos de ITO (15 Ω $\square^{-1}$), b) deposición de las capas delgadas mediante spin-coating, c) evaporación térmica en alto vacío del electrodo de aluminio en evaporador integrado en caja seca

(MBraun <0.1ppm O_2 y H_2O). De esta forma los dispositivos se prepararon utilizando la estructura tipo sándwich siguiente: ITO/PEDOT:PSS/Active Layer/Al. Tras la preparación de los dispositivos, se llevó a cabo la caracterización de los mismos utilizando una corriente pulsada (onda cuadrada, 1000 Hz, 50% ciclo de trabajo) o un voltaje constante y midiendo el voltaje, la corriente eléctrica y la luminancia frente al tiempo utilizando el equipo Botest OLT OLED Lifetime-Test System. Durante la preparación de los dispositivos, se ha determinado el espesor de las capas que forman los LECs utilizando un perfilómetro Ambios XP-1 profilometer. En las condiciones de trabajo, el espesor total de las diferentes capas que forman el dispositivo, debe situarse en 200 nm. De este modo, la caracterización del espesor de las capas resulta determinante para obtener resultados reproducibles.

El estudio de las propiedades fotofísicas de los compuestos presentados en esta tesis se llevó en estado sólido depositando el material sobre un sustrato de cuarzo o bien en disolución empleando una concentración 10^{-5} M. Una vez preparada la muestra, (en estado sólido o en disolución se determinó el rendimiento cuántico y espectro de fotoluminiscencia) excitando cada muestra preparada en un esfera integradora modelo C9920-02 Absolute PL Quantum Yield Measurement System.

6.4. Mejorando las prestaciones de los LECs mediante modificación química

El primer punto se discutió en el capitulo 3. Este estudio se llevó a cabo utilizando una familia de Ir-iTMCs derivados del complejo $[Ir(ppy)_2(phbpy)][PF_6]$ (ppy = fenilpiridina; phbpy = 6-fenil-2,2′-bipiridina). Este complejo es conocido por mostrar un alto tiempo de vida al presentar una interacción tipo π-π entre el grupo fenilo en posición 6 del ligando bipiridina y el fenilo coordinado de la fenilpiridina. Sin embargo, tanto el complejo de referencia como sus derivados presentan, en general, baja eficiencia en LECs. La familia estudiada consistió en la

modificación química del ligando auxiliar mediante dos estrategias. Por un lado, su funcionalización remota mediante grupos periféricos voluminosos (complejos A1-A4). Esta estrategia ha sido utilizada en trabajos previos a fin de aumentar el rendimiento quántico empleando grupos voluminosos que actúan como espaciadores de los centros emisores (iTMCs) de modo que se reducen los procesos de relajación no radiativos ("quenching"). Por otro lado, se estudió el efecto de substituir el grupo que forma la interacción π-π intramolecular incorporando un grupo naftilo (complejo A5) en lugar del grupo fenilo en el ligando auxiliar.

Los resultados mostraron que el uso de grupos voluminosos, tanto por funcionalización remota como usando un grupo naftilo no mejoró el ϕ_{PL}. En el caso concreto del complejo A5 se encontró, mediante el uso de cálculos teóricos la presencia de dos estados tripletes próximos en energía, T1 y T2, con carácter MLCT/LLCT y LC respectivamente y que compiten entre sí en los procesos de relajación. A pesar del bajo ϕ_{PL} observado para A5 (10.2%), su eficiencia en LECs fue superior al complejo de referencia $[Ir(ppy)_2(pbpy)][PF_6]$, el cual presenta un mayor ϕ_{PL} (21%). Además, el compuesto A5 permite la posibilidad de modular su nivel de luminancia variando la densidad de corriente aplicada sin afectar gravemente la eficiencia del dispositivo de forma contraria a lo que viene siendo habitual en LECs. Este último punto se consiguió sin comprometer la eficiencia del dispositivo. Por ultimó, se comprobó que la presencia de átomos de bromo en los grupos periféricos afecta negativamente las prestaciones de los LECs limitando considerablemente la estabilidad de operación del dispositivo.

6.5. Pureza de los iTMCs

En el cuarto capítulo, se estudió el efecto de la presencia de impurezas en el iTMCs sobre las prestaciones de los LECs. En general, en materiales luminiscentes, se atribuyen connotaciones negativas a la presencia de impurezas. Esta consideración, toma especial interés en

iTMCs, donde las técnicas de purificación más eficientes no pueden ser aplicadas debido a su baja volatilidad. Concretamente, la ruta habitual de síntesis de los Ir(III)-iTMCs conduce usualmente a la presencia de pequeñas cantidades de iones cloruro. Hasta la realización de esta tesis doctoral, no existía ningún estudio centrado en el efecto de estos iones sobre el funcionamiento de los LECs. Además, en general, en ocasiones se observa una variación importante entre los resultados obtenidos para LECs construidos con diferentes lotes de un mismo material. Por tanto, es interesante conocer si la dispersión de resultados es provocada por la presencia de pequeñas cantidades de cloruro. Los resultados obtenidos han permitido esclarecer que pequeñas cantidades de impurezas cloruro presentes como contra-anión en el complejo arquetipo $[Ir(ppy)_2(bpy)][PF_6]$ dar lugar a una significativa pérdida de eficiencia en LECs. Se determinó, mediante experimentos de ^{1}H-RMN y caracterización mediante rayos X, la presencia de una interacción entre los iones cloruro y los protones en posición 3 del ligando bipiridina, la cual da lugar a la formación de un par iónico. Finalmente, se estudió el efecto de la presencia de iones cloruro sobre el ϕ_{PL} de $[Ir(ppy)_2(bpy)][PF_6]$ en capas delgadas. Para ello se prepararon muestras en capas delgadas del complejo $[Ir(ppy)_2(bpy)][PF_6]$ con diferente contenido de cloruro de tetraetilamonio. Se observó que ϕ_{PL} disminuye desde un 33.2% hasta un 20.9% al incrementar el contenido de iones cloruro en la muestra. De este modo esta interacción debe ser la responsable de la dispersión de resultados entre los diferentes lotes, de modo que la presencia de pequeñas cantidades de cloruro reduce enormemente la eficiencia del dispositivo. El caso concreto estudiado, la eficacia puede se vió reducida desde 8.8 a 5.0 cd A^{-1}.

6.6. Sistemas Matriz-Dopante

Por último, en el quinto capítulo, se abordó el estudio de LECs basados en sistemas matriz-dopante a fin de mejorar ϕ_{PL} en capas delgadas. El uso de estos sistemas ha sido ampliamente utilizado en OLEDs.

La estrategia consiste en combinar, dentro de una misma capa activa, un material que actúa como matriz y un emisor en baja proporción (dopante). La capa activa estaría por tanto formada por un material orgánico que actúa de matriz y donde el material emisor está distribuido de forma aislada. En estas condiciones, se previenen procesos de relajación no radiativa ("self-quenching") lo que aumenta el rendimiento cuántico de la fotoluminiscencia ϕ_{PL}. La aplicación de la estrategia en dispositivos electroluminiscentes requiere que la matriz presente: a) propiedades de transporte electrónico, b) formación de capas homogéneas con el material emisor y c) compatibilidad con el huésped en las propiedades ópticas a fin de que el proceso de transferencia de carga sea eficiente. La estrategia cobra un especial interés en LECs, donde generalmente las capas emisoras presentan un único componente y los procesos de relajación no radiativa cobran elevado protagonismo. Además, los LECs con mejores prestaciones están basados en Ir-iTMCs y debido a su elevado coste y baja abundancia del iridio en la corteza terrestre, la estrategía permite reducir enormemente la cantidad de iTMC necesaria para la preparación del dispositivo.

Esta tesis se ha centrado en tres tipos de sistemas matriz-dopante. El primer sistema (A) emplea una unidad carbazol funcionalizada iónicamente (NMS25) y una molécula orgánica neutra (SPPO13) como matriz. Como dopante se utilizó un complejo de iridio neutro (FIrPic) con emisión de luz azul. El segundo sistema está basado en dos colorantes cianina (Dye H y Dye G). El colorante H fue empleado como matriz, mientras que Dye G se utilizó como emisor infrarrojo (dopante). El tercer sistema fue diseñado también utilizando dos moléculas orgánicas, una matriz iónica orgánica (MYW2) y el compuesto Dye H como dopante.

Tal y como se esperaba, los tres sistemas presentan un aumento de ϕ_{PL} en película delgada. Además, las propiedades fotofísicas se han traducido en una mejora de la eficiencia de los LECs. Concretamente, en el primer caso, se obtuvieron LECs con emisión en el azul con una eficacia de 5 cd A^{-1} y una luminancia superior a 400 cd m^{-2}. Este resultado destaca frente a otros LECs con emisión azul, ya que las mayores

eficiencias obtenidas en estos dispositivos se alcanzaron a bajos niveles de luminancia. En el segundo caso, los colorantes cianina seleccionados presentan buenas propiedades de transporte electrónico y su naturaleza iónica permite que funcionen bajo un régimen normal de operación en LECs dando lugar a dispositivos estables con un alto nivel de irradiancia. Sin embargo, la eficiencia alcanzada fue considerablemente inferior al máximo teórico esperado, lo que demuestra la necesidad de optimizar el diseño y funcionamiento de estos LECs basados en colorantes cianina. En el tercer caso, empleando la molécula MYW2 como matriz, se alcanzó un valor de eficiencia de 1.9%, lo que se aproxima al máximo teórico para el sistema concreto estudiado (2.2%), asumiendo un ϕ_{PL}=43.1% y una emisión fluorescente del dopante. Recalcar además, que el uso de estos sistemas matriz-dopante representan una prometedora alternativa a los Ir-iTMCs para la preparación de LECs.

6.7. Conclusiones generales

A largo de esta tesis se han demostrado, diferentes métodos de aumentar la eficiencia en LECs mediante la modificación del rendimiento cuántico de fotoluminiscencia.

En primer lugar, la modificación química del ligando auxiliar ha demostrado que, mediante la incorporación de grupos voluminosos no siempre se consigue aumentar el rendimiento cuántico de fotoluminiscencia. Además la presencia de estructuras conjugadas sobre el ligando auxilar puede dar origen a estados electrónicos próximos en energía que compitan entre sí, limitando el rendimiento cuántico de fotolumiscencia (complejo A5). Sin embargo, a pesar del bajo rendimiento cuántico de fotoluminiscencia, el complejo A5, ha demostrado interesantes propiedades cuando es incorporado en la fabricación de dispositivos LEC.

En segundo lugar, la presencia de impurezas contaminantes procedentes de precursores de síntesis en complejos iónicos de iridio, suponen una seria amenaza para el desempeño de dispositivos emisores de luz. En el caso concreto de los LEC, las prestaciones del dispositivo

se han visto considerablemente reducidas como consecuencia de la formación de pares iónicos entre el ligando bipiridina del complejo metálico y el ión cloruro.

En tercer lugar, el uso de sistemas matriz-dopante ha permitido aumentar la eficiencia en diversos LECs, basados en materiales orgánicos iónicos. Esta estrategia permite el uso de materiales que por sí mismos no serían aptos para su integración en este tipo de dispositivo electrolumiscente, como es el caso de los colorantes cianina.

References

[1] *Early Europeans unwarmed by fire*, http://www.nature.com/news/2011/110314/full/news.2011.158.html, Accessed September, 2015.

[2] *World Population Projected*, http://www.un.org/en/development/desa/news/population/un-report-world-population-projected-to-reach-9-6-billion-by-2050.html, Accessed September, 2015.

[3] *Energy Efficiency: Lighting*, http://www.iea.org/topics/energyefficiency/subtopics/lighting/, Accessed September, 2015.

[4] Bernanose, A.; M. Comte and P. Vouaux. ***Sur un nouveu mode demission lumineuse chez certains composes organiques,*** *Journal De Chimie Physique Et De Physico-Chimie Biologique*, 1953, **50**, 64-68.

[5] Bernanose, A. and P. Vouaux. ***Electroluminescence organique - Etude du mode demission,*** *Journal De Chimie Physique Et De Physico-Chimie Biologique*, 1953, **50**, 261-&.

[6] Bernanose, A. ***Electroluminescence in organic compounds,*** *British Journal of Applied Physics*, 1955, S54-S56.

[7] Helfrich, W. and W. Schneider. ***Recombination Radiation in Anthracene Crystals,*** *Phys. Rev. Lett.*, 1965, **14**, 229.

[8] Pope, M.; H. Kallmann and P. Magnante. ***Electroluminescence in Organic Crystals,*** *J. Chem. Phys.*, 1963, **38**, 2042.

[9] Chiang, C. K.; C. R. Fincher; Y. W. Park; A. J. Heeger; H. Shirakawa; E. J. Louis; S. C. Gau and A. G. MacDiarmid. *Phys. Rev. Lett.*, 1977, **39**, 1098.

[10] Tang, C. W. and S. A. VanSlyke. ***Organic electroluminescent diodes,*** *Applied Physics Letters*, 1987, **51**, 913-915.

[11] Baldo, M. A.; D. F. O'Brien; Y. You; A. Shoustikov; S. Sibley; M. E. Thompson and S. R. Forrest. ***Highly efficient phosphorescent emission from organic electroluminescent devices,*** *Nature*, 1998, **395**, 151-154.

[12] Kwon, H. and R. Pode (2011) *High Efficiency Red Phosphorescent Organic Light-Emitting Diodes with Simple Structure, Organic Light*

Emitting Diode (Chapter 4) - Material, Process and Devices, Prof. Seung Hwanko (Ed.); http://www.intechopen.com, P. S. Hwanko, 978-953-307-273-9, InTech. http://www.intechopen.com. Accessed September, 2015.

[13] Pei, Q. B.; G. Yu; C. Zhang; Y. Yang and A. J. Heeger. ***Polymer Light-Emitting Electrochemical-Cells,*** *Science*, 1995, **269**, 1086-1088.

[14] Costa, R. D.; E. Ortí; H. J. Bolink; F. Monti; G. Accorsi and N. Armaroli. ***Luminescent Ionic Transition-Metal Complexes for Light-Emitting Electrochemical Cells,*** *Angew Chem Int Edit*, 2012, **51**, 8178-8211.

[15] Maness, K. M.; R. H. Terrill; T. J. Meyer; R. W. Murray and R. M. Wightman. ***Solid-state diode-like chemiluminescence based on serial, immobilized concentration gradients in mixed-valent poly[Ru(vbpy)(3)](PF6)(2) films,*** *Journal of the American Chemical Society*, 1996, **118**, 10609-10616.

[16] Slinker, J. D.; J. Rivnay; J. S. Moskowitz; J. B. Parker; S. Bernhard; H. D. Abruna and G. G. Malliaras. ***Electroluminescent devices from ionic transition metal complexes,*** *Journal of Materials Chemistry*, 2007, **17**, 2976-2988.

[17] Gao, F. G. and A. J. Bard. ***Solid-state organic light-emitting diodes based on tris(2,2 '-bipyridine)ruthenium(II) complexes,*** *Journal of the American Chemical Society*, 2000, **122**, 7426-7427.

[18] Fang, J.; P. Matyba and L. Edman. ***The Design and Realization of Flexible, Long-Lived Light-Emitting Electrochemical Cells,*** *Adv. Funct. Mater.*, 2009, **19**, 2671.

[19] Sandstrom, A.; P. Matyba and L. Edman. ***Yellow-green light-emitting electrochemical cells with long lifetime and high efficiency,*** *Appl. Phys. Lett.*, 2010, **96**, 053303.

[20] Kaihovirta, N.; C. Larsen and L. Edman. ***Improving the Performance of Light-Emitting Electrochemical Cells by Optical Design,*** *Acs Applied Materials & Interfaces*, 2014, **6**, 2940-2947.

[21] Tang, S.; A. Sandstrom; J. F. Fang and L. Edman. ***A Solution-Processed Trilayer Electrochemical Device: Localizing the Light Emission for Optimized Performance,*** *Journal of the American Chemical Society*, 2012, **134**, 14050-14055.

[22] Li, X.; F. AlTal; G. Liu and J. Gao. ***Long-term, intermittent testing of sandwich polymer light-emitting electrochemical cells,*** *Applied Physics Letters*, 2013, **103**, -.

[23] Li, X.; J. Gao and G. Liu. ***Reversible luminance decay in polymer light-emitting electrochemical cells,*** *Applied Physics Letters*, 2013, **102**, 223303.

[24] Li, X.; J. Gao and G. Liu. ***Thickness dependent device characteristics of sandwich polymer light-emitting electrochemical cell,*** *Organic Electronics*, 2013, **14**, 1441-1446.

[25] Gautier, B. and J. Gao. ***Polymer light-emitting devices based on a polymer/salt mixture,*** *Applied Physics Letters*, 2012, **101**.

[26] Tang, S. and L. Edman. ***Quest for an Appropriate Electrolyte for High-Performance Light-Emitting Electrochemical Cells,*** *J Phys Chem Lett*, 2010, **1**, 2727-2732.

[27] van Reenen, S.; P. Matyba; A. Dzwilewski; R. A. J. Janssen; L. Edman and M. Kemerink. ***Salt Concentration Effects in Planar Light-Emitting Electrochemical Cells,*** *Advanced Functional Materials*, 2011, **21**, 1795-1802.

[28] van Reenen, S.; P. Matyba; A. Dzwilewski; R. A. J. Janssen; L. Edman and M. Kemerink. ***A Unifying Model for the Operation of Light-Emitting Electrochemical Cells,*** *Journal of the American Chemical Society*, 2010, **132**, 13776-13781.

[29] Sunesh, C. D.; G. Mathai and Y. Choe. ***Green and blue-green light-emitting electrochemical cells based on cationic iridium complexes with 2-(4-ethyl-2-pyridyl)-1H-imidazole ancillary ligand,*** *Organic Electronics*, 2014, **15**, 667-674.

[30] Zhang, J.; L. Zhou; H. A. Al-Attar; K. Z. Shao; L. Wang; D. X. Zhu; Z. M. Su; M. R. Bryce and A. P. Monkman. ***Efficient Light-Emitting Electrochemical Cells (LECs) Based on Ionic Iridium(III) Complexes with 1,3,4-Oxadiazole Ligands,*** *Advanced Functional Materials*, 2013, **23**, 4667-4677.

[31] Tordera, D.; J. Frey; D. Vonlanthen; E. Constable; A. Pertegás; E. Ortí; H. J. Bolink; E. Baranoff and M. K. Nazeeruddin. ***Low Current Density Driving Leads to Efficient, Bright and Stable Green Electroluminescence,*** *Advanced Energy Materials*, 2013, n/a-n/a.

[32] Dumur, F.; Y. Yuskevitch; G. Wantz; C. R. Mayer; D. Bertin and D. Gigmes. ***Light-emitting electrochemical cells based on a solution-processed multilayered device and an anionic iridium (III) complex,*** *Synthetic Metals*, 2013, **177**, 100-104.

[33] Dumur, F.; D. Bertin and D. Gigmes. ***Iridium (III) complexes as promising emitters for solid-state Light-Emitting Electrochemical Cells (LECs),*** *Int J Nanotechnol*, 2012, **9**, 377-395.

[34] Shen, Y. L.; D. D. Kuddes; C. A. Naquin; T. W. Hesterberg; C. Kusmierz; B. J. Holliday and J. D. Slinker. ***Improving light-emitting electrochemical cells with ionic additives,*** *Applied Physics Letters*, 2013, **102**, 5.

[35] Zhang, F.; L. Duan; J. Qiao; G. Dong; L. Wang and Y. Qiu. ***The intramolecular π–π stacking interaction does not always work for improving the stabilities of light-emitting electrochemical cells,*** *Organic Electronics*, 2012, **13**, 2442-2449.

[36] Slinker, J.; D. Bernards; P. L. Houston; H. D. Abruna; S. Bernhard and G. G. Malliaras. ***Solid-state electroluminescent devices based on transition metal complexes,*** *Chemical Communications*, 2003, 2392-2399.

[37] Bolink, H. J.; L. Cappelli; E. Coronado; A. Parham and P. Stossel. ***Green light-emitting solid-state electrochemical cell obtained from a homoleptic iridium(III) complex containing ionically charged ligands,*** *Chemistry of Materials*, 2006, **18**, 2778-2780.

[38] Hu, T.; L. He; L. Duan and Y. Qiu. ***Solid-state light-emitting electrochemical cells based on ionic iridium(III) complexes,*** *Journal of Materials Chemistry*, 2012, **22**, 4206-4215.

[39] Rudmann, H.; S. Shimada and M. F. Rubner. ***Solid-state light-emitting devices based on the tris-chelated ruthenium(II) complex. 4. High-efficiency light-emitting devices based on derivatives of the tris(2,2 '-bipyridyl) ruthenium(II) complex,*** *Journal of the American Chemical Society*, 2002, **124**, 4918-4921.

[40] Bolink, H. J.; L. Cappelli; E. Coronado; M. Gratzel; E. Orti; R. D. Costa; P. M. Viruela and M. K. Nazeeruddin. ***Stable single-layer light-emitting electrochemical cell using 4,7-diphenyl-1,10-phenanthroline-bis(2-phenylpyridine) iridium(III) hexafluorophosphate,*** *Journal of the American Chemical Society*, 2006, **128**, 14786-14787.

[41] Tordera, D.; A. M. Bünzli; A. Pertegás; J. M. Junquera-Hernández; E. C. Constable; J. A. Zampese; C. E. Housecroft; E. Ortí and H. J. Bolink. ***Efficient Green-Light-Emitting Electrochemical Cells Based on Ionic Iridium Complexes with Sulfone-Containing Cyclometalating Ligands,*** *Chemistry – A European Journal*, 2013, **19**, 8597-8609.

[42] Costa, R. D.; D. Tordera; E. Orti; H. J. Bolink; J. Schonle; S. Graber; C. E. Housecroft; E. C. Constable and J. A. Zampese. ***Copper(I) complexes for sustainable light-emitting electrochemical cells,*** *Journal of Materials Chemistry*, 2011, **21**, 16108-16118.

[43] Gao, F. G. and A. J. Bard. ***High-brightness and low-voltage light-emitting devices based on trischelated ruthenium(II) and tris(2,2 '-bipyridine)osmium(II) emitter layers and low melting point alloy cathode contacts,*** *Chemistry of Materials*, 2002, **14**, 3465-3470.

[44] Armaroli, N.; G. Accorsi; M. Holler; O. Moudam; J. F. Nierengarten; Z. Zhou; R. T. Wegh and R. Welter. ***Highly luminescent Cu-I complexes for light-emitting electrochemical cells,*** *Advanced Materials*, 2006, **18**, 1313-1316.

[45] Hosseini, A. R.; C. Y. Koh; J. D. Slinker; S. Flores-Torres; H. D. Abruna and G. G. Malliaras. ***Addition of a phosphorescent dopant in electroluminescent devices from ionic transition metal complexes,*** *Chemistry of Materials*, 2005, **17**, 6114-6116.

[46] Balzani, V. and S. Campagna, in *Photochemistry and Photophysics of Coordination Compounds I*, eds. V. Balzani and S. Campagna, Springer-Verlag Berlin, Berlin, Editon edn., 2007, vol. 280, pp. IX-XI.

[47] Balzani, V., in *Photochemistry and Photophysics of Coordination Compounds Ii*, eds. V. Balzani and S. Campagna, Springer-Verlag Berlin, Berlin, Editon edn., 2007, vol. 281, pp. IX-XI.

[48] Thompson, D. W.; J. F. Wishart; B. S. Brunschwig and N. Sutin. ***Efficient generation of the ligand field excited state of tris-(2,2 '-bipyridine)-ruthenium(II) through sequential two-photon capture by [Ru(bpy)(3)](2+) or electron capture by [Ru(bpy)(3)](3+),*** *J Phys Chem A*, 2001, **105**, 8117-8122.

[49] Kwon, T. H.; Y. H. Oh; I. S. Shin and J. I. Hong. ***New Approach Toward Fast Response Light-Emitting Electrochemical Cells Based on Neutral Iridium Complexes via Cation Transport,*** *Advanced Functional Materials*, 2009, **19**, 711-717.

[50] Slinker, J. D.; A. A. Gorodetsky; M. S. Lowry; J. J. Wang; S. Parker; R. Rohl; S. Bernhard and G. G. Malliaras. ***Efficient yellow electroluminescence from a single layer of a cyclometalated iridium complex,*** *Journal of the American Chemical Society*, 2004, **126**, 2763-2767.

[51] Costa, R. D.; E. Ortí; H. J. Bolink; S. Graber; C. E. Housecroft and E. C. Constable. ***Efficient and Long-Living Light-Emitting Electrochemical Cells,*** *Advanced Functional Materials*, 2010, **20**, 1511-1520.

[52] Ho, C. C.; H. F. Chen; Y. C. Ho; C. T. Liao; H. C. Su and K. T. Wong. ***Phosphorescent sensitized fluorescent solid-state near-infrared light-emitting electrochemical cells,*** *Physical Chemistry Chemical Physics*, 2011, **13**, 17729-17736.

[53] Tang, S.; W.-Y. Tan; X.-H. Zhu and L. Edman. ***Small-molecule light-emitting electrochemical cells: evidence for in situ electrochemical doping and functional operation,*** *Chemical Communications*, 2013, **49**, 4926-4928.

[54]deMello, J. C.; J. J. M. Halls; S. C. Graham; N. Tessler and R. H. Friend. ***Electric field distribution in polymer light-emitting electrochemical cells,*** *Physical Review Letters*, 2000, **85**, 421-424.

[55] deMello, J. C. ***Interfacial feedback dynamics in polymer light-emitting electrochemical cells,*** *Physical Review B*, 2002, **66**.

[56] deMello, J. C.; N. Tessler; S. C. Graham and R. H. Friend. ***Ionic space-charge effects in polymer light-emitting diodes,*** *Physical Review B*, 1998, **57**, 12951-12963.

[57] Pei, Q. B.; Y. Yang; G. Yu; C. Zhang and A. J. Heeger. ***Polymer light-emitting electrochemical cells: In situ formation of a light-emitting p-n junction,*** *Journal of the American Chemical Society*, 1996, **118**, 3922-3929.

[58] Dick, D. J.; A. J. Heeger; Y. Yang and Q. B. Pei. ***Imaging the structure of the p-n junction in polymer light-emitting electrochemical cells,*** *Advanced Materials*, 1996, **8**, 985-987.

[59] Slinker, J. D.; J. A. DeFranco; M. J. Jaquith; W. R. Silveira; Y. W. Zhong; J. M. Moran-Mirabal; H. G. Craighead; H. D. Abruna; J. A. Marohn and G. G. Malliaras. ***Direct measurement of the electric-field distribution in a light-emitting electrochemical cell,*** *Nature Materials*, 2007, **6**, 894-899.

[60] Yu, Z. B.; M. L. Wang; G. T. Lei; J. Liu; L. Li and Q. B. Pei. ***Stabilizing the Dynamic p-i-n Junction in Polymer Light-Emitting Electrochemical Cells,*** *J Phys Chem Lett*, 2011, **2**, 367-372.

[61] Gao, J.; A. J. Heeger; I. H. Campbell and D. L. Smith. ***Direct observation of junction formation in polymer light-emitting electrochemical cells,*** *Physical Review B*, 1999, **59**, R2482-R2485.

[62] Rudmann, H.; S. Shimada and M. F. Rubner. ***Operational mechanism of light-emitting devices based on Ru(II) complexes: Evidence for electrochemical junction formation,*** *Journal of Applied Physics*, 2003, **94**, 115-122.

[63] Matyba, P.; K. Maturova; M. Kemerink; N. D. Robinson and L. Edman. ***The dynamic organic p-n junction,*** *Nature Materials*, 2009, **8**, 672-676.

[64] Meier, S. B.; S. van Reenen; B. Lefevre; D. Hartmann; H. J. Bolink; A. Winnacker; W. Sarfert and M. Kemerink. ***Dynamic Doping in Planar Ionic Transition Metal Complex-Based Light-Emitting Electrochemical Cells,*** *Advanced Functional Materials*, 2013, n/a-n/a.

[65] Lenes, M.; Garcia-Belmonte, G.; Tordera, D.; Pertegas, A.; Bisquert, J. and H. J. Bolink. ***Operating modes of Sandwiched Light-Emitting Electrochemical Cells,*** *Advanced Functional Materials*, 2011, **21**, 1581-1586.

[66] Meier, S. B.; D. Hartmann; W. Sarfert; D. Tordera; H. J. Bolink and A. Winnacker. ***In situ photoluminescence spectroscopy study of dynamic doping in sandwich-type light-emitting electrochemical cells,*** *Proceedings of SPIE - The International Society for Optical Engineering*, 2012, 847617-847617.

[67] Meier, S. B.; D. Hartmann; D. Tordera; H. J. Bolink; A. Winnacker and W. Sarfert. ***Dynamic doping and degradation in sandwich-type light-emitting electrochemical cells,*** *Physical Chemistry Chemical Physics*, 2012, **14**, 10886-10890.

[68] Costa, R. D.; E. Ortí; H. J. Bolink; S. Graber; S. Schaffner; M. Neuburger; C. E. Housecroft and E. C. Constable. ***Archetype Cationic Iridium Complexes and Their Use in Solid-State Light-Emitting Electrochemical Cells,*** *Advanced Functional Materials*, 2009, **19**, 3456-3463.

[69] Parker, S. T.; J. D. Slinker; M. S. Lowry; M. P. Cox; S. Bernhard and G. G. Malliaras. ***Improved turn-on times of iridium electroluminescent devices by use of ionic liquids,*** *Chemistry of Materials*, 2005, **17**, 3187-3190.

[70] Tordera, D.; S. Meier; M. Lenes; R. D. Costa; E. Orti; W. Sarfert and H. J. Bolink. ***Simple, Fast, Bright, and Stable Light Sources,*** *Advanced Materials*, 2012, **24**, 897-+.

[71] Bolink, H. J.; E. Coronado; R. D. Costa; N. Lardies and E. Orti. ***Near-Quantitative Internal Quantum Efficiency in a Light-Emitting Electrochemical Cell,*** *Inorg Chem*, 2008, **47**, 9149-9151.

[72] Liao, C. T.; H. F. Chen; H. C. Su and K. T. Wong. ***Tailoring balance of carrier mobilities in solid-state light-emitting electrochemical cells by doping a carrier trapper to enhance device efficiencies,*** *Journal of Materials Chemistry*, 2011, **21**, 17855-17862.

[73] Su, H. C.; F. C. Fang; T. Y. Hwu; H. H. Hsieh; H. F. Chen; G. H. Lee; S. M. Peng; K. T. Wong and C. C. Wu. ***Highly efficient orange and green solid-state light-emitting electrochemical cells based on cationic Ir-III complexes with enhanced steric hindrance,*** *Advanced Functional Materials*, 2007, **17**, 1019-1027.

[74] Shavaleev, N. M.; R. Scopelliti; M. Gratzel; M. K. Nazeeruddin; A. Pertegas; C. Roldan-Carmona; D. Tordera and H. J. Bolink. ***Pulsed-current versus constant-voltage light-emitting electrochemical cells with trifluoromethyl-substituted cationic iridium(iii) complexes,*** *Journal of Materials Chemistry C*, 2013, **1**, 2241-2248.

[75] He, L.; J. Qiao; L. Duan; G. F. Dong; D. Q. Zhang; L. D. Wang and Y. Qiu. ***Toward Highly Efficient Solid-State White Light-Emitting Electrochemical Cells: Blue-Green to Red Emitting Cationic Iridium Complexes with Imidazole-Type Ancillary Ligands,*** *Advanced Functional Materials*, 2009, **19**, 2950-2960.

[76] He, L.; L. Duan; J. Qiao; R. J. Wang; P. Wei; L. D. Wang and Y. Qiu. ***Blue-emitting cationic iridium complexes with 2-(1H-pyrazol-1-yl)pyridine as the ancillary ligand for efficient light-emitting electrochemical cells,*** *Advanced Functional Materials*, 2008, **18**, 2123-2131.

[77] Meier, S. B.; W. Sarfert; J. M. Junquera-Hernandez; M. Delgado; D. Tordera; E. Orti; H. J. Bolink; F. Kessler; R. Scopelliti; M. Gratzel; M. K. Nazeeruddin and E. Baranoff. ***A deep-blue emitting charged bis-***

cyclometallated iridium(iii) complex for light-emitting electrochemical cells, *Journal of Materials Chemistry C*, 2013, **1**, 58-68.

[78] Monti, F.; F. Kessler; M. Delgado; J. Frey; F. Bazzanini; G. Accorsi; N. Armaroli; H. J. Bolink; E. Ortí; R. Scopelliti; M. K. Nazeeruddin and E. Baranoff. ***Charged Bis-Cyclometalated Iridium(III) Complexes with Carbene-Based Ancillary Ligands,*** *Inorganic Chemistry*, 2013, **52**, 10292-10305.

[79] Sessolo, M.; D. Tordera and H. J. Bolink. ***Ionic Iridium Complex and Conjugated Polymer Used To Solution-Process a Bilayer White Light-Emitting Diode,*** *Acs Applied Materials & Interfaces*, 2013, **5**, 630-634.

[80] Bolink, H. J.; L. Cappelli; S. Cheylan; E. Coronado; R. D. Costa; N. Lardies; M. K. Nazeeruddin and E. Orti. ***Origin of the large spectral shift in electroluminescence in a blue light emitting cationic iridium(III) complex,*** *Journal of Materials Chemistry*, 2007, **17**, 5032-5041.

[81] Bernhard, S.; J. A. Barron; P. L. Houston; H. D. Abruna; J. L. Ruglovksy; X. C. Gao and G. G. Malliaras. ***Electroluminescence in ruthenium(II) complexes,*** *Journal of the American Chemical Society*, 2002, **124**, 13624-13628.

[82] Kalyuzhny, G.; M. Buda; J. McNeill; P. Barbara and A. J. Bard. ***Stability of thin-film solid-state electroluminescent devices based on tris(2,2 '-bipyridine)ruthenium(II) complexes,*** *Journal of the American Chemical Society*, 2003, **125**, 6272-6283.

[83] Malliaras, G. G. and J. C. Scott. *J. Appl. Phys.*, 1998, **83**, 5399.

[84] Bolink, H. J.; E. Coronado; R. D. Costa; E. Ortí; M. Sessolo; S. Graber; K. Doyle; M. Neuburger; C. E. Housecroft and E. C. Constable. ***Long-Living Light-Emitting Electrochemical Cells - Control through Supramolecular Interactions,*** *Advanced Materials*, 2008, **20**, 3910-3913.

[85] Graber, S.; K. Doyle; M. Neuburger; C. E. Housecroft; E. C. Constable; R. D. Costa; E. Ortí; D. Repetto and H. J. Bolink. ***A Supramolecularly-Caged Ionic Iridium(III) Complex Yielding Bright and Very Stable Solid-State Light-Emitting Electrochemical Cells,*** *Journal of the American Chemical Society*, 2008, **130**, 14944-14945.

[86] Costa, R. D.; E. Ortí; H. J. Bolink; S. Graber; C. E. Housecroft; M. Neuburger; S. Schaffner and E. C. Constable. ***Two are not always better***

than one: ligand optimisation for long-living light-emitting electrochemical cells, *Chemical Communications*, 2009, 2029-2031.

[87] Costa, R. D.; E. Ortí; H. J. Bolink; S. Graber; C. E. Housecroft and E. C. Constable. ***Light-emitting electrochemical cells based on a supramolecularly-caged phenanthroline-based iridium complex,*** *Chemical Communications*, 2011, **47**, 3207-3209.

[88] Costa, R. D.; E. Ortí; D. Tordera; A. Pertegás; H. J. Bolink; S. Graber; C. E. Housecroft; L. Sachno; M. Neuburger and E. C. Constable. ***Stable and Efficient Solid-State Light-Emitting Electrochemical Cells Based on a Series of Hydrophobic Iridium Complexes,*** *Advanced Energy Materials*, 2011, **1**, 282-290.

[89] He, L.; L. A. Duan; J. A. Qiao; G. F. Dong; L. D. Wang and Y. Qiu. ***Highly Efficient Blue-Green and White Light-Emitting Electrochemical Cells Based on a Cationic Iridium Complex with a Bulky Side Group,*** *Chemistry of Materials*, 2010, **22**, 3535-3542.

[90] Jeon, H. G.; Y. Kondo; S. Maki; E. Matsumoto; Y. Taniguchi and M. Ichikawa. ***A highly efficient sublimation purification system using baffles with orifices,*** *Organic Electronics*, 2010, **11**, 794-800.

[91] Jeon, H. G.; M. Inoue; N. Hirarnatsu; M. Ichikawa and Y. Taniguchi. ***A modified sublimation purification system using arrays of partitions,*** *Organic Electronics*, 2008, **9**, 903-905.

[92] Forrest, S. R. ***Ultrathin Organic Films Grown by Organic Molecular Beam Deposition and Related Techniques,*** *Chemical Reviews*, 1997, **97**, 1793-1896.

[93] Hu, T.; L. Duan; J. Qiao; L. He; D. Q. Zhang; R. J. Wang; L. D. Wang and Y. Qiu. ***Stable blue-green light-emitting electrochemical cells based on a cationic iridium complex with phenylpyrazole as the cyclometalated ligands,*** *Organic Electronics*, 2012, **13**, 1948-1955.

[94] Zysman-Colman, E.; J. D. Slinker; J. B. Parker; G. G. Malliaras and S. Bernhard. ***Improved turn-on times of light-emitting electrochemical cells,*** *Chemistry of Materials*, 2008, **20**, 388-396.

[95] Tordera, D.; A. Pertegás; N. M. Shavaleev; R. Scopelliti; E. Ortí; H. J. Bolink; E. Baranoff; M. Grätzel and M. K. Nazeeruddin. ***Efficient orange light-emitting electrochemical cells,*** *Journal of Materials Chemistry*, 2012, **22**, 19264-19268.

[96] Pile, D. L. and A. J. Bard. ***Effect of water vapor on the operation and stability of tris(2,2 '-bipyridine)ruthenium(II)-based light-emitting electrochemical cells,*** *Chemistry of Materials*, 2005, **17**, 4212-4217.

[97] Zhao, W.; C. Y. Liu; Q. Wang; J. M. White and A. J. Bard. ***Effect of residual solvent on Ru(bpy)(3)(ClO4)(2)-based light-emitting electrochemical cells,*** *Chemistry of Materials*, 2005, **17**, 6403-6406.

[98] Soltzberg, L. J.; J. D. Slinker; S. Flores-Torres; D. A. Bernards; G. G. Malliaras; H. D. Abruna; J. S. Kim; R. H. Friend; M. D. Kaplan and V. Goldberg. ***Identification of a quenching species in ruthenium tris-bipyridine electroluminescent devices,*** *Journal of the American Chemical Society*, 2006, **128**, 7761-7764.

[99] Slinker, J. D.; J. S. Kim; S. Flores-Torres; J. H. Delcamp; H. D. Abruna; R. H. Friend and G. G. Malliaras. ***In situ identification of a luminescence quencher in an organic light-emitting device,*** *Journal of Materials Chemistry*, 2007, **17**, 76-81.

[100] Constable, E. C. and K. R. Seddon. ***A deuterium exchange reaction of the tris-(2,2′-bipyridine)ruthenium(II) cation: evidence for the acidity of the 3,3′-protons,*** *J. Chem. Soc., Chem. Commun.*, 1982, 34-36.

[101] Walzer, K.; B. Maennig; M. Pfeiffer and K. Leo. ***Highly efficient organic devices based on electrically doped transport layers,*** *Chemical Reviews*, 2007, **107**, 1233-1271.

[102] Su, H. C.; C. C. Wu; F. C. Fang and K. T. Wong. ***Efficient solid-state host-guest light-emitting electrochemical cells based on cationic transition metal complexes,*** *Applied Physics Letters*, 2006, **89**.

[103] Su, H. C.; H. F. Chen; Y. C. Shen; C. T. Liao and K. T. Wong. ***Highly efficient double-doped solid-state white light-emitting electrochemical cells,*** *Journal of Materials Chemistry*, 2011, **21**, 9653-9660.

[104] Liao, C.-T.; H.-F. Chen; H.-C. Su and K.-T. Wong. ***Improving the balance of carrier mobilities of host-guest solid-state light-emitting electrochemical cells,*** *Physical Chemistry Chemical Physics*, 2012, **14**, 1262-1269.

[105] Ho, C.-C.; H.-F. Chen; Y.-C. Ho; C.-T. Liao; H.-C. Su and K.-T. Wong. ***Phosphorescent sensitized fluorescent solid-state near-infrared light-emitting electrochemical cells,*** *Physical Chemistry Chemical Physics*, 2011, **13**, 17729-17736.

Index of figures

Index of tables

Index of abbreviations

LED	Light emitting diode
OLED	Organic light emitting diode
EIA	Energy Information Administration
EL	Electroluminiscence
PL	Photoluminescence
HIL	Hole injection layer
HTL	Hole transport layer
EML	Emitting material layer
HBL	Hole blocking layer
ETL	Electron transport layer
LEC	Light-emitting electrochemical cell
TMC	Transition metal complex
iTMC	Ionic transition metal complex
SM	Small molecular
HOMO	High occupied molecular orbital
LUMO	Low unoccupied molecular orbital
$t_{1/2}$	Life-time
t_{on}	Turn-on time
Lum	Luminance
ϕ_{PL}	Photoluminescence quantum yield
EQE	External quantum efficiency
PCE	Power conversion efficiency
CIE	Commision Internationale de l´Eclairage coordinates
HPLC	High performance liquid chromatography
λ_{max}^{PL}	Photoluminescence wavelength peak
MLCT	Metal to ligand charge transfer
LLCT	Ligand to ligand charge transfer
LC	Ligand centered
TADF	Thermal-activated delayed fluorescence
PEDOT:PSS	poly(3,4-ethylenedioxythiophene) polystyrene sulfonate
SPPO13	2,7-Bis(diphenylphosphoryl)-9,9′-spirobifluorene
ITO	Indium tin oxide

IL	Ionic liquid
[Bmim][PF_6]	1-butyl-3-methyl-imidazolium hexafluorophosphate
C^N	phenyl pyridine based ligand
N^N	bipyridine based ligand
Ppy	Phenylpyridine
Bpy	bipyridine
ppyF_2	2-(2′,4′-difluorophenyl)pyridine
pbpy	6-phenyl-2,2′-bipyridine
dtb-bpy	4,4′-di-tert-butyl-2,2′-dipyridil
C_{10}ppbpypy	4-(3,5-bis(decyloxylphenyl)-6-phenyl-2,2′-bipyridine
Dasb	4,5-diaza-9,9′-spirobifluoroene

Other contributions during this thesis

6. R. D. Costa, A. Pertegás, E.Ortí and H. J. Bolink "Improving the turn-on time of light-emitting electrochemical cells without sacrificing their stability" *Chem. Mat.* **2010,** *22*, 1288-1290.

7. M. Lenes, G. Gracia-Belmonte, D. Tordera, A. Pertegás, J. Bisquert and H. J. Bolink "Operating modes of sandwiched light-emitting electrochemical cells" *Adv. Funct. Mater* **2011,** *21***,** 1581-1586.

8. R. D. Costa, E. Ortí, D. Tordera, A. Pertegás, H. J. Bolink, S. Graber, C. E. Housecroft, L. Sachno, M. Neuburger and E. C. Constable "Stable and efficient solid-state light-emitting electrochemical cells based on a series of hydrophobic Iridium complexes" *Adv. Ener. Mater.* **2011**, *1*, 282-289.

9. W.-J. Xu, S.-J. Liu, T.-C. Ma, Q. Zhao, A. Pertegás, D. Tordera, H. J. Bolink, S.-H. Ye, X.-M. Liu and S. S. W. Huang "p-n metallophosphor based on cationic Iridium (III) complex for solid-state light emitting electrochemical cells" *J. Mater. Chem.* **2011,** *21*, 13999-14007.

10. D. Tordera, A. Pertegás, N. M. Shavaleev, R. Scopelliti, E. Orti, H. J. Bolink, E. D. Baranoff, M. Gratzel and M. K. Nazeeruddin "Efficient Orange Light-Emitting Electrochemical Cells" *J. Mater. Chem.* **2012,** *22*, 19264-19268.

11. N. M. Shavaleev, R. Scopelliti, M. Grätzel, M. K. Nazeeruddin, A. Pertegás, Cristina Roldán, D. Tordera, H. J. Bolink "Pulsed-current versus constant-voltage light-emitting electrochemical cells with trifluoromethyl-substituted cationic iridium(III) complexes"*J. Mater. Chem. C* **2013,** *1*, 2241-2248.

12. D. Tordera, J. Frey, D. Vonlanthen, E. Constable, A. Pertegás, E. Ortí, H. J. Bolink, E. Baranoff, M. K. Nazeeruddin "Low Current Density Driving Leads to Efficient, Bright and Stable Green Electroluminescence" *Adv. Energy. Mater.* **2013**, *3*, 1338-1343.

13. E. C. Constable, C. E. Housecroft, P. Kopecky, C. J. Martin, I. A. Wright, J. A. Zampese, H. J. Bolink, A. Pertegás "Solution, structural and photophysical aspects of substituent effects in the N^N ligand in [Ir(C^N)2(N^N)]+ complexes" *Dalton Trans.* **2013** *42*, 8086-8103.

14. D. Tordera, A. M. Bünzli, A. Pertegás, J. M. Junquera-Hernández, E. C. Constable, J. A. Zampese, C. E. Housecroft, E. Ortí, H. J. Bolink "Efficient Green-Light-Emitting Electrochemical Cells Based on Ionic Iridium Complexes with Sulfone-Containing Cyclometalating Ligands" *Chem. Eur. J.* **2013,** *19,* 8597-8609.

15. D. Tordera, J. J. Serrano-Pérez, A. Pertegás, E. Ortí, H. J. Bolink, E. Baranoff, Md. K. Nazeeruddin, J. Frey "Correlating the Lifetime and Fluorine Content of Iridium(III) Emitters in Green Light-Emitting Electrochemical Cells" *Chem. Mater.* **2013**, *25*, 3391-3397.

16. A. M. Bünzli, H. J. Bolink, E. C. Constable, C. E. Housecroft, J. M. Junquera-Hernández, M. Neuburger, E. Ortí; A. Pertegás, J. J. Serrano-Pérez, D. Tordera, J. A. Zampese "Thienylpyridine-based cyclometallated iridium(III) complexes and their use in solid state light-emitting electrochemical cells" *Dalton Trans.* **2014**, *43*, 738-750.

17. S. B. Meier, D. Tordera, A. Pertegás, C. Roldán-Carmona, E. Ortí, H. J. Bolink "Light-emitting electrochemical cells: recent progress and future prospects" *Mater. Today* **2014**, *17*, 217-223.

Agradecimientos

A mis dos tutores, Enrique y Henk que han hecho posible, gracias a su esfuerzo y dedicación la elaboración de esta tesis doctoral. También, darles las gracias a ambos por su confianza y comprensión a lo largo de todo este periodo.

Al grupo del Prof. Edwin Constable y Prof. Catherine Housecroft, al grupo del Prof. Md. Nazeeruddin y al grupo del Prof. Eli Zysman-Colman por confiar en nosotros para llevar a cabo la preparación de dispositivos utilizando sus materiales.

Agradecer sinceramente a todas las personas que forman o han formado del grupo de investigación por contribuir y ayudarme en la elaboración de esta tesis.

Agradecer a mi familia por mostrarme su apoyo durante este periodo.